Fireball of 24 February 2018 at 00h11m UT
All Sky camera at Wilderen (EN92), Belgium, by Jean-Marie Biets

Contents

Detailed analysis of the fireball 20160317_031654 over the United Kingdom

Jakub Koukal

Valašské Meziříčí Observatory, Vsetínská 78, 75701 Valašské Meziříčí, Czech Republic
j.koukal@post.cz

On March 17, 2016 in the early morning hours the UKMON network (United Kingdom Meteor Observation Network) cameras recorded a bright fireball with an absolute magnitude of -12.5 ± 0.4m, its atmospheric path began above the Dorset County and ended up above the Oxford County in the southern part of England. This fireball belonging to the Northern March gamma Virginids (IAU MDC #749 NMV) meteor shower was recorded from 8 cameras of the UKMON network. The atmospheric path of the bolide and the heliocentric orbit of the meteoroid are analyzed in this article. The flight of the fireball, whose absolute magnitude was comparable with the brightness of the Full Moon, was also observed by numerous random observers from the public in the United Kingdom, the Netherlands, Belgium and France. Numerical integration of the heliocentric orbit of the body and its clones was performed to find the potential parent body of the fireball and also the potential parent body of the meteor shower #749 NMV. However, no potential parent body of the fireball 20160317_031654 was found in the comets (periodic, non-periodic and lost) and asteroids database.

1 Introduction

Fireball 20160317_031654 was recorded by the UKMON network cameras on March 17, 2016 at $3^h16^m54.0 ± 0.1^s$ UT. Records from the cameras were significantly saturated due to the intense brightness of the fireball. The fireball flight was recorded by the following UKMON network stations (*Figure 2*): Clanfield NW (Hampshire Astronomy Group, *Steve Bosley*), Church Crookham (*Peter Campbell-Burns*), Lockyer L1, L2 (Norman Lockyer Observatory, *Dave Jones*), Scotch Street C1 (*Steve Hooks*) and Wilcot NE, N (*Richard Fleet*).

In this case, it was necessary to perform the astrometry of the recorded fireball manually. From the NHM station (Natural History Museum, London), only a flash of the flight of the fireball at the edge (or outside) of the field of view was recorded. The bolide was included in the EDMOND database (Kornoš et al., 2014a,b) with the designation 20160317_031654, which accurately identifies the observation time in the YYYYMMDD_HHMMSS (UT) format. The Northern March gamma Virginids meteor shower (IAU MDC #749 NMV) is one of the less active and poorly known showers. In the IAU MDC meteor showers database (Jopek et al., 2014), there are only two mean orbits of this shower (Jenniskens et al., 2016; 2018) that were taken from the CAMS network observations. The orbital elements of the shower mean orbit (Jenniskens et al., 2018; in parentheses Jenniskens et al., 2016) are as follows: v_g = 38.3 (42.7) km/s, a = 1.54 (2.40) AU, q = 0.082 (0.071) AU, e = 0.935 (0.979), i = 21.1 (23.7)°, ω = 334.8 (332.5)°, Ω = 346.7 (338.9)°, coordinates of the geocentric radiant (J2000.0) are RA = 198.5 (189.1)°, DEC = –1.2 (3.0)°. The mean orbit was calculated from the 138 (13) individual orbits belonging to the shower. The possible parent body of the NMV shower has not yet been established.

2 Visual observations

Visual observations of fireballs are collected in the IMO database[1] and reports to this database are sent by visual observers from around the world. The reports of the fireball 20160317_031654 (Event 1027–2016[2]), were sent by 62 observers from the United Kingdom, the Netherlands, Belgium and France (*Figure 1*). Many observers reported a terminal explosion, no fragmentation or sound effects during the flight were observed. The average relative brightness of the fireball from visual reports was between –15m and –20m, but many observers reported the fireball brighter than –20m.

3 Trajectory, radiant and orbit

Records taken from the stations Lockyer L1, Clanfield NW, and Scotch Street C1 were used to calculate the atmospheric path of the fireball 20160317_031654 and the meteoroid orbit in the Solar System.

---

[1] http://fireballs.imo.net/members/imo_view/browse_events
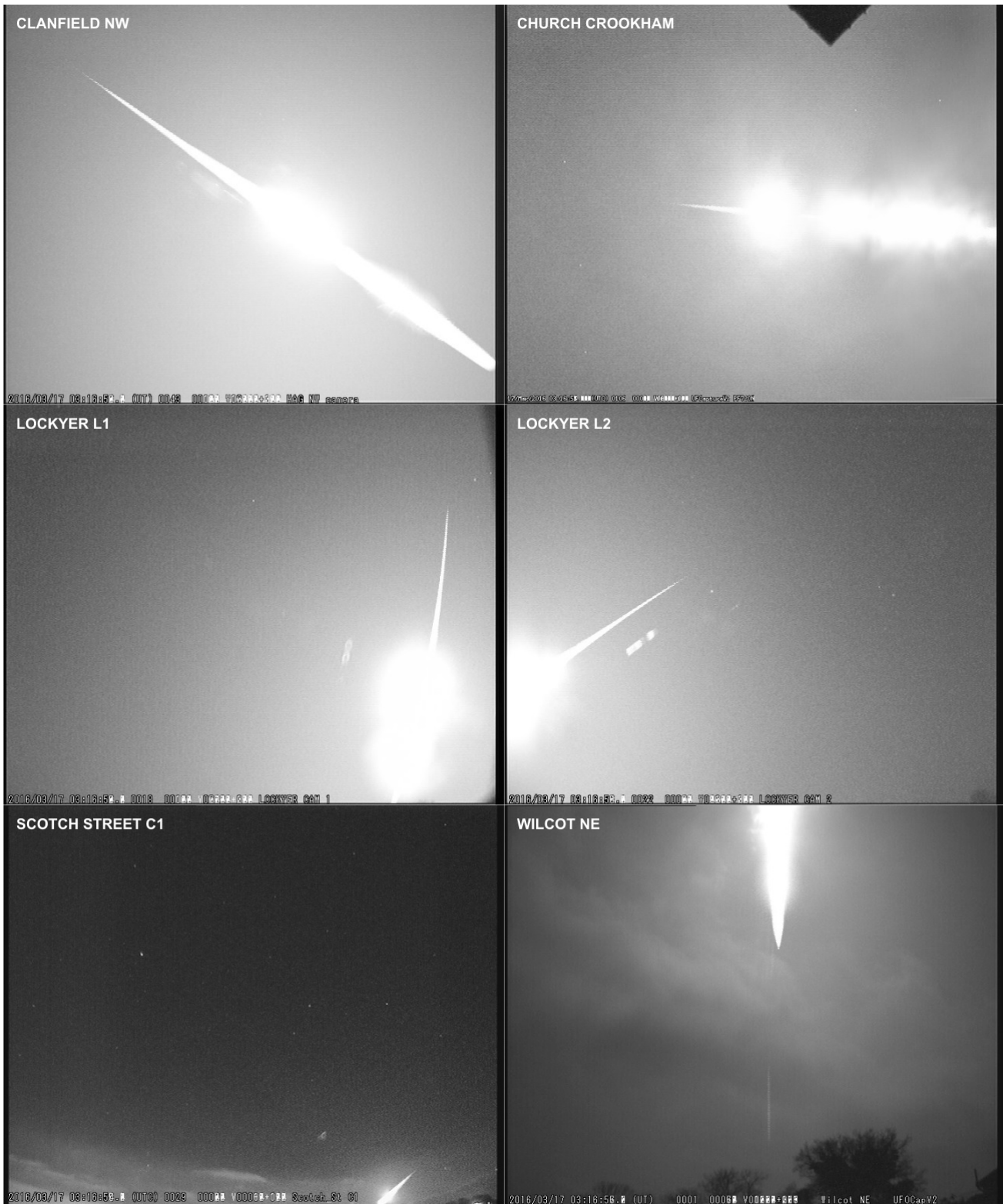[2] http://fireballs.imo.net/members/imo_view/event/2016/1027

Figure 2 – Summary images of the fireball 20160317_031654 from stations Clanfield NW (Hampshire Astronomy Group, Steve Bosley), Church Crookham (Peter Campbell-Burns), Lockyer L1, L2 (Norman Lockyer Observatory, Dave Jones), Scotch Street C1 (Steve Hooks) and Wilcot NE (Richard Fleet). The saturated parts of the sequence (saturated frames) have been omitted from the summary images. Author: UKMON.

The projection of the beginning of the atmospheric path was located at the coordinates N50.671666° W2.138888° near the city of Wareham (East Holme, Dorset County, UK), the height of the fireball at this time was 119.3 ± 0.1 kilometers above the Earth's surface. The end of the projection of the atmospheric path was located at the coordinates N51.810555° W1.504166° near the city of Witney (Crawley, Oxford County, UK), the height of the

fireball at this time was 35.2 ± 0.1 kilometers above the Earth's surface (*Figure 3*). The fireball reached an absolute brightness of -12.5 ± 0.4m.

It was a relatively fast meteor, the geocentric velocity of the meteoroid before entering the gravitational field of the Earth was 43.37 ± 0.03 km/s (including the deceleration effect), the orbital elements of the meteoroid orbit were as

follows: a = 2.933 ± 0.123 AU, q = 0.0489 ± 0.0002 AU, e = 0.983 ± 0.001, i = 18.14 ± 0.03°, ω = 336.61 ± 0.01°, Ω = 356.7476°. The fireball belonged to the meteor shower Northern March gamma Virginids (IAU MDC #749 NMV) with a geocentric radiant position at RA = 205.39 ± 0.11°, DEC = –6.42 ± 0.05° (*Figure 4*). The orbital heliocentric parameters of the fireball orbit are shown in *Table 1*, the geocentric orbit parameters are shown in *Table 2*.

Table 1 – Heliocentric orbital elements (J2000.0) of the fireball 20160317_031654, calculated using the software UFOOrbit (SonotaCo, 2009), the effect of deceleration is considered in the calculation.

Heliocentric orbital element		Fireball 20160317_031654
Semi-major axis	a	2.933 ± 0.123 AU
Eccentricity	e	0.983 ± 0.001
Perihelion distance	q	0.0489 ± 0.0002 AU
Aphelion distance	Q	5.866 ± 0.246 AU
Argument of perihelion	ω	336.61 ± 0.01°
Longitude of ascending node	Ω	356.7476°
Inclination	i	18.14 ± 0.03°
Orbital period	P	5.02 ± 0.32 y
Heliocentric velocity	v_s	38.48 ± 0.03 km/s
Tisserand´s parameter	TP_J	2.03 ± 0.04

Table 2 – Geocentric radiant, geocentric velocity, beginning and terminal height of the fireball 20160317_031654, calculated using the software UFOOrbit (SonotaCo, 2009), the effect of deceleration is considered in the calculation.

| Geocentric element		Fireball 20160317_031654
Geocentric velocity	v_g	43.37 ± 0.03 km/s
Initial velocity	v_i	44.73 ± 1.13 km/s
Radiant right ascension	RA	205.39 ± 0.11°
Radiant declination	DEC	-6.42 ± 0.05°
Beginning height of the atmospheric path	H_B	119.3 ± 0.1 km
Terminal height of the atmospheric path	H_E	35.2 ± 0.1 km
Absolute magnitude	a_{mag}	-12.5 ± 0.4^m
Initial dynamic mass	m_d	87.057 ± 15.287 kg
Terminal velocity	v_t	19.82 ± 0.84 km/s
Terminal dynamic mass	m_{dt}	0.139 ± 0.071 kg
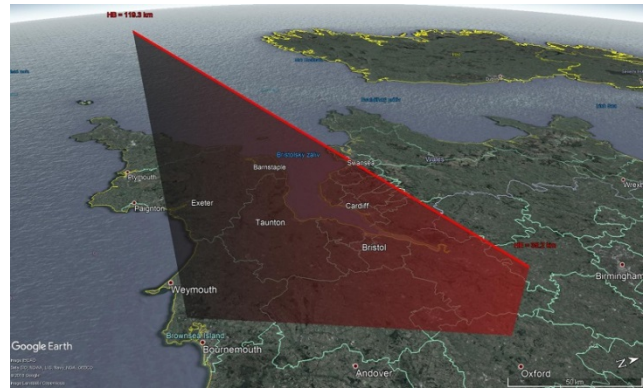
Figure 3 – 3D projection of the atmospheric path of the fireball 20160317_031654 on the Earth´s surface. Source of the map background: Google Earth, Google Inc.
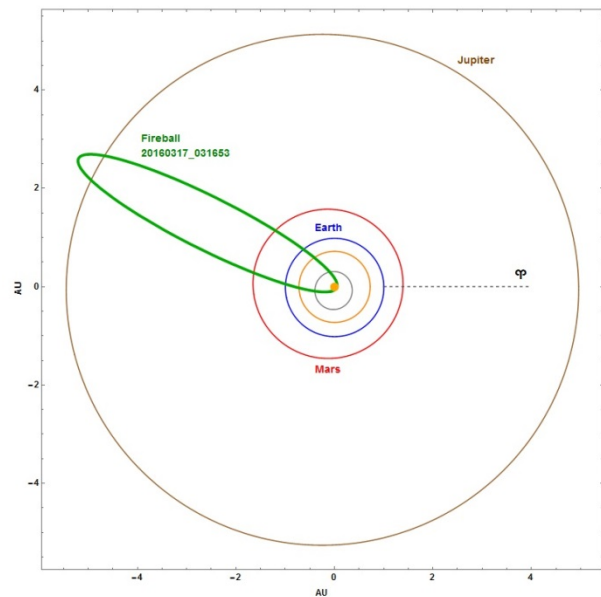

Figure 4 – Projection of the fireball 20160317_031654 orbit in the Solar System, including the effect of deceleration (polar coordinates system). Author: Jakub Koukal.

4   Physical properties of the fireball 20160317_031654

To estimate the initial weight of the body and its other physical properties, only the heliocentric orbital elements and the atmospheric path can be used in the case of fireball 20160317_031654. Because there is no spectrum available from the bolide flight, it is not possible to estimate its chemical composition. For the initial determination of the heliocentric orbit parameters, the Tisserand´s parameter in relation to the planet Jupiter was calculated (*Equation 1*).

$$TP_J = \frac{a_J}{a} + 2\sqrt{(1 - e^2)\frac{a}{a_J}}\cos i \qquad (1)$$

where a_J is the semi-major axis of the planet Jupiter, a the semi-major axis of the orbit, e the eccentricity of the orbit and i the inclination of the object.

Depending on the value of the Tisserand´s parameter, the inclination of the orbit and the distance of the aphelion, the bodies can be divided into 5 groups (Borovička et al., 2005). Fireball 20160317_031654 has the Tisserand´s

parameter $TP_J = 2.03 \pm 0.04$, but the inclination of the orbit $i = 18.14 \pm 0.03°$ and the perihelion distance $q = 0.0489 \pm 0.0002$ AU (*Table 1*). Therefore the fireball belongs to the group 1/SA (Sun-approaching orbits: $q < 0.2$ AU) according to this classification. The density of the bodies in this group varies within a wide range (Kikwaya et al., 2011), from 1000 kg/m³ to 4000 kg/m³. The K_B parameter (Ceplecha, 1958) was used to determine a more accurate body density estimate. The K_B parameter is a function of the material properties of the body and surface temperature (*Equation 2*) and changes of this parameter are closely related to the meteoroid composition.

$$K_B = \log \rho_B + 2.5 \log v_\infty - 0.5 \log(\cos Z_R) \qquad (2)$$

where ρ_B is the air density, v_∞ the approach velocity and Z_R the zenith distance of the radiant.

The value of the K_B parameter for the fireball is 6.617 ± 0.035. According to the classification criteria for groups of bodies (Ceplecha, 1988), this fireball belongs to the group C1 ($a < 5$ AU, $i < 35°$). However, the fireball is located on the boundary of groups C1 and D ($K_B < 6.60$), therefore the meteoroid density is considered $\rho_m = 800$ kg/m³ (Kikwaya et al., 2011).

To calculate the initial mass of the meteoroid, an equation (*Equation 3*) of the momentum transfer from the air molecules that collide with the meteoroid during the ablation phase (e.g. Ceplecha, 1966) is used.

$$\frac{dv}{dt} = \frac{\Gamma \rho_a v^2}{m_d} A \left(\frac{m_d}{\rho_m}\right)^{2/3} \qquad (3)$$

where m_d is the dynamic mass of the meteor, Γ the drag coefficient, A the shape factor, ρ_m the meteor density, v the meteor velocity, ρ_a the atmospheric density.
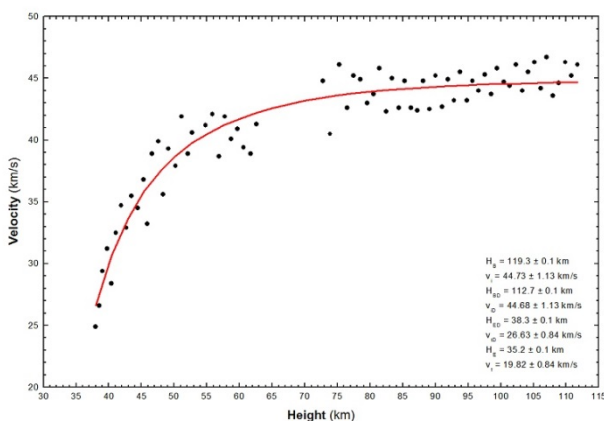

Figure 5 – Deceleration course of the fireball 20160317_031654 from Clanfield NW station. Author: Jakub Koukal.

The calculation of the meteoroid deceleration was performed using data from Clanfield NW station (*Figure 5*). The shape factor $A = 1.209$ is considered for the spherical body and the drag coefficient is considered

$\Gamma = 1.0$ (Ceplecha, 1966). The resulting initial dynamic mass of the fireball is for the given body density $m_d = 87.057 \pm 15.287$ kg (*Table 2*).

Calculation of the photometric initial mass m_{ph} was not performed because the calculation procedure (Ceplecha, 1966) is not suitable for use without further modifications. The resulting photometric initial mass values vary in many cases up to several orders from real values, or from the dynamic initial mass (Gritsevich, 2008).

To calculate the body mass loss during the ablation phase, it is assumed that the drag coefficient Γ and the coefficient of the heat transfer Λ are constant. Under these circumstances, it is possible to simplify the calculation (*Equation 4*) of the body mass loss during the ablation phase. However, this procedure is not suitable for bodies that penetrate into low heights (Ceplecha, 1961). This procedure calculates the terminal dynamic mass of the fireball $m_{dt} = 0.139 \pm 0.071$ kg (*Table 2*).

$$\frac{m}{m_d} = e^{-\frac{\sigma}{2}(v_\infty^2 - v^2)} \qquad (4)$$

where m is the actual mass of the meteor, m_d the initial dynamic mass of the meteor, v_∞ the initial velocity, v the actual velocity and σ the ablation coefficient.

The calculation of the mechanical strength of the meteoroid is based on the equality of the dynamic pressure and the mechanical strength of the body (*Equation 5*) at the time of the meteoroid fragmentation. The density of the atmosphere at a given fragmentation height is calculated according to the U.S. Standard Atmosphere 1976 model (NOAA, NASA and USAF, 1976), including values at altitudes above 86 km (NASA 1976).

$$P = \rho_a v^2 \qquad (5)$$

where ρ_a is the atmospheric density and v the actual velocity.

The moments of meteoroid fragmentation were determined from the course of the absolute brightness values of the fireball 20160317_031654 from the Clanfield NW station (*Figure 6*). The mechanical strength values of the meteoroid at individual moments of body fragmentation are shown in *Table 3*.

Table 3 – Mechanical strength of the meteoroid at individual moments of fragmentation. The mechanical strength of the fireball is determined by fragmentation at point B.

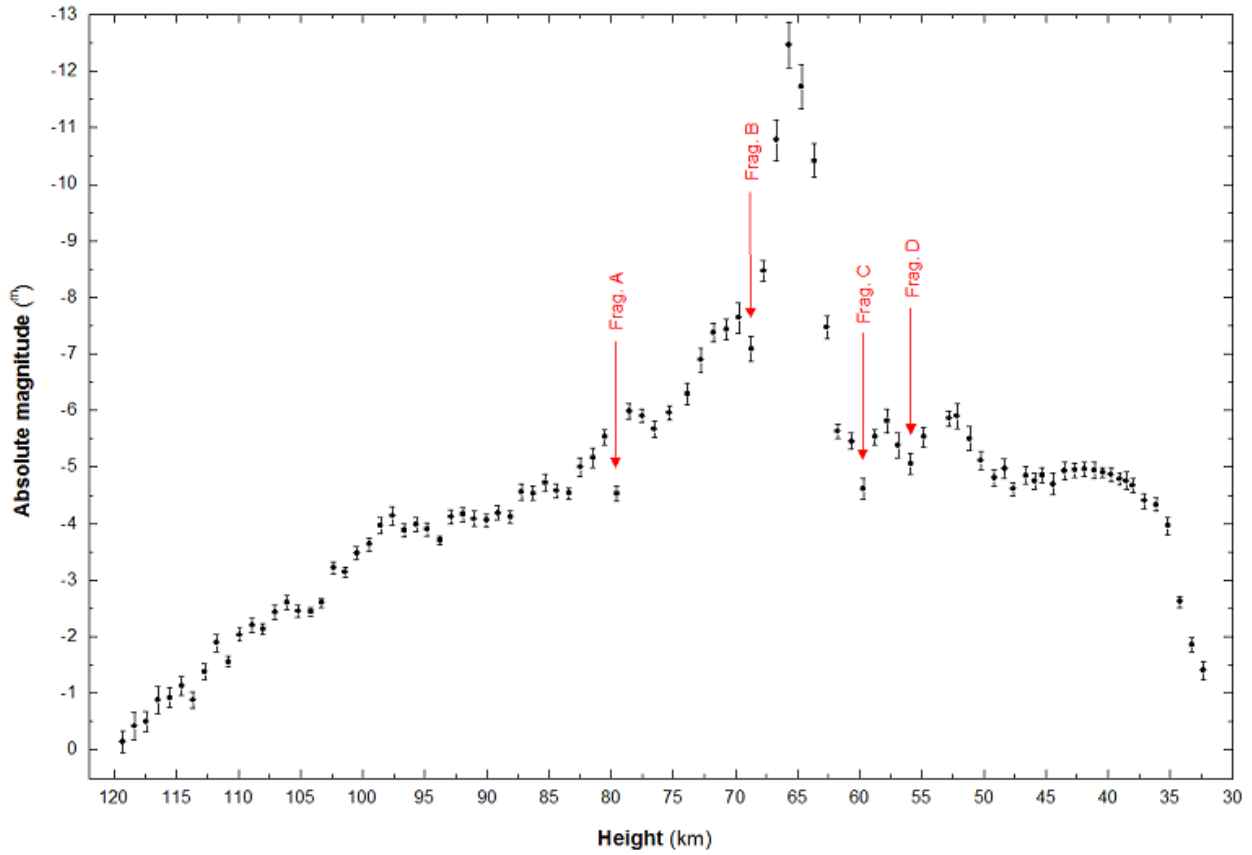| Fragmentation	H km	ρ_a kg/m³	v km/s	σ_d MPa	$\Delta\sigma_d$ MPa
A	79.6	1.6878E-05	43.90	0.033	0.004
B	68.7	8.9339E-05	43.04	0.165	0.018
C	59.7	2.9972E-04	41.67	0.520	0.056
D	55.9	4.8335E-04	40.75	0.803	0.090

Figure 6 – Absolute brightness curve of the fireball 20160317_031654 from the station Clanfield NW. The moments of fragmentation of the meteoroid are marked with symbols A–D. Author: Jakub Koukal.
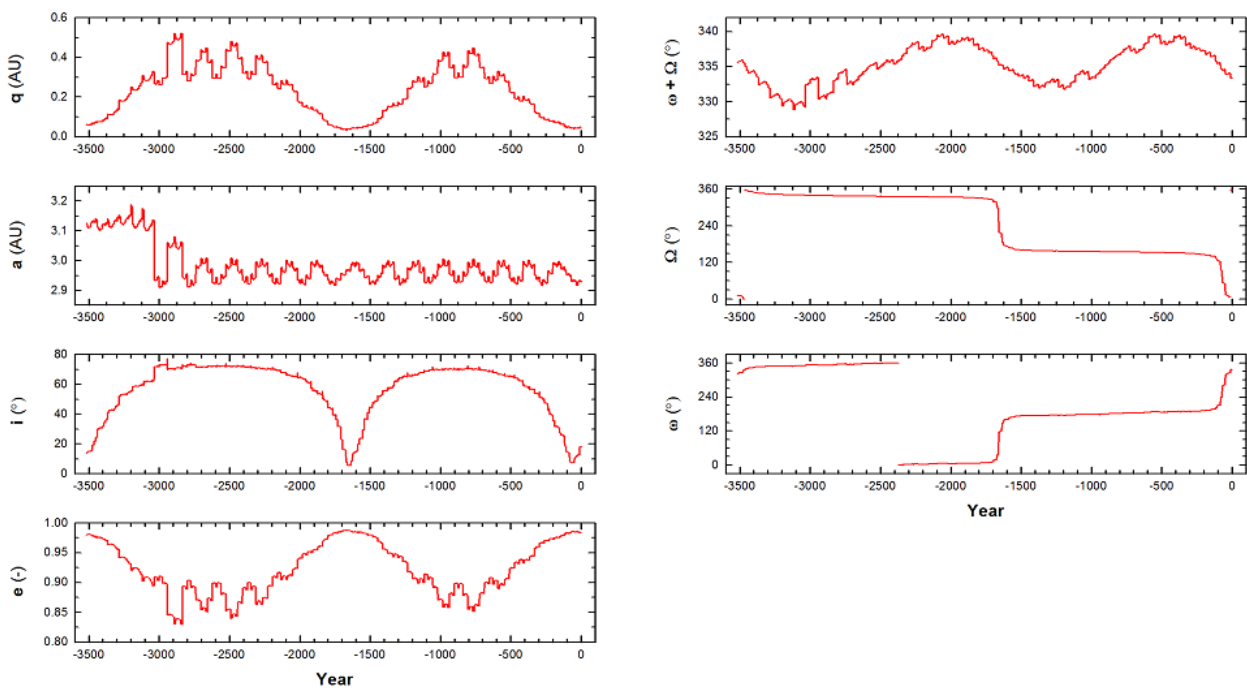

Figure 7 – Reverse numerical integration of the orbital elements of the fireball 20160317_031654 orbit. Column to the left (from the top): perihelion distance (q), semi-major axis (a), inclination (i) and eccentricity (e). Column to the right (from the top): sum of ascending node and argument of perihelion (peri + node), length of ascending node (node) and argument of perihelion (peri). Author: Jakub Koukal.

5   Origin of the fireball 20160317_031654

In order to look for the potential parent bodies of the fireball 20160317_031654, a reverse integration of the heliocentric orbit was performed. In addition, a reverse integration of the heliocentric orbits of the fireball clones was also performed. The reverse integration of the fireball orbit was performed using numerical-integration software SOLEX (Vitagliano, 1997). This software is based on a 18th-order polynomial extrapolation method of the Bulirsh-Stoer type, the method of calculation is entirely based on the numerical integration of the Newton equation of motion. Due to the geometry of the fireball orbit, there are frequent approaches to the Solar System bodies and thus significant changes in orbital elements (*Figures 7 and 8*). The periodicity in the changes of the orbital elements (q, e, i) is approximately 1600 y.

In addition, the reverse integration of the heliocentric orbits of the individual meteoroid clones along the fireball orbit was performed (*Figure 9*). $\Delta M = 15°$ (mean anomaly) was determined as a step for clone formation. A total of 24 clones were created spread across the entire circumference of the fireball orbit. Only 6 clones of the meteoroid have a stable orbit within the considered time interval (3500 y), including the meteoroid itself. The results of the reverse integration of the clone orbits indicate a probable age for the fireball 20160317_031654 of maximum 3700 ± 100 y. However, no potential parent body was not found for the fireball 20160317_031654 in the comets (periodic, non-periodic and lost) and asteroids database.
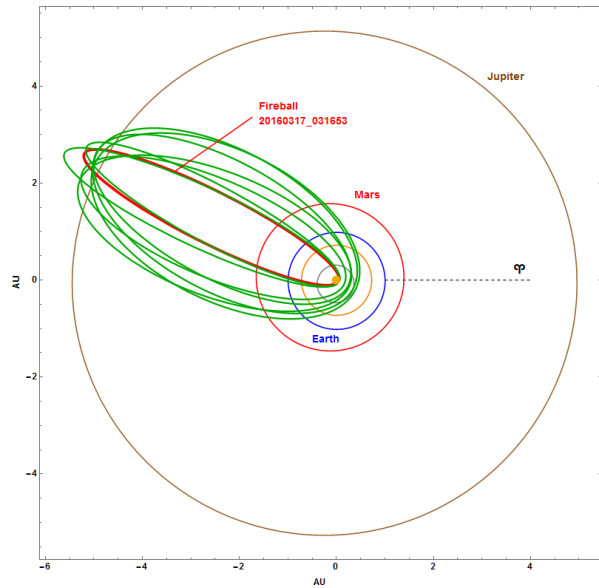

Figure 8 – Projection of the meteoroid orbits (reverse integration) in the Solar System with an interval of 500 years (polar coordinates system). Author: Jakub Koukal.
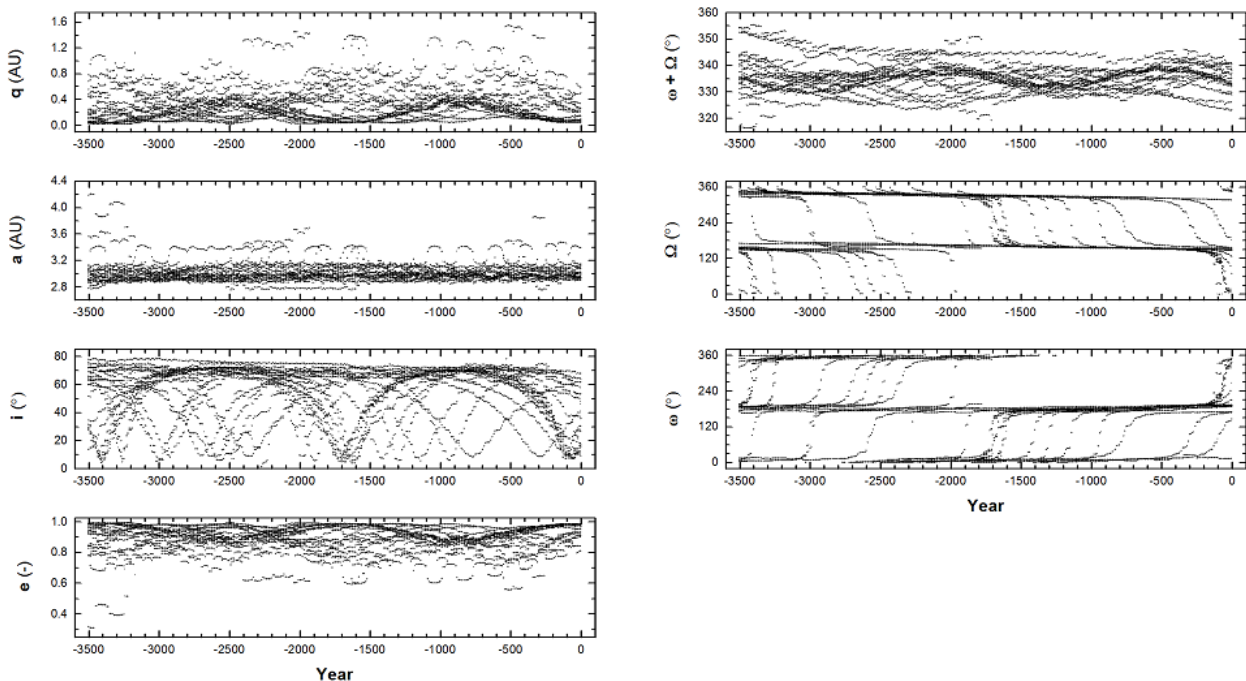

Figure 9 – Reverse numerical integration of the orbital elements of the meteoroid clones within the orbit of the meteoroid. Column to the left (from the top): perihelion distance (q), semi-major axis (a), inclination (i) and eccentricity (e). Column to the right (from the top): sum of ascending node and argument of perihelion (peri + node), length of ascending node (node) and argument of perihelion (peri). Author: Jakub Koukal.

Acknowledgment

References

Borovička J., Koten P., Spurný P., Boček J., Štork R. (2005). "A survey of meteor spectra and orbits: evidence for three populations of Na-free meteoroids". *Icarus*, **174**, 15–30.

Ceplecha Z. (1958). "On the composition of meteors". *Bulletin of the Astronomical Institute of Czechoslovakia*, **9**, 154–159.

Ceplecha Z. (1961). "Multiple fall of Přibram meteorites photographed". *Bulletin of the Astronomical Institute of Czechoslovakia*, **12**, 21–47.

Ceplecha Z. (1966). "Dynamic and photometric mass of meteors". *Bulletin of the Astronomical Institute of Czechoslovakia*, **17**, 347–354.

Ceplecha Z. (1988). "Earth's influx of different populations of sporadic meteoroids from photographic and television data". *Bulletin of the Astronomical Institute of Czechoslovakia*, **39**, 221–236.

Gritsevich M. I. (2008). "Validity of the photometric formula for estimating the mass of a fireball projectile". *Doklady Physics*, **53**, 97–102.

Jenniskens P., Nénon Q., Gural P. S., Albers J., Haberman B., Johnson B., Morales R., Grigsby B. J., Samuels D., Johannink C. (2016). "CAMS newly detected meteor showers and the sporadic background". *Icarus*, **266**, 384–409.

Jenniskens P., Baggaley J., Crumpton I., Aldous P., Pokorny P., Janches D., Gural P.S., Samuels D., Albers J., Howell A., Johannink C., Breukers M., Odeh M., Moskovitz N., Collison J., and Ganjuag

S. (2018). "A survey of southern hemisphere meteor showers". *Planetary Space Science*, **154**, 21–29.

Jopek T. J., Kanuchova Z. (2014). "Current status of the IAU MDC Meteor Shower Database". In Jopek T. J., Rietmeijer F. J. M., Watanabe J., Williams I. P., editors. *Proceedings of the Meteoroids 2013 Conference*, Aug. 26-30, 2013, A.M. University, Poznań, Poland, pages 353–364.

Kikwaya J. B., Campbell-Brown M., Brown P. G. (2011). "Bulk density of small meteoroids". *Astronomy & Astrophysics*, **530**, A113, 17p.

Kornoš L., Koukal J., Piffl R., and Tóth J. (2014a). "EDMOND Meteor Database". In Gyssens M. and Roggemans P., editors, *Proceedings of the International Meteor Conference*, Poznań, Poland, Aug. 22-25, 2013. International Meteor Organization, pages 23–25.

Kornoš L., Matlovič P., Rudawska R., Tóth J., Hajduková M. Jr., Koukal J., Piffl R. (2014b). "Confirmation and characterization of IAU temporary meteor showers in EDMOND database". In Jopek T. J., Rietmeijer F. J. M., Watanabe J., Williams I. P., editors. *Proceedings of the Meteoroids 2013 Conference*, Aug. 26-30, 2013, A.M. University, Poznań, Poland, pages 225–233.

NASA (1976). "The 1976 Standard Atmosphere Above 86-km Altitude". Edited by R. A. Minzner, Goddard Space Flight Center, NASA SP-398, October 1976.

NOAA, NASA and USAF (1976). "U. S. Standard Atmosphere. NOAA-S/T 76-1562", Washington, D.C., October 1976.

SonotaCo (2009). "A meteor shower catalog based on video observations in 2007-2008". *WGN, Journal of the International Meteor Organization*, **37**, 55–62.

Vitagliano A (1997). "Numerical Integration for the Real Time Production of Fundamental Ephemerides over a Wide Time Span". *Celestial Mechanics and Dynamical Astronomy*, **66**, 293–308.

The 2018 February 24 fireball results

Paul Roggemans[1], Carl Johannink[2] and Jean-Marie Biets[3]

[1] **Pijnboomstraat 25, 2800 Mechelen, Belgium**
paul.roggemans@gmail.com

[2] **Dutch Meteor Society, the Netherlands**
c.johannink@t-online.de

[3] **Dutch Meteor Society, the Netherlands**
jean-mariebiets@telenet.be

A spectacular fireball has been recorded by different cameras of the CAMS BeNeLux network as well as by EN all-sky cameras. Both systems allowed trajectory and orbit calculations and the results from both analyses are compared in this paper. The fireball could not be associated with any known meteor shower. An attempt was made to check if any concentration of orbits occurred at the position of the fireball orbit but no trace of any unknown meteor shower could be detected. The fireball was caused by a sporadic meteoroid.

1   Introduction

A very bright fireball had been registered on February 24 at $0^h11^m33^s$ UT by many cameras of the BeNeLux CAMS network, several EN all-sky cameras (*Figure 1*) as well as FRIPON network cameras. A description of the event with a photo gallery of this spectacular fireball has been published in eMeteorNews (Roggemans, 2018). Meanwhile the trajectory and orbit of this fireball have been calculated based on the CAMS data and independently using the all-sky data. The results from both analyses are compared in this article.

Figure 1 – The fireball captured on the All-sky camera by Jos Nijland at Benningbroek (EN95), the Netherlands.

2   Fireball trajectory

Pavel Spurný used the all-sky images obtained by *Koen Miskotte*, *Jos Nijland* and *Jean-Marie Biets*. The all-sky camera EN95 (Jos) uses a mechanic shutter while the all-sky cameras EN92 (Jean-Marie) and EN98 (Koen) are equipped with a Liquid Cristal Shutter (LCS).

The images of Jos and Koen got the fireball trail saturated due to the brightness of the event and the shortness of the trail due to the large distance between the fireball and their geographic position. The image obtained by *Jean-Marie Biets* also failed to provide sector breaks due to a technical problem with the LCS during that night. Only the image obtained by Jos barely displays breaks which could be used for the velocity computation.
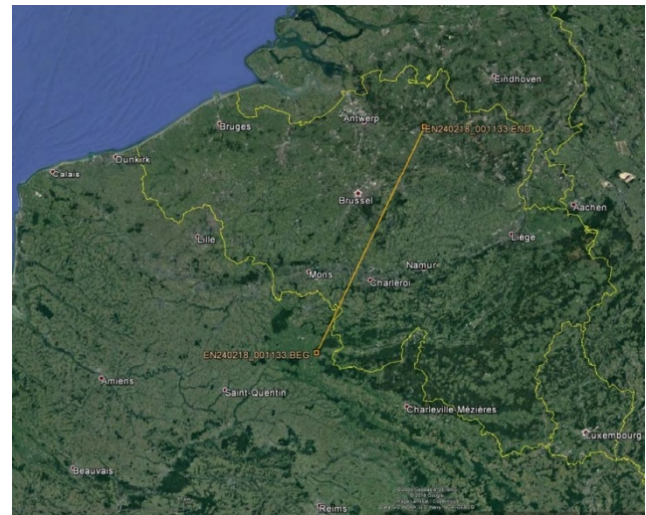

Figure 2 – Ground projection of the fireball trajectory calculated by Pavel Spurný.

Pavel excluded all possibility for any meteorite dropping with an ending height above 30 km. Indeed not every bright fireball results in a meteorite dropping. *Pavel Spurný* also provided the orbital elements together with a map of the atmospheric trajectory (*Figure 2*). Based on the all-sky data the fireball had an initial velocity $v_\infty = 20.9 \pm 0.9$ km/s, an entrance angle of 34.1 ± 0.8 ° and a total length of 157.3 km.
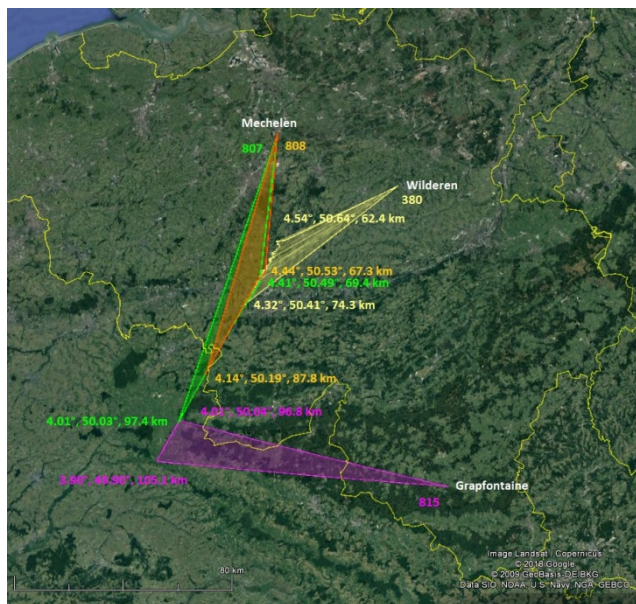
Figure 3 – The ground projection of the fireball based on the images of CAMS 807 and 808 at Mechelen (Luc Gobin), CAMS 380 at Wilderen (Jean-Marie Biets) and CAMS 815 at Grapfontaine (Jean-Paul Dumoulin).
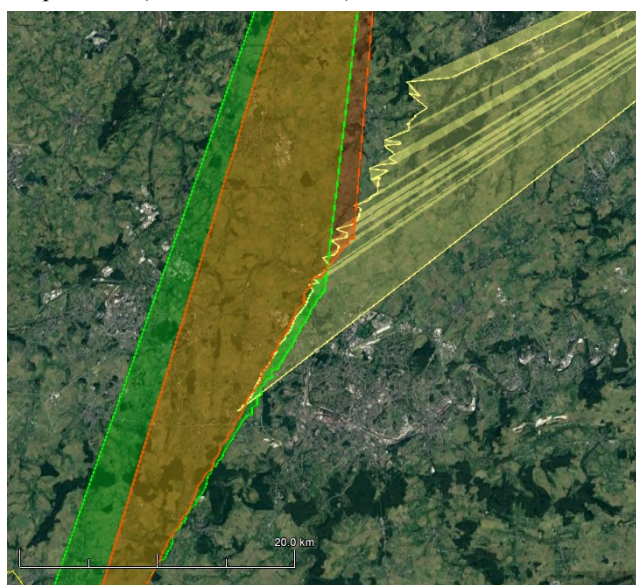

Figure 4 – Close-up of the projection of the individual measured points of the CAMS data where the brightness saturated the CAMS image, causing considerable scatter on the trajectory determination.

These data can be compared with the results that were independently obtained from the CAMS data. CAMS 815 detected the fireball a bit higher before the all-sky got it. The trajectory is about identical in position but the overexposure on the CAMS cameras results in a visible scatter of the individual measuring points for CAMS 807 and 808. This scatter becomes very large on the positions of CAMS 380 where the fireball was between 75 and 60 km elevation (*Figures 3 and 4*).

3 Fireball orbit

It is indeed interesting to compare the orbital elements between the all-sky and CAMS. The CAMS project collects data for meteors in the magnitude range of –3 to +5 while everything in the magnitude range brighter

than –4 fits typically the all-sky camera project. The results for both are listed in *Table 1*.

Table 1 – The radiant and orbital data as obtained from CAMS data (Carl Johannink) and obtained from All-sky data (Pavel Spurný).

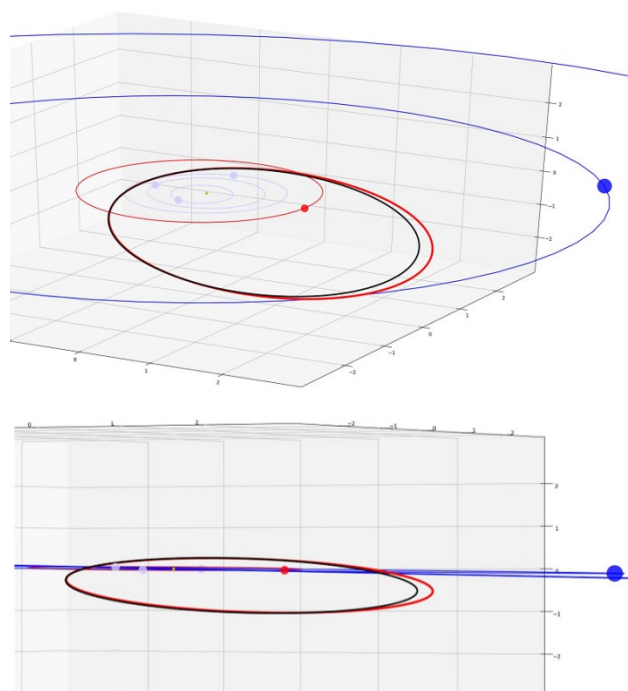|	CAMS	All-sky
λ_O (°)	335.085	
α (°)	133.03 ± 0.02	137.0 ± 0.3
δ (°)	−16.68 ± 0.07	−12.2 ± 0.3
v_g (km/s)	17.6	
a (A.U.)	2.39	2.3
e	0.658	0.65
q (A.U.)	0.816	0.81
i (°)	15.83	16.5
ω (°)	56.10	57.9
Ω (°)	155.08	155.09

Figure 5 – The orbits obtained for this fireball, red for CAMS, black for the All-Sky. Top: a 3D view with the inner planets, planet Mars shown in red and Jupiter in blue. Bottom: the orbits as seen from a position in the ecliptic plane. Note the aphelion is situated in the asteroid belt. These plots were provided by Peter Campbell-Burns.

The orbit is situated near the ecliptic with an aphelion in the asteroid belt, well within the orbit of Jupiter in a region very rich in dust (*Figure 5*).

4 Shower or sporadic fireball?

The orbit of the fireball has been compared to the 1776 reference orbits of the showers of the IAU working list of meteor showers. This list contains 1031 meteor shower numbers, 64 of which were removed leaving 967 showers, most of which remain to be confirmed. The orbit of the

fireball did not match with any of the 1776 reference orbits, not even with the weak discrimination threshold of $D_{SH} < 0.25$, $D_D < 0.105$ and $D_H < 0.25$.

An attempt was made to find out if this fireball could be part of some so far unknown meteor shower. We therefore used 483449 orbits from EDMOND (Kornos et al., 2014), and SonotaCo (SonotaCo, 2009). We selected all orbits that radiated from the same area at the sky with a comparable velocity in the same month of time ($\alpha \pm 10°$, $\delta \pm 10°$, $\lambda_O \pm 15°$, $v_g \pm 5$ km/s).

With 83 orbits found within these criteria with at a glimpse several similar orbits there might be some concentration of orbits. We took the fireball orbit as parent orbit and compared all 83 orbits applying the discrimination criteria of Southworth and Hawkins (1963), Drummond (1981) and Jopek (1993). The results confirmed the presence of several comparable orbits, considering the different thresholds, weak, medium weak, medium high and high:

- $D_{SH} < 0.25$ & $D_D < 0.105$ & $D_H < 0.25$, 65 orbits;
- $D_{SH} < 0.2$ & $D_D < 0.08$ & $D_H < 0.2$, 51 orbits;
- $D_{SH} < 0.15$ & $D_D < 0.06$ & $D_H < 0.15$, 30 orbits;
- $D_{SH} < 0.1$ & $D_D < 0.04$ & $D_H < 0.1$, 4 orbits.

Although the D-criteria indicate the presence of a significant number of comparable orbits, the final test with the inclination i versus length of perihelion Π (*Figure 6*), shows no concentration at all!
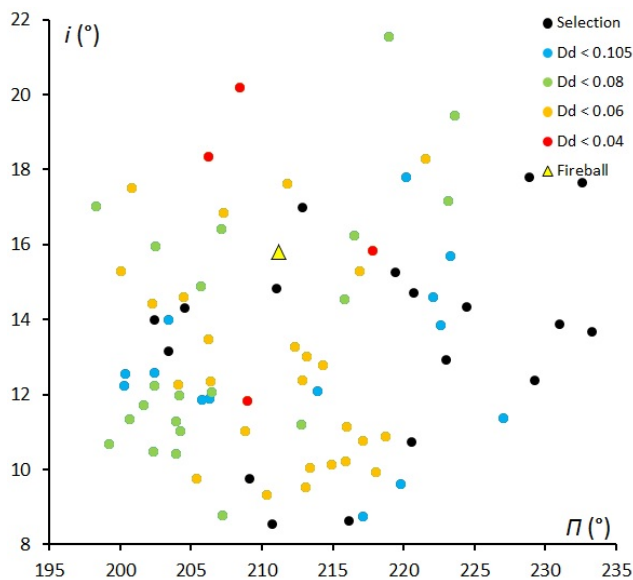

Figure 6 – The inclination i versus length of perihelion Π. The colors indicate the different degrees of similarity according to the D-criteria.

When we ignore the fireball and calculate the median values for the 83 selected orbits and take these as parent orbit to apply the D-criteria we get an even better score on our similarity criteria:

- $D_{SH} < 0.25$ & $D_D < 0.105$ & $D_H < 0.25$, 67 orbits;
- $D_{SH} < 0.2$ & $D_D < 0.08$ & $D_H < 0.2$, 53 orbits;
- $D_{SH} < 0.15$ & $D_D < 0.06$ & $D_H < 0.15$, 36 orbits;
- $D_{SH} < 0.1$ & $D_D < 0.04$ & $D_H < 0.1$, 13 orbits.

Also here the plot of the inclination i versus length of perihelion Π, shows a random mixture of orbits with low and high threshold D-criteria without any indication for some concentration of orbits. With other words, all these orbits are no more than similar sporadic orbits, all with a short periodicity close to the ecliptic plane. If some of these orbits are effectively physically related, it is most difficult, if not impossible to determine such relationship unless the orbital evolution can be reconstructed to find a similar origin, if any. We can conclude that the fireball was caused by a sporadic meteoroid.

Acknowledgment

References

Drummond J. D. (1981). "A test of comet and meteor shower associations". *Icarus*, **45**, 545–553.

Jopek T. J. (1993). "Remarks on the meteor orbital similarity D-criterion". *Icarus*, **106**, 603–607.

Kornoš L., Matlovič P., Rudawska R., Tóth J., Hajduková M. Jr., Koukal J., and Piffl R. (2014). "Confirmation and characterization of IAU temporary meteor showers in EDMOND database". In Jopek T. J., Rietmeijer F. J. M., Watanabe J., Williams I. P., editors, *Proceedings of the Meteoroids 2013 Conference*, Poznań, Poland, Aug. 26-30, 2013. A.M. University, pages 225–233.

Roggemans P. (2018). "Fireball over Belgium 2018 February 24, 0h11m UT". *eMetN*, **3**, 81–83.

SonotaCo (2009). "A meteor shower catalog based on video observations in 2007-2008". *WGN, Journal of the International Meteor Organization*, **37**, 55–62.

Southworth R. R. and Hawkins G. S. (1963). "Statistics of meteor streams". *Smithson. Contrib. Astrophys.*, **7**, 261–286.

Re-entry of the Soyuz MS-08 carrier rocket
25 March 2018

Enrico Stomeo

Venice Planetarium and Italian Meteor Group
via Umbria 21/d, 30037 Scorze' (VE), Italy
stom@iol.it

The re-entry of the Soyuz MS-08 carrier rocket on 2018 March 25 could be observed from a large part of the central Mediterranean Sea. The radio station of the Planetarium in Venice was able to record the return into the atmosphere. The radio signal was perceived in Venice from 01h23m52,5s UTC with a frequency of 1431,363 Hz until 01h24m02,0s with a frequency of 805,487 Hz. Considering the recorded frequency variations due to the Doppler effect, it can be deduced that the object was drastically decelerating in those last moments by about 1.3 km/s.

1   Introduction

On March 25th at 01[h]24[m] UTC the radio station located in the Planetarium in Venice was able to record the return to the atmosphere of a stage (2018-026B) of the rocket carrier which left from Kazakhstan four days earlier to bring the spacecraft Soyuz MS-08 into orbit, with some astronauts on board towards the International Space Station (ISS).

The forecasts of the reentry of the space debris were given by the Joint Space Operations Center (JSpOC) for 01[h]36[m] UTC ± 1[m] (03[h]25[m] Italian time) near our country, in the Ligurian Sea just west of Corsica at about 41.9°N latitude and 8.1°E longitude.

During the reentry, the large metal object, impacting with the atmosphere, strongly ionized the atmospheric layers at high altitude, producing a remarkable show for all the witnesses of the surrounding regions. It appears that the event was followed by almost all coastal areas of the central Mediterranean. In Italy it was observed obviously well from Sardinia, but also from all the Tyrrhenian lands up to the southern latitudes (e.g. Lazio, Campania, Calabria and Sicily). Many movies and photographic pictures immortalized the transit of the spatial debris. Online[3] is one of the most significant videos taken by Vallo di Diano in Campania.

2   The trajectory

The map shows the ground projection of the atmospheric path from north-west to south-east of the debris resulting from the forecasts based on the last calculated orbital elements. The estimated point of reentry is also indicated west of Corsica (*Figure 1*).

The radio station located in the Planetarium of Venice is oriented in the direction of the Graves radar (central France) in order to receive radio pulses transmitted by the radar in case of meteoritic events. In the case of a meteor, but also of any other moving object, the radio signal is reflected back to the ground from the atmospheric zones as long as these remain ionized, and consequently the transmitted pulses can be received without difficulty.

Despite the considerable distance between Venice and the area of the return (over 550 km), the radio echoes were recorded sequentially by the receiver of the Planetarium's radio station (a Yaesu FT-713), and from these an audio signal was instantly generated through a demodulator (USB) with a frequency more or less shifted by the Doppler effect. The audio of the object recorded during the reentry can be heard clicking here[4].

The spatial relict, now below 90 km in height, flying over the Ligurian Sea at a speed of probably around 8 km/s, began to melt and dissolve because of the high temperature and friction.

Figure 1 – The ground projection of the predicted atmospheric path in the re-entry area.

[3] http://www.ondanews.it/strana-scia-luminosa-avvistata-nel-cielo-del-vallo-diano-si-pensa-alla-stazione-cinese-tingong-1/

[4] http://www.astrovenezia.net/radio_meteore/2018/20180325_0124_soyuz_reentry_aav.mp4

3   The spectogram of the event

The second image shows the spectrogram of the event as a function of time (Greenwich Time) and radio frequency, as generated by the analysis software of Spectrum_Lab (*Figure 2*). The intensity of the reflection is shown by false colors, from blue (low intensity) to red-yellow (high intensity).

The window in which the radio signal was perceived in Venice goes from $01^h23^m52,5^s$ UTC with a frequency of 1431,363 Hz until $01^h24^m02,0^s$ with a frequency of 805,487 Hz, according to the recorded reception. A few moments before $01^h24^m00^s$ the object began to move away from the receiving station. Considering the recorded frequency variations due to the Doppler effect, it can be deduced that the object was drastically decelerating in those last moments by about 1.3 km/s.

It can be assumed that it continued its journey beyond the point provided by the JSpOC to the west of Corsica, and that, if any metallic debris survived the fall, it occurred in the Tyrrhenian Sea, if not beyond. The many visual testimonies from Tuscany may prove this, describing that the object was splitting up into several trails, similar to meteors, of different persistence.
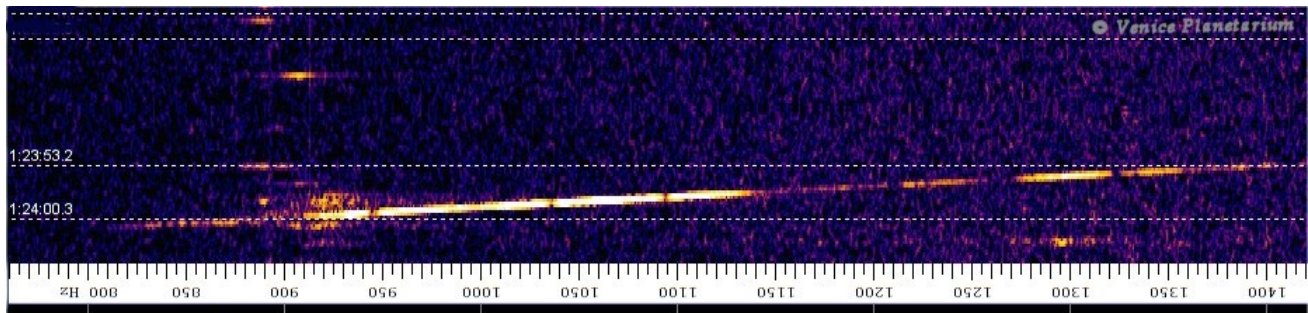

Figure 2 – Spectrogram of the event according to time and radio frequency.

2017 Report BOAM
French meteor observation database

Tioga Gulon

6, rue Rodin, F-54710 Fléville-devant-Nancy, France
france.allsky.camera@free.fr

An overview of the 2017 activity report of the French network BOAM (Base d'Observation Amateur des Météores) is presented.

1   Introduction

In 2010 a group of French amateurs with cameras for meteor observations (*Figure 1*) decided to organize themselves as a network and to combine their detections in a database by creating BOAM (Base d'Observation Amateur des Météores[5]).
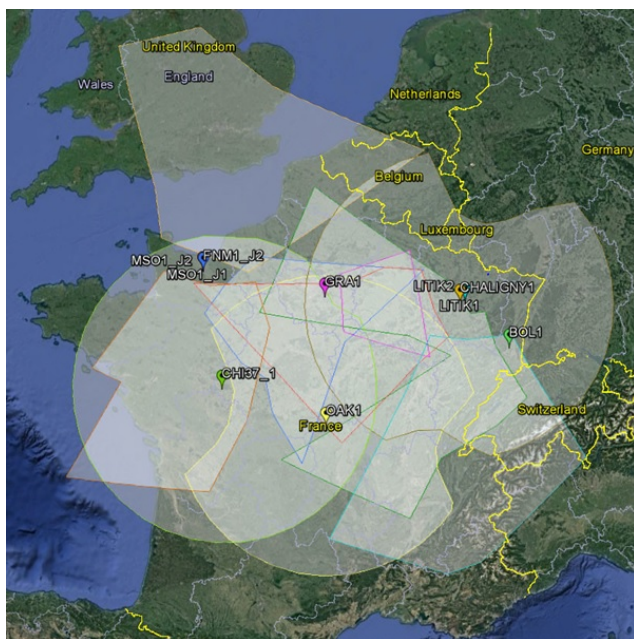

Figure 1 – Field of view at 100 km of altitude.

2   Overview of the 2017 statistics

The network is currently composed of a dozen of cameras running with UFOsuite softwares. After 8 years of operating, the database contains almost 75000 meteors.

2017 was quite disappointing for the network. Only 7763 meteors have been recorded, that is a decrease of 40% compared to 2016 (*Figure 2 and 3*). This is partly due to the fact that the most productive camera of our network was not operating during this year. However, we also noticed a decrease in detections for all cameras, 32% less. May be this was due to more cloud cover in 2017? In any case, bad weather was present around the time of the

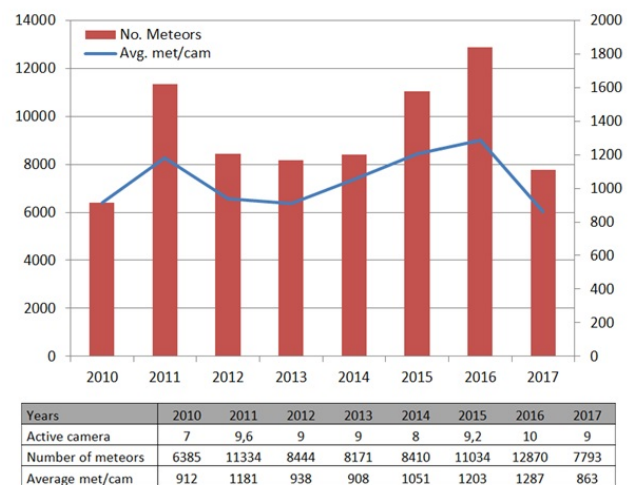maximum of the Perseids, we recorded 2422 Perseids less than in 2016.

Years	2010	2011	2012	2013	2014	2015	2016	2017
Active camera	7	9,6	9	9	8	9,2	10	9
Number of meteors	6385	11334	8444	8171	8410	11034	12870	7793
Average met/cam	912	1181	938	908	1051	1203	1287	863

Figure 2 – Comparing 2017 with previous years.

Figure 3 – 2017 the number of detections per camera.

Thanks to direct sharing data with our close friends of the video observing networks, UKMON[6] in United-Kingdom and FMA[7] in Switzerland, both using the same software, we could calculate 1849 meteor orbits and trajectories (*Figures 4 and 5*). All were detected by several cameras and at least one BOAM camera.

Acknowledgment

---

[5] http://boam.fr/?lang=en

[6] https://ukmeteornetwork.co.uk/
[7] http://www.meteorastronomie.ch/

Figure 4 – 1849 meteor trajectories on the ground map. UFOorbit software settings : Q₁, dt < 10.0s, GD > 10km, dD < 0.5° (Q_1 : preset quality conditions dt : maximum time difference between 2 stations, GD : minimum ground distance between 2 stations, dD : maximum angle difference of radiant and ground pole).

Figure 5 – 1849 meteor radiants on a sinusoidal projection sky map (Hammer projection). Vertical : declination, Horizontal : right ascension, v_g : geocentric velocity.

2017 Report BOAM
January to May 2017

Tioga Gulon

6, rue Rodin, F-54710 Fléville-devant-Nancy, France
france.allsky.camera@free.fr

A summary of the major shower events and an overview of the peculiar meteor events recorded by the French network BOAM during the period of January until May 2017 are presented.
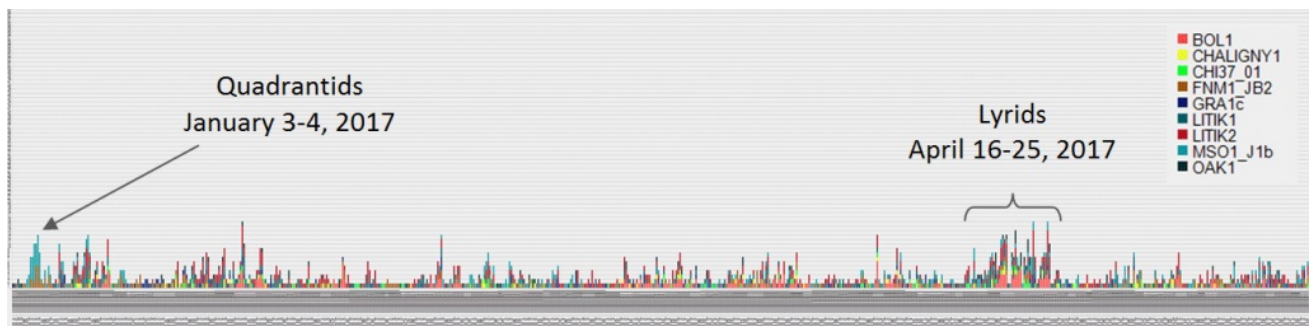
Figure 1 – Overview of the number of captures for the period January to May 2017 – GraphBoam.

1 Introduction

The first half of the year is known to be rather weak for meteor activity but we were able to enjoy the first major shower of the year, the Quadrantids and the well-known Lyrids, it is also a period where we could observe bright fireballs.

2 December 28 – January 12: Quadrantids

The Quadrantids activity is very low over the period except few hours before and after the peak which occurred January 3rd to 4th. The Zenithal Hourly Rate (ZHR) increases up to 120 meteors per hour and the shower becomes the first of the three major showers of the year.

Table 1 – The Quadrantid meteor stream characteristics.

Period of activity	December 28 – January 12
Maximum	January 3–4
Radiant position (max)	$\alpha = 230°$ and $\delta = +49°$
Zenithal Hourly Rate (max)	120 meteors per hour
Velocity	41 km/s
Population index r	2.1
Parent body	2003 EH1, 96P/Machholz

Their origin is complex. Peter Jenniskens found evidence that Quadrantid meteoroids are associated with the asteroid 2003 EH1, discovered on March 6th 2003 by B. A. Skiff (Lowell Observatory-LONEOS). The radiant of this extinct comet which became an asteroid matches with the Quadrantid meteoroid stream. Quadrantids are also related to comet 96P / Machholz.

In 2017, the maximum activity of the Quadrantids was forecasted on January 03th around 14h UTC and was not favorable for European observers. The radiant was at a low elevation in the first part of the night rising at the sky in the morning, the best observing conditions for France were on January 3rd at the end of the night.
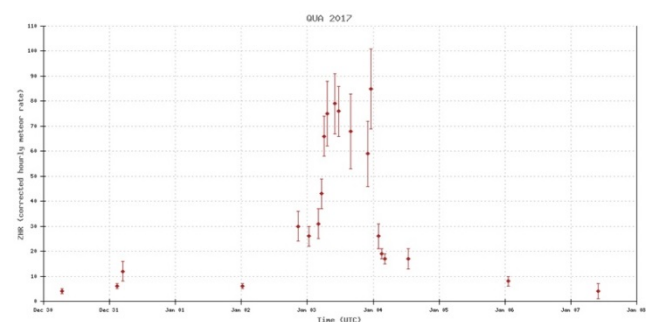

Figure 2 – QUA 2017 – activity profile based on visual observations © IMO.

85 single detections are attributed to Quadrantids by UFOAnalyzer in the BOAM database; half of them were recorded by the stations in Normandy which had good weather during the peak. 30 orbits, radiant positions and trajectories could be calculated with the data from UKMON and FMA.
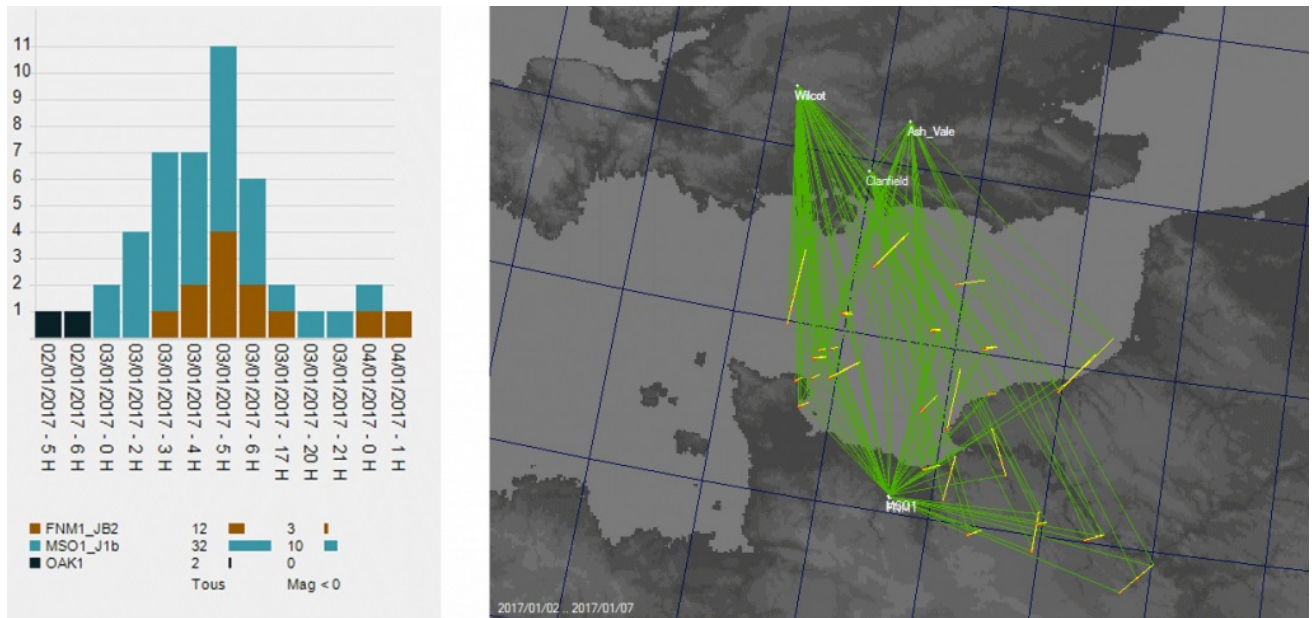
Figure 3 – Left: January 2–5 single detections Right: 25 trajectories from FNM1_JB2, MSO1_J1, UKMON stations.
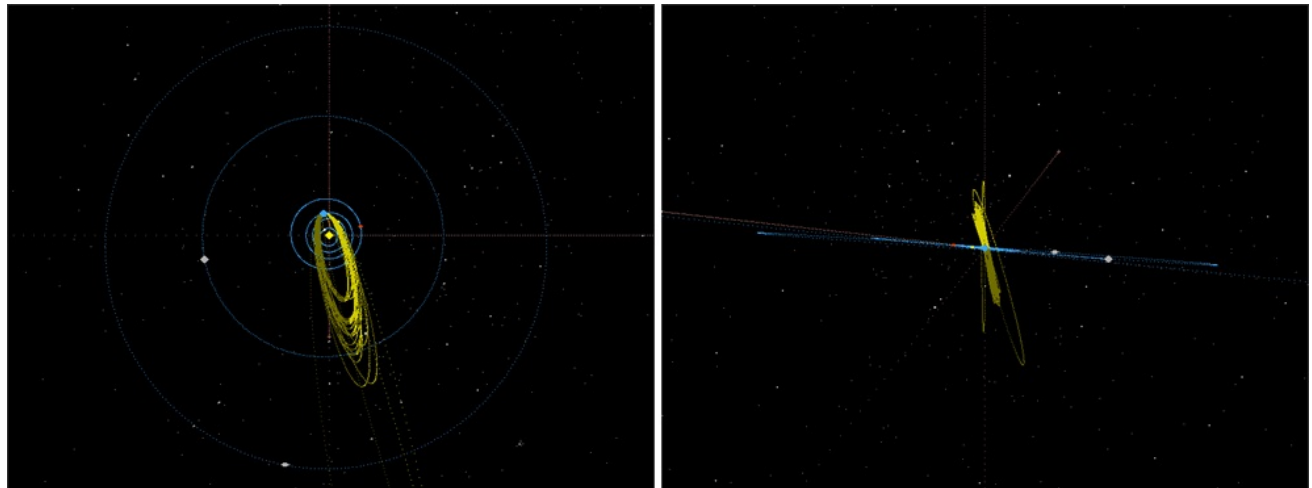

Figure 4 – 30 Quadrantid orbits: top view side view (Red = Mars, Gray = Jupiter) UFOorbit. Rq: The semi-major axis of the calculated orbit depends a lot on the velocity of the meteor, the accuracy for the semi-major axis is rather low.
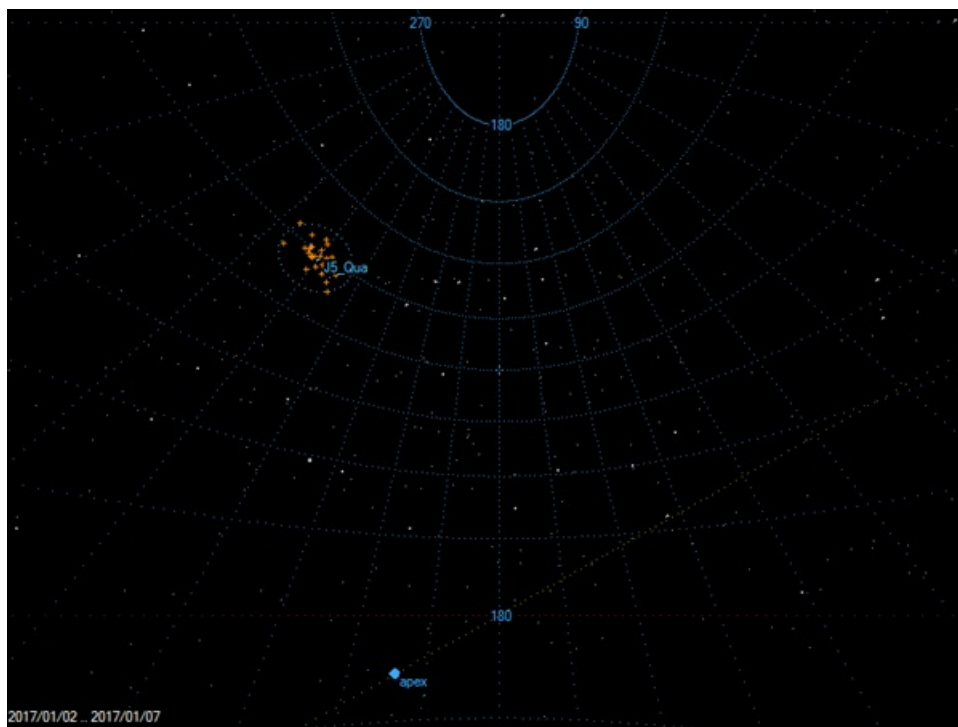

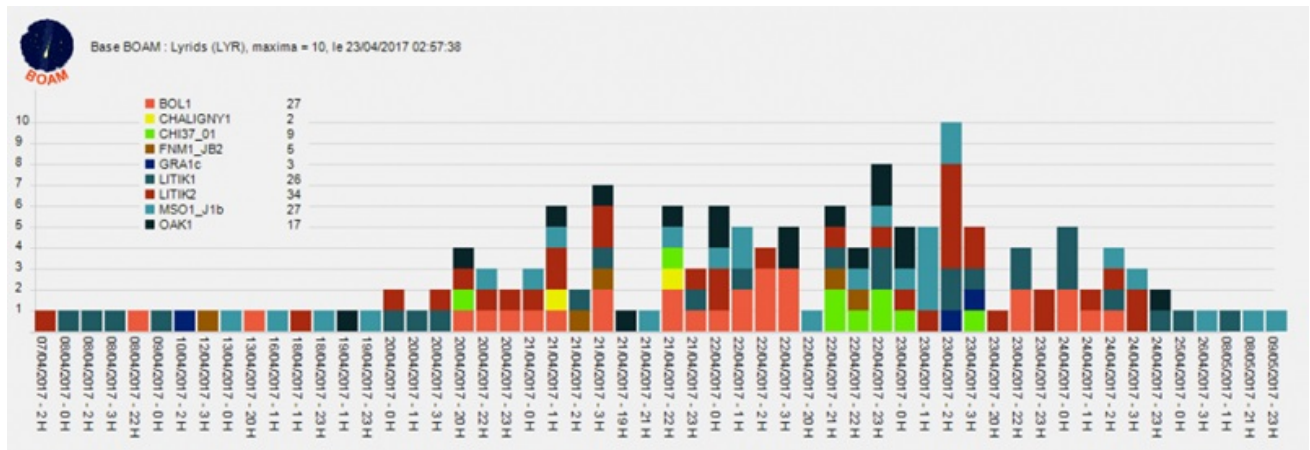*Figure 5* – 30 Quadrantid radiants on a gnomonic projection sky map.

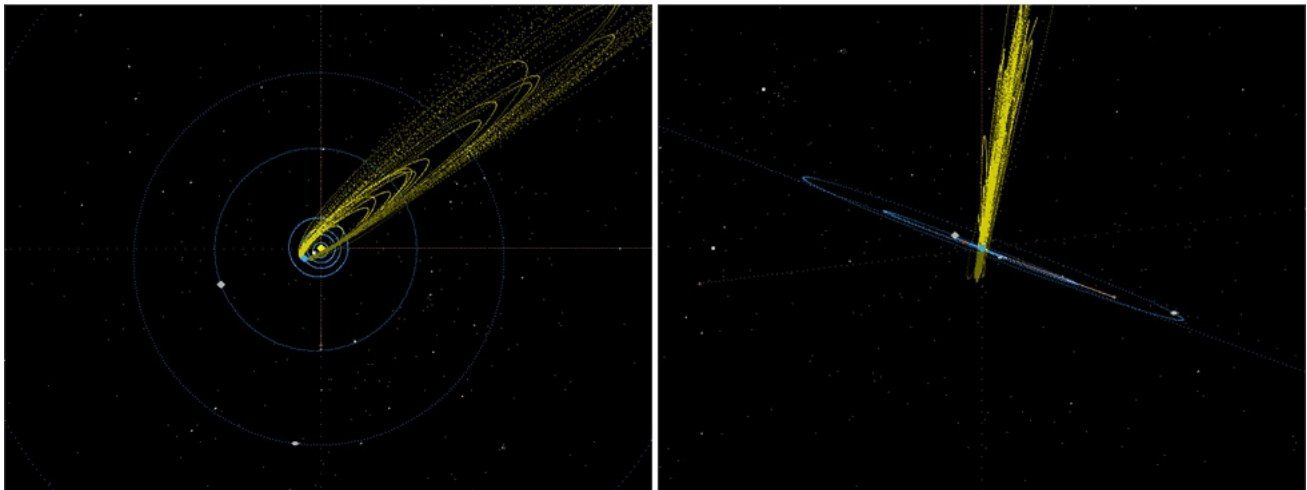*Figure 6* – Chronological distribution of the 150 single detections of Lyrids – GraphBoam.

Figure 7 – 60 Lyrid orbits in the solar system map: top view side view – UFOorbit. Rq: The semi-major axis of the orbit calculated depends a lot on the velocity of the meteor, the accuracy is rather poor for this element.
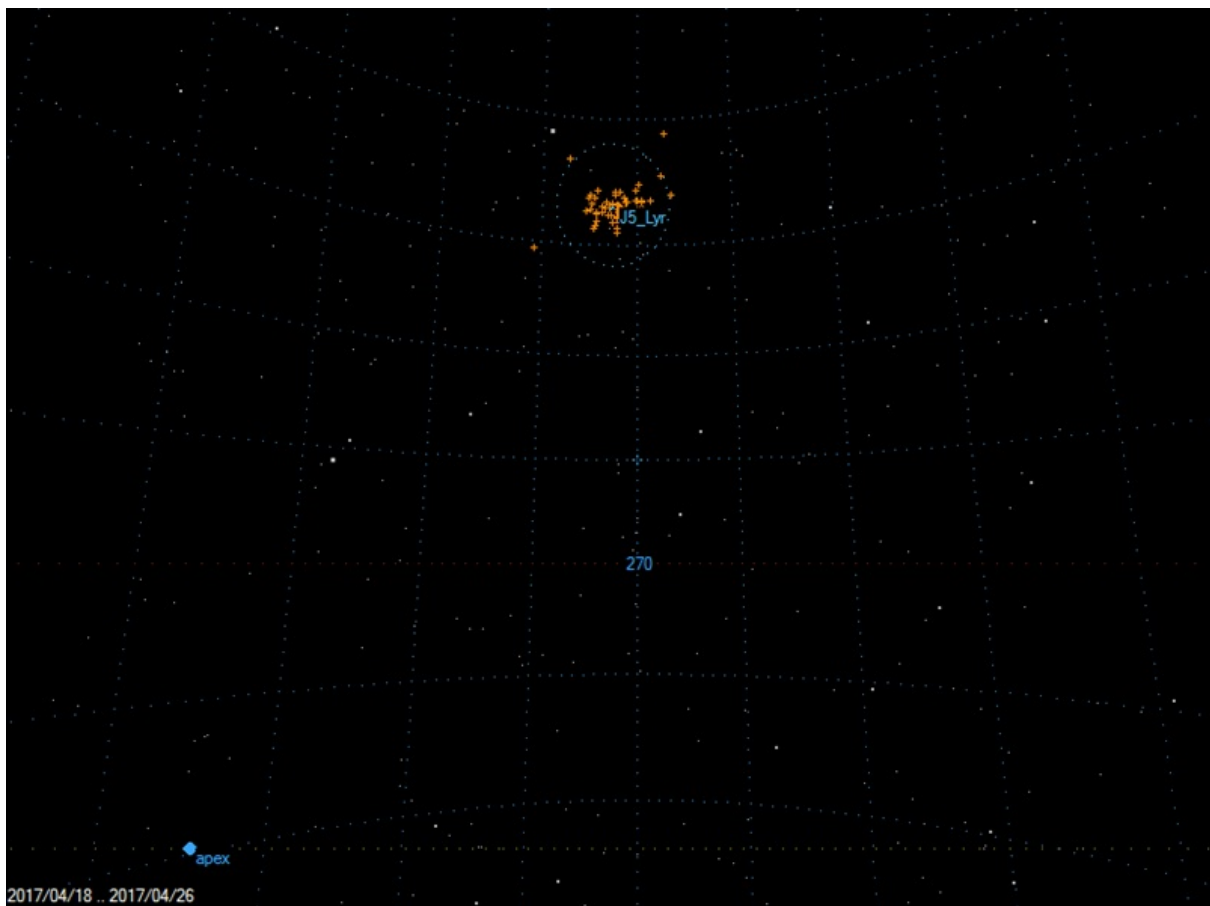

Figure 8 – 60 Lyrid radiants on a sinusoidal projection sky map – UFOorbit.

3   April 16 – 25: Lyrids

The Lyrid shower is the oldest meteor shower to be observed. First reports of high meteor activity associated with the Lyrids were found in Zuo Zhang, China.

According to IMO's data (1988-2000) the activity of the Lyrids is variable. The maximum occurs between solar longitude 32.0° and 32.45°, corresponding to 2017 April 22, 04[h] to April 22, 15[h] UT. Peak width is also variable 15 hours (in 1993) to 62 hours (in 2000).

Table 2 – The Lyrids meteor stream characteristics.

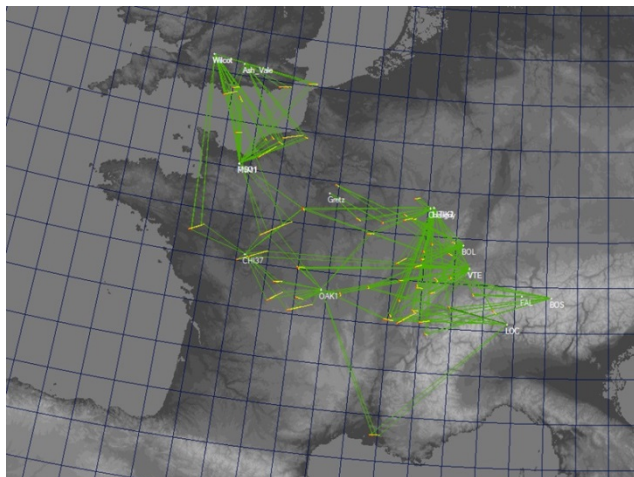| Period of activity	April 16–25
Maximum	April 22
Radiant position (max)	$\alpha = 271°$ and $\delta = +34°$
Zenithal Hourly Rate (max)	18 (var. max. 90)
Velocity	49 km/s
Population index *r*	2.1
Parent body	C/1861 G1 (Thatcher)

Figure 9 – 60 Lyrid trajectories on the ground map – UFOorbit.

The Lyrids with an average velocity of 49 km/s, are a meteor stream rich in rather bright meteors but without leaving many persistent trails.

Last Year, observing conditions were favorable without moonlight (New Moon on April 26th), the radiant was quite high in the sky from 22[h]30[m] UT and rising all night long.

4   Peculiar meteor events

2017/01/06 – 22:44:23 UT: Long meteor M20170106_224423

A –0.5 magnitude, sporadic meteor crossed the field of view of the camera at Fléville during 9.86 seconds. Unfortunately, it was recorded just by on station[8].

---

[8] https://meteornews-assets.ams3.digitaloceanspaces.com/videos/M20170106_224423_LITIK1_.mp4

Figure 10 – M20170106_224423_LITIK1_.

2017/01/29 – 17:36:48 UT: M20170129_173648

This objet entered the atmosphere with a slow speed of 13 km/s, a steep slope of 63° and ended at a height of 35 km.

Stream: Sporadic. Absolute magnitude: –3.0, Duration time: 1.87 s, Velocity: 13 km/s, Altitude of start: 76 km, Altitude of end: 35 km, Trajectory length: 46 km, Inclination: 63°, Radiant: ra = 71° dec.= +34°

Figure 11 – M20170129_173648 Meteor – Fléville (France) – T.Gulon.

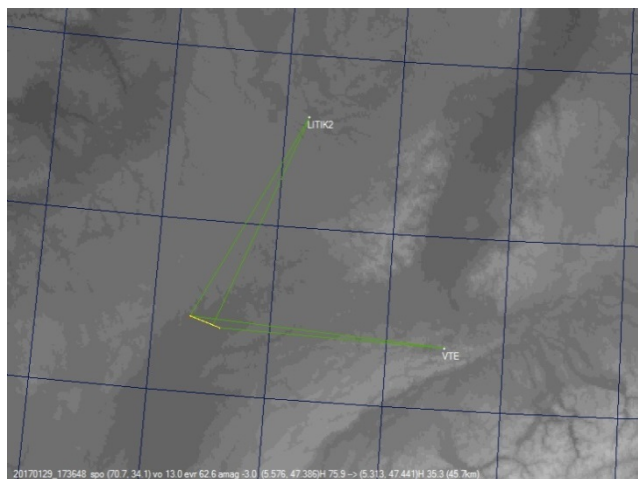*Figure 12* – M20170129_173648 Meteor – Val Terbi (Switzerland) – R.Spinner.

Figure 13 – M20170129_173648 trajectory on ground map.

2017/03/12 – 05:01:31 UT: M20170312_050131

A fast fireball caught by 4 cameras and ending by a flare of magnitude –6.7.

A radar reflection by the geophysical observatory[9] in Montsevelier, Val Terbi (Switzerland) receiver was also recorded.

Sporadic. Absolute magnitude: –6.7, Duration time: 0.86 s, Velocity: 68 km/s, Altitude of start: 121 km, Altitude of end: 78 km, Trajectory length: 86 km, Inclination: 53°, Radiant: ra = 266° dec.= +10°.

Figure 14 – M20170312_050131 – Fleville (France) – T.Gulon.

Figure 15 – M20170312_050131 – Chaligny (France) – Marco.

Figure 16 – M20170312_050131 – Bos-Cha (Switzerland) – J. Richert/FMA.

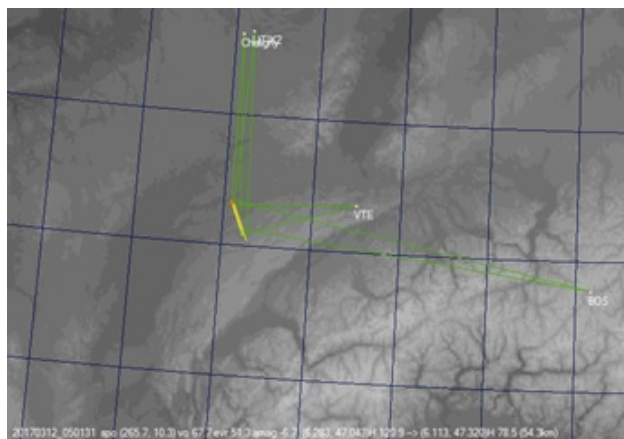*Figure 17* – M20170312_050131 – Val Terbi (Switzerland) – R.Spinner/FMA.

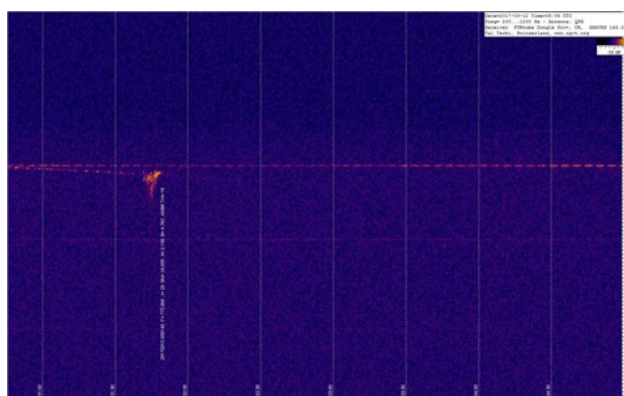*Figure 18* – M20170312_050131 trajectory on the ground map.

Figure 19 – M20170312_050131 GRAVE radar reflection – Val Terbi (Switzerland) – R.Spinner.

---

[9] http://www.ogvt.org/en.html

2017/03/25 00:03:35 UT: exploding fireball over the Channel

This short and bright fireball has been observed from both sides of the channel by French BOAM and British UKMON cameras and 11 visual observers from the UK, the Netherlands, France and Belgium. You can find information on UKMON's page for this event online[10].

Stream: Sporadic. Absolute magnitude: –6.2, Duration time: 1.38 s, Velocity: 45 km/s, Altitude of start: 109 km, Altitude of end: 71 km, Trajectory length: 63 km, Inclination: 37°, Radiant, ra= 263° dec.= +43°.
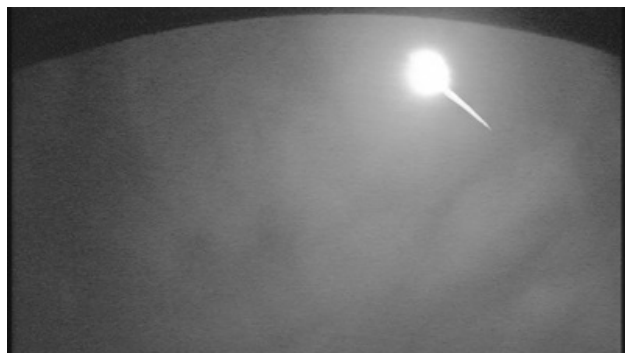

Figure 20 – 11 visual reports – IMO.

Figure 21 – M20170325_000335 – May-sur-Orne (France) – S.Jouin.

Figure 22 – M20170325_000335 Fireball – Wilcot (UK) – UKMON.

---

[10] https://ukmeteornetwork.co.uk/fireballs/large-meteor-over-the-channel-on-25-march-2017/

Figure 23 – M20170325_000335 Fireball – Ash Vale (UK) – UKMON.

Figure 24 – M20170325_000335 Fireball – Clanfield (UK) – Hampshire Astronomical Group.
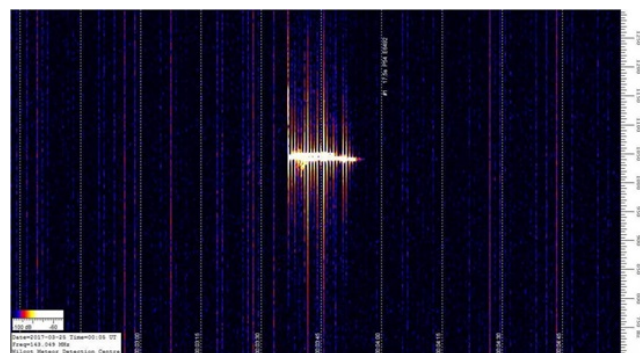

Figure 25 – M20170325_000335 GRAVE radar reflection – Wilcot (UK) – UKMON.
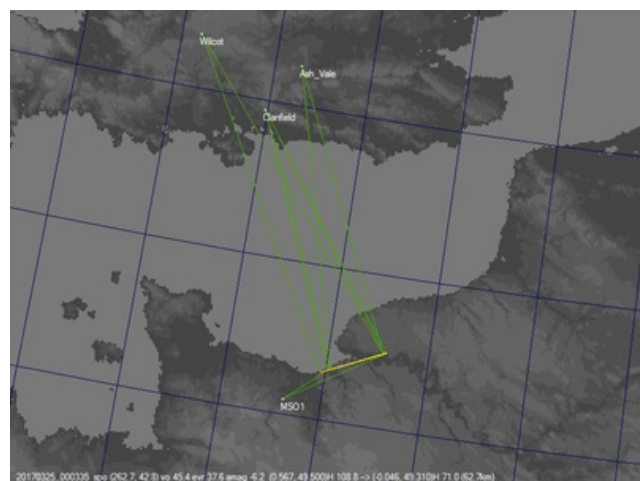

Figure 26 – M20170325_000335 trajectory on the ground map.

2017/03/14 23:42:51 UT: A –10 magnitude Fireball

The object crossed the sky through the zenith over AstroChinon observatory and was recorded by the camera at Chaligny, 470 km away. The duration time was 3.6 seconds and the maximum brightness was probably around –10 mag.
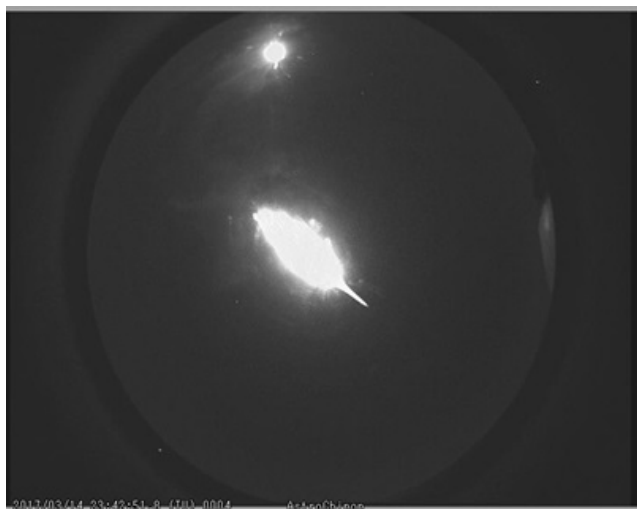

Figure 27 – M20170314_234251 – Chinon (France) – AstroChinon.

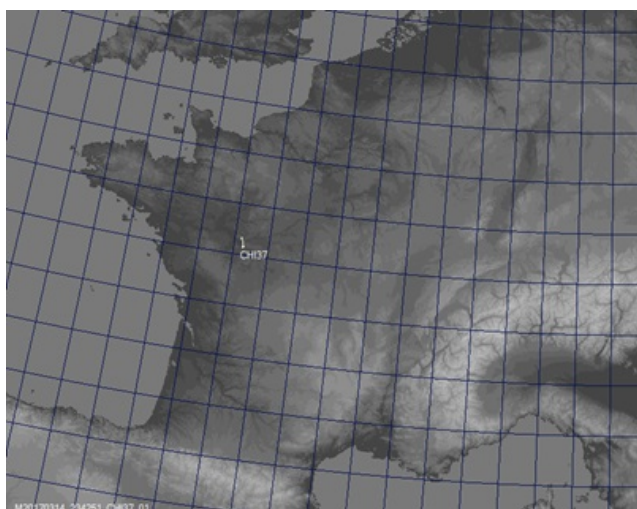*Figure 28* – M20170314_234251 Fireball – Chaligny (France) – Marco.

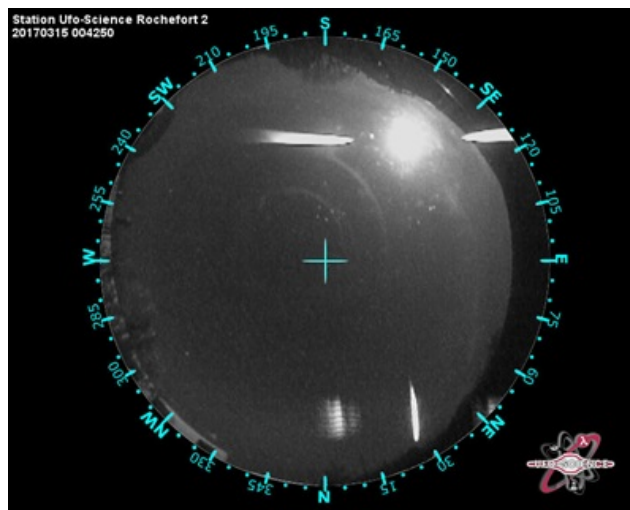*Figure 29* – Location on ground map (estimate for 100 km of altitude).

Figure 30 – Fireball from La Rochelle (France) – Jean-Christophe Doré.

2017/03/27 20:32:23 UT: A deep and straight atmospheric entry

This fireball has gone relatively unnoticed by BOAM observers but it was reported by 16 visual testimonials and resulted in a meteorite prospection on the strewn field by the FRIPON's team. No more information on their investigation except a summary[11]: "The meteorite remaining to be found."

Stream: Sporadic, Absolute magnitude: –4.3, Duration time: 4.1 s, Velocity: 13 km/s, Altitude of start: 80 km, Altitude of end: 40 km, Trajectory length: 41 km, Inclination: 90°.
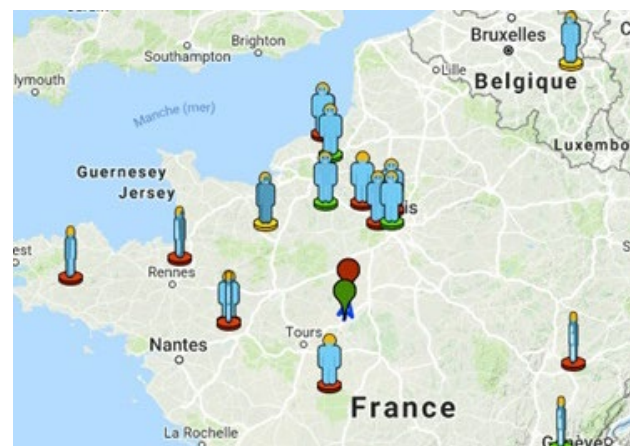

Figure 31 – 16 visual reports from IMO.

Figure 32 – M20170327_203223 Fireball – Fontenay (France) – J. Brunet.

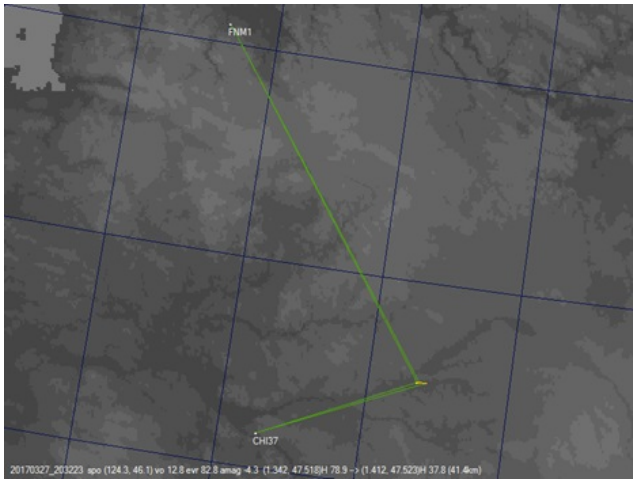[11] http://www.vigie-ciel.org/la-recherche-de-meteorites-a-chambord/

Figure 33 – M20170327_203223 ground map.

The two captures made by BOAM cameras do not allow calculating an accurate trajectory but just an estimation of velocities and coordinates. A very steep slope ~ 90 °, slow speed ~ 12 km/s and the end point of the fireball at an altitude below 30 km are a good clue for the survival of an object.

Figure 34 – M20170327_203223 Fireball – Chinon (France) – Astrochinon.

2017/03/29 00:17:43 UT: M20170329_001743
A nice fireball with a slow speed of 15 km/s ending at a height of 35 km.

Figure 35 – M20170329_001743 Fireball – Cerilly (France) – T. Gulon.

Stream: Sporadic, Absolute magnitude: –5.2, Duration time: 4.1 s, Velocity: 15 km/s, Altitude of start: 72 km, Altitude of end: 35 km, Trajectory length: 57 km, Inclination: 40°, Radiant: ra = 172° dec.= +2.5°.

Figure 36 – M20170329_001743 Fireball – Bollwiller (France) – C.Demeautis.

Figure 37 – M20170329_001743 – Val Terbi (Switzerland) – R.Spinner/FMA.
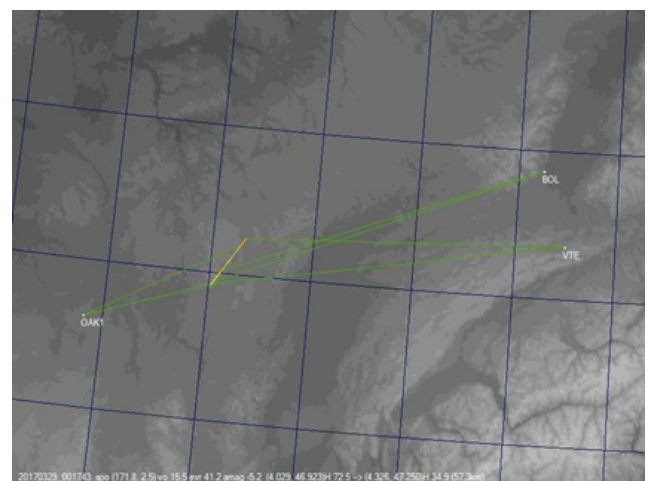
Figure 38 – M20170329_001743 trajectory on the ground map.

2017/04/10 23:40:34 UT: A –9 fireball with persistent trail M20170410_234034

Stream: Sporadic, Absolute magnitude: –8.8, Duration time: 2.35 s, Velocity: 31 km/s, Altitude of start: 119 km, Altitude of end: 72 km, Trajectory length: 72 km, Inclination: 40°, Radiant ra. = 250° dec. = +23°.

Figure 39 – M20170410_234034 – Gretz (France) – A. Leroy/R. Trangosi[12].

Figure 40 – M20170410_234034 Fireball – Fléville (France) – T.Gulon[13].
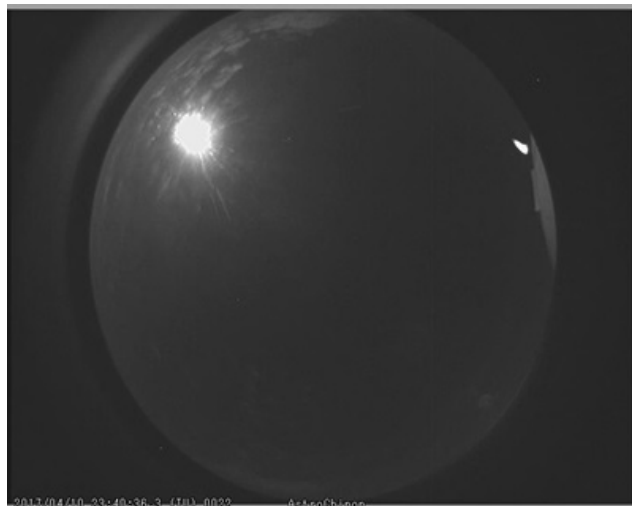
Figure 41 – M20170410_234034 Fireball – Chinon (France) – Astrochinon.
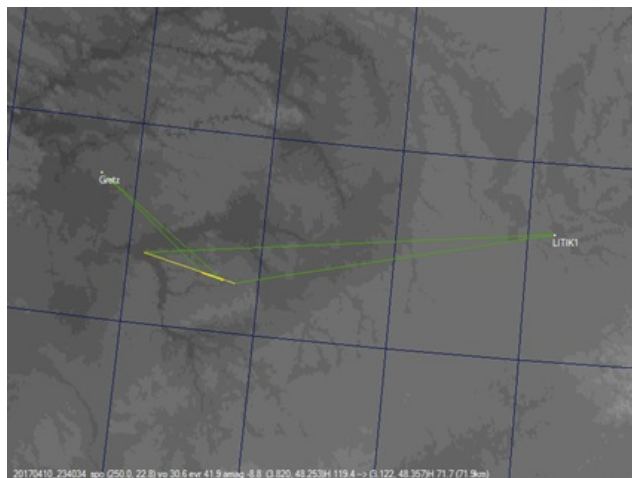
Figure 42 – M20170410_234034 trajectory on the ground map.

References

Rendtel J. (2016). "2017 Meteor Shower Calendar". International Meteor Organization.

---

[12] http://video.boam.free.fr/detection/video/M20170410_234035_ Gretz_Wa.flv
[13] http://video.boam.free.fr/detection/video/M20170410_234034_ LITIK1_.flv

CAMS meeting 11 March 2018

Paul Roggemans

Pijnboomstraat 25, 2800 Mechelen, Belgium
paul.roggemans@gmail.com

The annual CAMS BeNeLux meeting took place in Bussloo, Netherlands on 11 March 2018 and was attended by about 25 people. Recent CAMS results were presented and various hardware and software aspects were considered. A summary is presented of the different presentations.

1   Introduction

The CAMS BeNeLux network is managed by a team of 20 volunteers operating more than 90 cameras at 22 CAMS stations. The greatest distance between two CAMS stations is about 400 km (for instance Grapfontaine–Terschelling is 395 km or Zillebeke–Burlage, 400 km) and although the most northern stations are operated with remote control, a CAMS meeting requires a long ride for several participants. Nevertheless the network participants are very eager to meet each other to share experience and to discuss all aspects of their CAMS activities.

For the March 2018 meeting the gathering was hosted by Volkssterrenwacht Bussloo, near Apeldoorn in the Netherlands. About 25 people attended the meeting, most of them camera operators, but also some meteor observers interested to hear about CAMS.

2   6th anniversary and the 100000th orbit

The first orbits of the network were registered in the night of 14–15 March 2012 by *Klaas Jobse* and *Piet Neels* and this date marks the birthdate of the CAMS BeNeLux network.

Figure 1 – Koen Miskotte presenting the CAMS cake, not to be confused with space cake.

But this was not the only reason for a celebration. A few weeks before the meeting, the network had obtained its 100000th orbit. *Koen Miskotte* (Ermelo, 351,352, 353 and 354) surprised his colleagues with a delicious cake which he prepared especially for this occasion (see *Figure 1*

and 2). *Paul and Adriana Roggemans* (Mechelen, 383, 384, 388, 389, 399 and 809) offered some bottles of Romanian wine to help celebrate the event.

Figure 2 – The delicious cake offered by Koen Miskotte.

3   Welcome and CAMS developments

Carl Johannink, the CAMS BeNeLux Network coordinator, opened the meeting at 11 o'clock and introduced the program for the day.

2017 has been a very busy year for CAMS BeNeLux. Carl presented an overview of the main achievements of 2017:

- 35591 orbits were collected in 2017;
- 13 papers were published in eRadiant;
- 14 papers were published in eMeteorNews;
- 2 papers were published in WGN;
- 1 contribution was made to the IAU Working List of meteor streams (#228 OLY);
- Activity recorded of #281 OCT;
- 1 orbit of #246 AMO recorded 22/23 Nov.;
- Activity of #523 AGC registered;
- Tau Herculids detected on 30/31 May.

While December 2017 and January 2018 brought exceptionally bad weather, February 2018 was a once in a lifetime exceptional good month with as many as 4147 orbits. This total is exceptional for February, but about the same number of orbits as what we had in the normal month of October 2017 while meteor activity is much higher in October than in February. This gives some idea about the number of orbits we may have *if* we once get an exceptional clear month of October.

In the night of 13-14 February 2018 *Dr. Peter Jenniskens* draw Carl's attention to a possible outburst for which CAMS BeNeLux had a number of orbits. The new shower got listed as #1032 FCM ($\alpha = 124°$, $\delta = 2°$, $\lambda_{\Theta} = 324°$, $v_g = 16.5$ km/s) and was also detected by LO CAMS (Arizona). More orbits of this shower were meanwhile found in the period 9–16 February as well as in previous years.
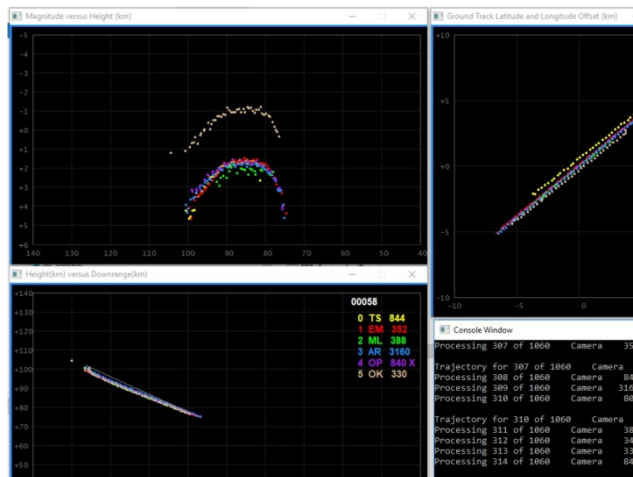

Figure 3 – One of the examples with anomalies presented by Carl Johannink.

Next Carl described a number of points that require attention from all camera operators. For example:

- The name of the FtpDetectInfo.txt should always refer to the *day that the night started*. With other words this must be adapted manually if the capture session was started after midnight UT.
- All detectfiles must refer to the most recent Cal-files and these Cal-files must be sent with the detectinfo.

- If no Cal file could be obtained, then it should be carefully checked why. In case that the camera was moved, be sure to recalibrate manually and do not send data unless you have a valid Cal-file.
- Always double check what you send (correct date, correct cal-files, correct detectinfo, etc.).
- Verify if your time synchronization functions correctly. Check D4 and do not just trust it blindly.

In practice mistakes and unexpected errors do occur and most of these catch the attention when the data of all stations is merged and analyzed on double station events by the program Coincidence. Carl presented a number of situations where he has to interpret the possible source of some anomaly in order to decide which camera is at the origin of the problem. In most cases a valid trajectory and orbit can be obtained if the camera data of the source of the anomaly is rejected. Unfavorable geometrics or too poor accuracy in certain detection cases are among different possible explanations.

4   The weird meteor of 2018 February 16

In the morning of 16 February at 4ʰ55ᵐ UT a remarkable long meteor trail passed through several cameras and confused some camera operators whether or not this should be confirmed as a meteor or not. As many as 18 cameras captured this unusual long trail: 313 (Gronau, Germany), 324 (Hengelo, Netherlands), 331 and 334 (Oostkapelle, Netherlands), 342 and 343 (Ooltgenplaat, Netherlands), 352 (Ermelo, Netherlands), 380 (Wilderen, Belgium), 389, 807 and 808 (Mechelen, Belgium), 804 (Zoersel, Belgium), 814 and 815 (Grapfontaine, Belgium), 844 (Terschelling, Netherlands), 3160, 3166 and 3167 (Alphen aan de Rijn, Netherlands).
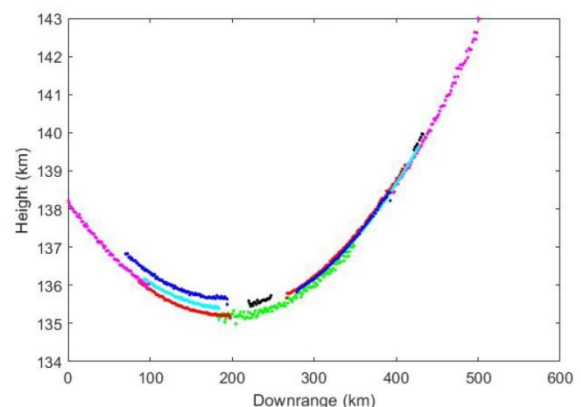
Figure 4 – A plot of the variation in height along the trajectory.

This meteor was in more than one way peculiar as it was an earth grazer with an exceptional long trajectory of over 500 km which occurred at an exceptional high elevation with an even more remarkable high entrance velocity. The standard analyses with the CAMS app Coincidence could not handle this case. All the data was transferred to the CAMS headquarters in California where *Dr. Peter Jenniskens* investigated the data. *Pete Gural* could apply some ad hoc analyzing techniques to get more information from the available images. The first preliminary results

indicate that this could be a most remarkable appearance. Carl presented some of the first results and browsed the lists with questions and requests for additional investigations. The case is still under investigation and more will be published as soon as the final results and conclusions are ready.

5   Minor showers and D-criteria

Paul Roggemans gave a presentation how minor showers can be detected within a huge number of orbits. The CAMS project generated a large number of newly discovered minor showers. In about 10 years an impressive working list with concentrations of orbits has been compiled which recalls bad memories of the radiant catalogues of 40 years ago which were mainly based on single station work. Most minor showers from the past proved to a large extend fake. How real are the many minor showers that are currently being listed?
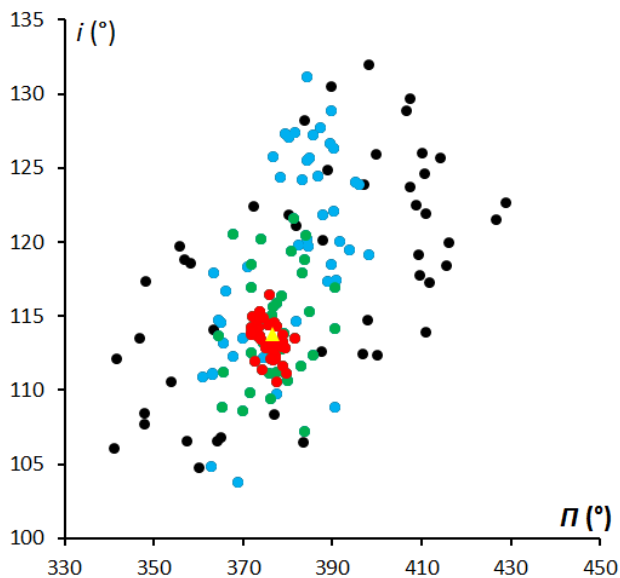

Figure 5 – An example of a statistical significant concentration of December alpha Bootids in a diagram of inclination i against length of perihelion Π.

Amateurs tend to overlook that even the most sophisticated video observing techniques still have error margins on their measurements. Most people assume there is a solid methodology to analyze and to define orbit concentrations and therefore tend to believe all reported minor showers are real. However this is not how science works, nobody should believe anything. The most common way to try to detect clusters of similar orbits are the so called discrimination criteria, (Roggemans and Johannink, 2018). With some practical examples the relative significance of these criteria was shown. The famous D-criteria only indicate a degree of similarity between orbits but do not prove any physical relationship between the orbits. When searching worlds' major orbit datasets of CAMS, EDMOND and SonotaCo, clusters of similar orbits should be considered with great care and caution. Random dust concentrations in the solar system explain why in some regions the 'contamination' with random distributed sporadic orbits includes similar orbits

that fulfill the D criteria. In these cases the D criteria are rather misleading as many of these pure sporadic orbits will fulfil the D-criteria within a high threshold.

The complex nature of the shower association based on orbits with a rather accurately determined radiant position and velocity raises questions about the reliability of single station meteor work. For visual observations the focus is to count the number of meteors and their magnitudes for a limited number of meteor showers known as major showers with statistical significant numbers of meteors. These observations make statistically sense as the dominant activity of such visually observed shower is far above the sporadic contamination of the sample. The problem is more with single station video work that pretends to detect minor shower radiants from backwards produced trails, assuming that any concentration of intersection points indicates a shower radiant. This assumption will work for a number of minor showers, but the sporadic contamination of the sample will be rather problematic in many cases. Radio work does not allow detecting any shower association and can be considered as of no use in the challenge to study minor showers.

6   Fireball EN240218

Jean-Marie Biets presented an overview of the results obtained for the fireball of 24 February at $00^h11^m31^s$ UT, such disturbing bright event for CAMS and such a delight for the All-sky cameras.

Figure 6 – Jean-Marie Biets during his presentation.

Figure 7 – The 24 February fireball registered by EN92 at Wilderen (Belgium).

The fireball was recorded by 5 all-sky stations: Ermelo

(*Koen Miskotte*), Benningbroek (*Jos Nijland*), Wilderen (*Jean-Marie Biets*), Niederkruechten (*Hans Schremmer*) and Oostkapelle (*Klaas Jobse*). The fireball was also captured on several CAMS cameras.

Jean-Marie presented an overview of all the images collected for this fireball and compared the results obtained from the all-sky data provided by *Dr. Pavel Spurný* with the results provided by *Carl Johannink* based on the CAMS data. Based on the all-sky data the fireball started at 97 km height and ended at 33.5 km after a trajectory of 157.3 km. No need to make any field searches for meteorites as there is no chance for anything that could have hit the surface of the Earth.
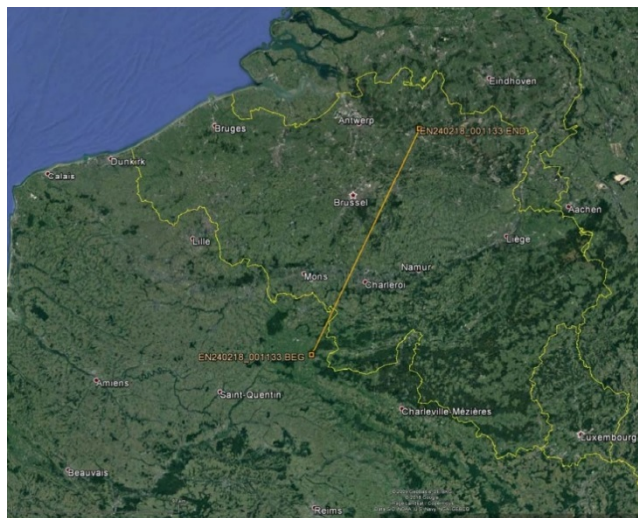

Figure 8 – The projected ground trajectory of the fireball.

7   Hardware issues of CAMS

The volunteers of Volkssterrenwacht Bussloo offered soup, coffee and tea during lunchtime, a perfect time for socializing and informal contacts. After the lunch *Robert Haas* explained a number of technical aspects that interfere. With several posts attempting to operate more cameras on a single PC combined with Auto CAMS, the demands on the hardware and the software configuration caused quite a bit of technical problems. The weak point in the CAMS configuration turns out to be the EzCap 116 dongles and their interaction with the USB ports. Problems with the dongles, some call these EzCrap, are responsible for various, sometimes unexpected malfunctioning.

Figure 9 – Typical CAMS hardware configuration.

Robert explained the characteristics of the different Watec models and how resolution and contrast are defined. Some examples were given to modify the settings. Typical problems like hot pixels, video smear, and different kinds of erroneous interferences in the video images were discussed. The problems with dongles, USB capacity and connections got detailed attention.

The differences between Watec 902H Ultimate and the Watec 902H were discussed in detail. A number of practical advices were given as how to obtain a new calibration file.

8   CAMS 2.2 and CamsGUI

Steve Rau presented the new Auto CAMS (based on CAMS 2.2) and CamsGui. All participants received a printed copy of the 113 pages thick CAMS manual with a lot of information about CAMS, practical tips, detailed descriptions of all the different CAMS programs, the manual procedures to operate CAMS and the details about AutoCAMS and CamGui.
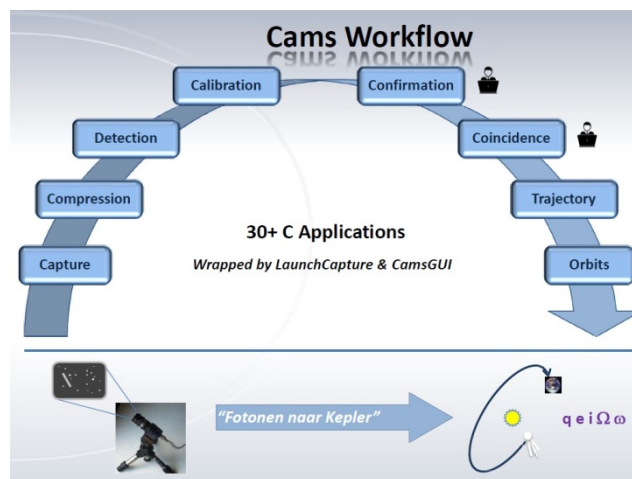

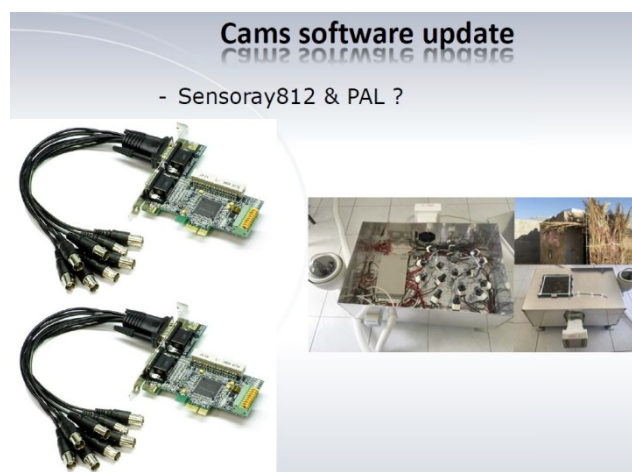*Figure 10 – The CAMS workflow.*

Figure 11 – The CAMS installation in the United Arab Emirates.

The workflow of CAMS consists of a sequence of procedures that have been automated to a large extend. Human intervention is only required at two steps in the loop. The confirmation requires on sight decision which detection is most likely a real meteor and which are

obvious false detections. Coincidence requires visual quality control of the obtained trajectory and orbit. Also these aspects have been automated at the CAMS headquarters, applying AI technology. Step by step Steve went through the procedures demonstrating the advantages of the tools.

Steve described how to install the new CAMS software version, which parameter files that had to be adapted. The use of CAMSGui.exe was explained and information was provided about the use of the Sensoray 812 with Pal which functions perfectly at the CAMS stations in the United Arab Emirates (*Figure 11*).

A live demo was giving and since the CAMS station in the United Arab Emirates were already capturing towards the end of the CAMS day in the BeNeLux, everybody could watch the ongoing CAMS session live via TeamViewer.

Steve summarized some frequently reported problems and provided his advices what to do in case these problems do occur. Log files are helpful to identify most problems. Some CAMS stations were confronted with so called sectored meteor trails, which make the determination of the correct duration and thus velocity impossible. The reason for this is that the number of cameras exceeds the capacity of the PC used for CAMS. Other system processes may interfere, USB capacity may be exceeded, the hard disk may be too slow to handle the storage of the data, etc.

9 Camera fields optimization

Paul Roggemans gave an overview of the current orientation of all the camera fields compared to the situation as presented at the previous CAMS day of 12 March 2017. The number of cameras has increased with about 50% since last meeting. Most stations have pointed their cameras in function of an optimal coverage of the atmosphere above 80 km, taking into account that the variable weather circumstances require multiple instead of double station coverage. The large number of cameras and the occurrence of many multiple station meteors during perfect clear nights feed the perception that the camera network got saturated and that no new posts or cameras should be admitted. However, the number of perfectly clear nights for the network remains rather rare, at best once or twice a month. The bulk of the orbits collected by the network are being harvested during partial clear nights, often under very unfavorable circumstances. This success despite mediocre weather conditions is due to two factors: the organization of the camera fields with multiple overlap combined with AutoCAMS at 2/3 of the CAMS stations.

CAMS Benelux with more than 90 cameras is about the 3rd camera network after SonotaCo with ~100 cameras in Japan and EDMOND which unites many networks with in total 311 cameras. We are about the only network that so far does not struggle with delay in reduction. With 1/3 of our network functioning only occasionally according to

the weather we are the only network that does not operate all cameras all nights.

The technical problems that occurred in 2017 had a serious impact on the final harvest of orbits. More supervision of automated stations is required to anticipate on erroneous data, e.g. when clock synchronization problems ruin identification of coincidence.
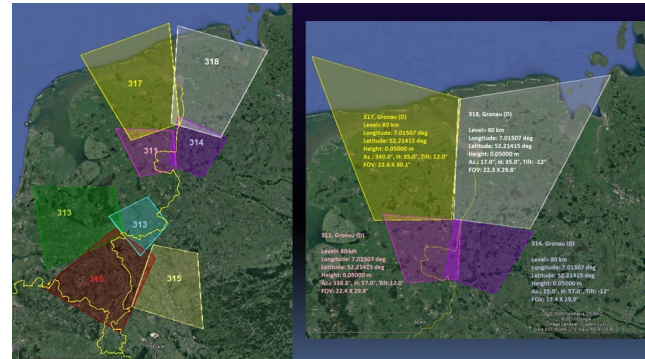
Figure 12 – Camerafields should be oriented in such a way that a large block of the sky is being monitored.

Finally a comparison was made between CAMS 1.3, 1.6 and 2.2 for the number of false detections. Based on the data of the capture sessions, it appeared that the number of false detections was reduced by a factor of 3 comparing version 1.6 to 1.3, and reduced by a factor of 30 comparing version 2.2 to 1.3. Everybody is highly recommended to upgrade to version 2.2 a.s.a.p.

Figure 13 – The positions of the CAMS stations in March 2018.

10 Closing of the CAMS day

Before the meeting was closed, *Paul Roggemans* took a moment to thank *Carl Johannink* and *Martin Breukers* for their efforts as coordinators to provide regular feedback to the camera operators, a considerable amount of work which is essential for the motivation of all. A bottle of Romanian wine was offered to Carl and Martin with a sincere warm applause from the audience.

Carl closed the CAMS meeting a bit past 17h, later than initially planned. Reactions from the participants were very positive. We already look forward to a next CAMS meeting!

Many thanks to the team of the Volkssterrenwacht Bussloo for their hospitality and support to have this meeting.

Figure 14 – The CAMS team with the camera operators present at the meeting. From Left to right: ***Paul Roggemans*** and ***Adriana Roggemans*** (Mechelen, 383, 384, 388, 389, 399 and 809), ***Ian Rau***, ***Robert Haas*** (Alphen aan de Rijn, 3160, 3161, 3162, 3163, 3164, 3165, 3166 and 3167; Burlage, 801, 802, 821 and 822; Texel, 811, 812, 813 and 814). ***Tim Polfliet*** (Gent, 396), ***Steve Rau*** (Zillebeke, 3151 and 3152), ***Luc Gobin*** (Mechelen, 390, 391, 807 and 808), ***Carl Johannink*** (Gronau, 311, 312, 313, 314, 315, 316, 317 and 318), ***Piet Neels*** (Ooltgenplaat, 340, 341, 342, 343, 344, 345, 349 and 840; Terschelling, 841, 842, 843 and 844), ***Hans Betlem*** (Leiden, 371, 372 and 373), ***Erwin van Ballegoij*** (Heesch, 347 and 348), ***Jos Nijland*** (Benningbroek, 358 and 359), ***Jean-Marie Biets*** (Wilderen, 380, 381 and 382), ***Martin Breukers*** (Hengelo, 320, 321, 322, 323, 324, 325, 326, 327) and ***Koen Miskotte*** (Ermelo, 351, 352, 353 and 354).

Not in this picture: ***Felix Bettonvil*** (Utrecht, 376 and 377), ***Bart Dessoy*** (Zoersel, 397, 398, 804, 805 and 806), ***Franky Dubois*** (Langemark, 386), ***Jean-Paul Dumoulin & Christian Wanlin*** (Grapfontaine, 814 and 815), ***Klaas Jobse*** (Oostkapelle, 330, 331, 332, 333, 334, 337, 338 and 339), ***Hervé Lamy*** (Dourbes, 394 and 395; Humain, 816, Ukkel, 393) and ***Hans Schremmer*** (Niederkruechten, 803) (Photo Carl Johannink).

Geminids 2017: a tricky analysis

Koen Miskotte

Dutch Meteor Society
k.miskotte@upcmail.nl

An analysis of the Geminids 2017 based on visual meteor observations is presented. A ZHR profile has been computed based on observations reported to the website of the International Meteor Organization and data from observers that were sent directly to the author. This article provides an overview of the method, the difficulties and the final results of this analysis. The results from 2017 are also being compared with previous analyzes of the Geminids from 1985, 2001 and 2009.

1   Introduction

The Geminids of 2017 have been looked forward to for years. After all, the parent body of the Geminids, 3200 Phaethon, would have had its closest approach in 2017 and this just around the Geminids maximum (Miskotte, 2010; Miskotte et al., 2011; Ryabova and Rendtel, 2018). According to Galina Ryabova and Jürgen Rendtel (2018) there was a very small chance for some increased activity on December 14 just after 12^h UT ($\lambda_O = 262.45 \pm 0.005°$). Furthermore, Galina and Jürgen state in the same article that the Geminid activity has increased in the period 1985–2016.

In addition, it is true that previous analyzes state that the Geminids series 1985–2001–2009 and 2017 are the best returns to verify if the Geminids activity increases, remains stable or decreases (Miskotte et al., 2010; Miskotte et al.,2011).
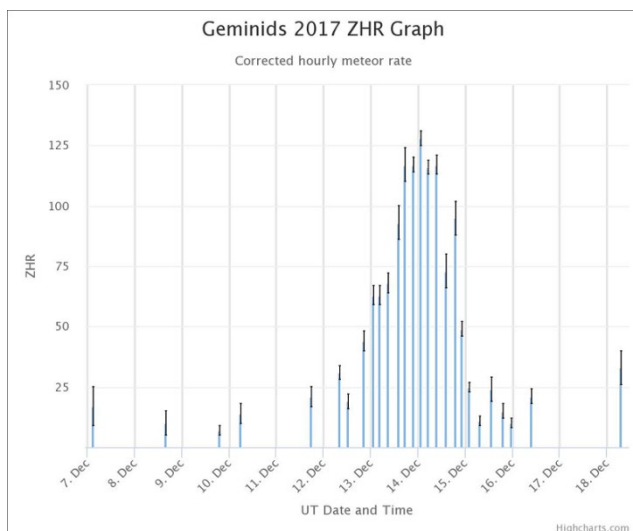

Figure 1 – On the fly ZHR curve of the Geminids 2017. The curve is based on 8568 Geminids and an assumed population index r of 2.6. Furthermore, only data with a limiting magnitude of +5.0 or better was used.

Unfortunately, the Geminid maximum in the BeNeLux was not a success. The weather was pretty bad and again it was proven that the best opportunities for clear skies were in the southern part of the BeNeLux. Of course we also looked at data from well-known observers provided via the IMO site. However, it could also be seen that the weather in 2017 had a negative impact on the observational results.

At the IMO site[14], up to 14 January 2018, 8568 different meteors were reported by 71 different observers. This resulted in the *Figures 1 and 2*, the well-known "on the fly" curves. An overview of the results from 2017 will be compared in this article with previous returns of 1985–2001 and 2009.
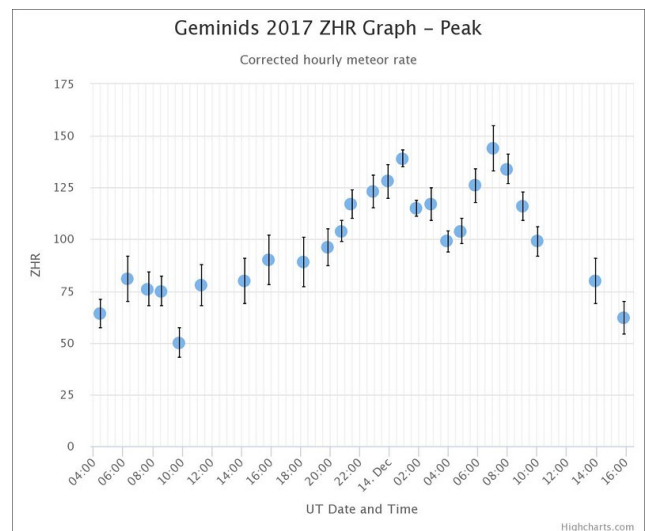

Figure 2 – This ZHR curve is zoomed in on the maximum of the Geminids between 13 December 2017, 4^h00^m UT and 14 December 2017 14^h00^m UT. The curve is based on 6065 Geminids and an assumed population index r of 2.4. Furthermore, only data with a limiting magnitude of +5.5 or higher was used. This immediately yields a better result compared to Figure 1.

2   Assessment of the data

Because the weather in the BeNeLux was disappointing and because we wanted to analyze the results on a global scale, we looked at the data that were reported to IMO. In addition, some observers sent their data directly to the author. Because few data were available from the observers with a reliable C_p determination, an attempt was

---

[14] http://www.imo.net/members/imo_live_shower?shower=GEM&year=2017

first made to make an analysis with data from all observers with a limiting magnitude of +5.9 or better and with an overall percentage of obstruction of no more than 10%. Also radiant heights below 25 degrees were not used. This data was then stored in the well-known ZHR spreadsheet (the interval counts) and the magnitude distribution check sheet (for the population index r determination). During the collection of the data it turned out that a large part of the observations were rather fragmented. Many observers had to deal with variable circumstances or could only observe a short period. When everything was entered in the spreadsheets, 6588 Geminids could be used for the analysis. This is roughly 70% of all the data reported to IMO.

3   Determination of the population index

Determining a profile for the population index r turned out to be an impossible task. Only data from experienced observers has been used here. The control of the magnitude distributions indicated that only 20% (!) of the submitted data of 3189 Geminids was suitable for the calculation of r-values. The rule in this spreadsheet is that the difference between the average magnitude of the Geminids and the limiting magnitude may not be greater than 4 magnitudes. This number (~700) of meteors is far too little for a reliable determination of the population index profile. In spite of that we tried to get a good picture of the Geminids 2017. Therefore we decided to maintain an r-value of 2.5 until $\lambda_\Theta = 262.2°$ for the ZHR calculations and to use a value of 2.3 after that time. This makes it possible to compare directly with the ZHR curves from the series 1985, 2001 and 2009, since in the large Geminids analysis (Miskotte et al., 2010) calculations were also made with those r values up to and from the same solar longitude.

4   ZHR calculations

In first instance, all data from all observers who submitted observations that met the requirements set out in section 2 were used for ZHR calculations. Observers with a known C_p were selected, while for observers with no known C_p, a C_p of 1.0 was maintained. As stated in section 3, a population index r of 2.5 was assumed for observations done before $\lambda_\Theta = 262.2°$, followed by a population index r of 2.3 after $\lambda_\Theta = 262.2°$. This resulted in *Figure 3*.

The two visible peaks of *Figure 2* on the IMO site are also clearly visible here, both with a peak ZHR of just less than 140. Furthermore, the high ZHRs obtained above Europe and the US from the night 12–13 December 2017, with peaks at $\lambda_\Theta = 261.1°$ (13 December 2017 4.3ʰ UT, ZHR 70) and 261.3° (13 December 2017 8.6ʰ UT, ZHR 70) and two strong outliers at $\lambda_\Theta = 260.7°$ (12 December 2017 18.9ʰ UT, ZHR 70) and $\lambda_\Theta = 261.0°$ (13 December 2017 02.3ʰ UT, ZHR 90!).

Because of the mentioned outliers, the rather messy build up in the night of 12–13 December and the rather high ZHR values that night, the author zoomed in on the data

gathered between $\lambda_\Theta = 260.7°$ and $\lambda_\Theta = 261.5°$. Usually there is a fairly regular build-up of activity around that solar longitude, with the ZHR slowly increasing. Further inspection of the observations shows that there seems to be a problem with the data of one observer, for who a good C_p determination is available (surprisingly enough). This observer has very high individual ZHR values for the night 12–13 December, just over 100! His C_p was once determined at 0.7 (found from the period 2014–2015). To be sure, I have recalculated his C_p and added it with data from August 2017. Indeed the C_p is now a bit higher with 0.9. But even then I still found high ZHR values between 70–90. The observer reported ZHR values that are twice as high compared to those of other observers with a good C_p, observing at the same time.
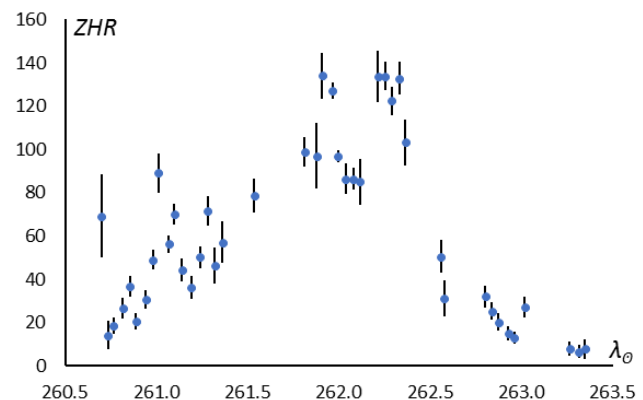

Figure 3 – Geminids 2017 ZHR curve based on all observers with a minimum limiting magnitude of +5.9. This curve is based on 6443 Geminids with an assumed population index value of 2.5 before $\lambda_\Theta = 262.2°$ and 2.3 after $\lambda_\Theta = 262.2°$.

That is why I decided to do another complete ZHR analysis in which data was used according to the following method:

- All data from observers without a reliable C_p determination were removed.
- All data from the observer with the very high ZHR values of 12–13 December 2017 were removed, this observer could only observe the night of 12–13 December. The high ZHR outlier of $\lambda_\Theta = 261.011°$ immediately disappeared.
- The high ZHR at $\lambda_\Theta = 260.70°$ was removed; this was an observation by one observer for who the C_p was well known, an outlier.

Of the 6565 Geminids mentioned, 3995 then remained. From these data a new ZHR curve was made, the result is displayed in *Figure 4*. It is immediately apparent that the structure of 12–13 December looks a lot more "stable". The double peak remains, even though the first peak has been reduced by 1 ZHR point. *Figure 5* is a combination of *Figures 3* (ZHR curve of all observers) and *Figure 4* (ZHR curve based only on data of observers with a known C_p) to better emphasize the differences.

This shows again that for a good accurate ZHR determination, only data from observers with a good C_p determination must be used. One cannot throw data into

one pile without controlling the data and just process it. The author insists that for a good C_p determination, sporadic data collected between July 25 and the entire month of August between 0^h and 4^h pm local time, should be used.
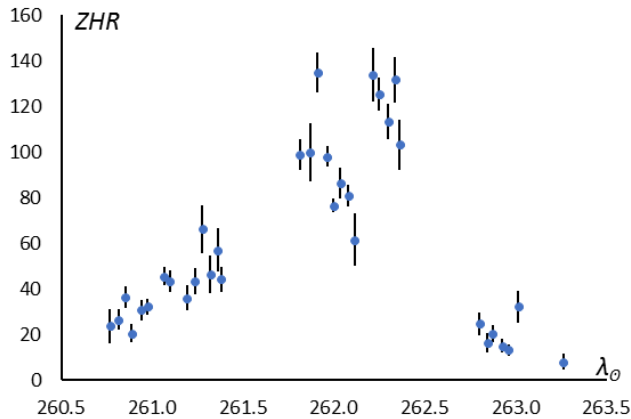

Figure 4 – ZHR profile for the Geminids 2017 based on 3995 Geminids. This is the final version of the 2017 ZHR profile for the Geminids and is the reference to compare with 1985, 2001 and 2009.
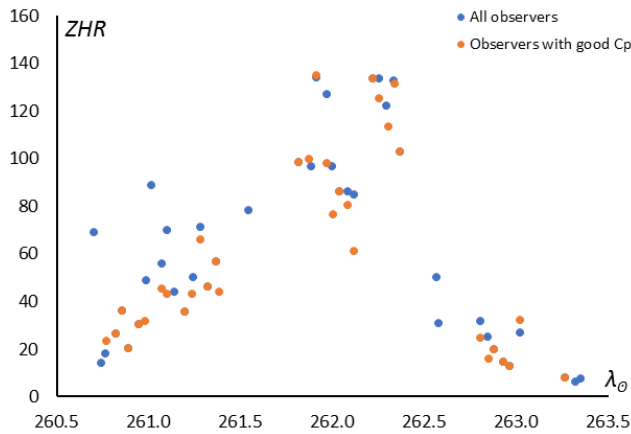

Figure 5 – Comparison between ZHR profiles of Figures 3 and 4. The lower ZHRs of 12–13 December are very clearly visible; the differences in the night of 13–14 December are smaller.

5   The series 1985–2001–2009–2017

Despite the fact that most observers had moderate weather conditions during the Geminids, a "reasonable" reliable ZHR curve emerged from the calculations. It remains a pity that there was not a lot of relatively good data this year to make this analysis more robust. Nevertheless, an attempt has been made to compare the ZHR curve from 2017 with older ZHR curves. This analysis is good for comparison with the years 1985, 1993, 2001 and 2009.

For the sake of clarity, I repeat the conclusions from (Miskotte et al., 2010) again with regard to the series of 1985–2001–2009.

"*To summarize: this series is the best thing to look at the possible evolution in ZHR. It is clearly visible that 1985 was the year with the least activity in this series. The year 2001 scores the highest in terms of ZHR and in 2009 the ZHR is a bit lower than in 2001. If the ZHR in 2017 is lower than in 2009, it is clear that we are in a downward*

trend of the activity of the Geminids. Then the years with the highest ZHRs are already behind us. This period with highest activity will have to be somewhere between 1996 and 2004, see also chapter 6.1".
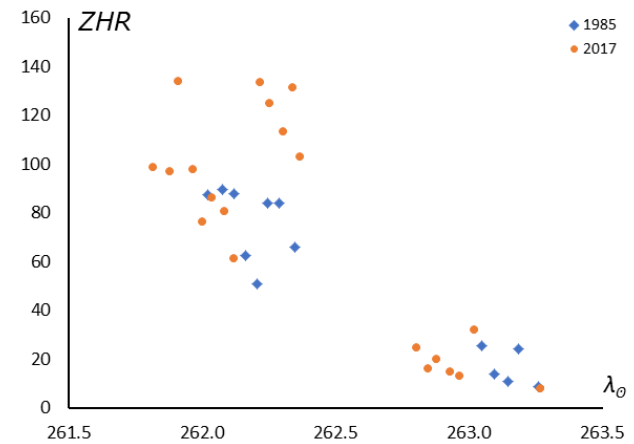
1985–2017 (32 years)

Figure 6 – Comparison between the ZHR curves from 1985 and 2017. It is striking here that the ZHR in 1985 is much lower.

In 1985 the author (Miskotte, 2010 et al.; Miskotte et al., 2011) and Peter Jenniskens (1986) found a double peak. The ZHR curve is based on data from two good observers at one location (Puimichel, southern France), so we must also exercise caution. It would be better when more good data was available from 1985. It is also questionable to what extend the passage of a cirrus field (Jobse, 1986) influences the "dip" between the two peaks. Furthermore, the curve seems to have shifted in solar longitude compared to 2017 by about 0.2 degree, earlier than in 1985. In *Figure 7* we have the same equation as in *Figure 6*, but the ZHR profile for 1985 is moved forward by 0.2 degrees (= ~5 hours).
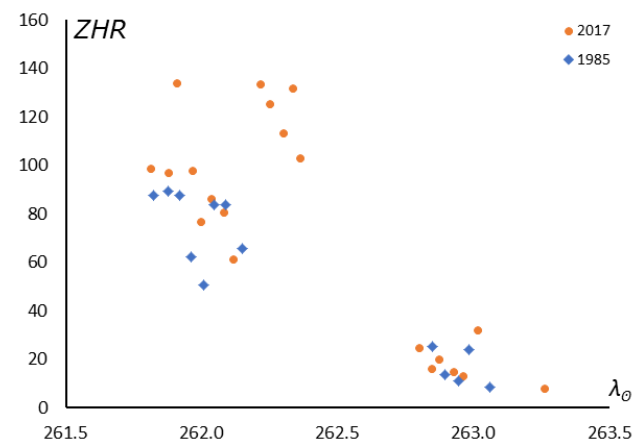

Figure 7 – The same figure as Figure 6, but now the ZHR profile of 1985 has been moved forward by 0.2 degrees. Really good conclusions cannot be drawn here.

The profile of 1985 is based on data from 2 observers at Puimichel (*Klaas Jobse* and *Paul Roggemans*). No observational data is available from $\lambda_\odot = 262.2°$ or later on the IMO site for comparison with the peak in 2017.

2001–2017 (16 years)

Because a peak in activity above America was noticed in 2017, the author decided to look at the IMO site for observational data from known observers in the period of 14 December 2001 after 05ʰ UT. Indeed, about seven North American observers had sent data. However, I was only able to add a limited dataset from two observers with a good C_p determination. These were *Robert Lunsford* (3 hours effective) and *Pierre Martin* (2 hours effective). Their data mutually connects nicely and is included in the *Figures 8 and 9* below.
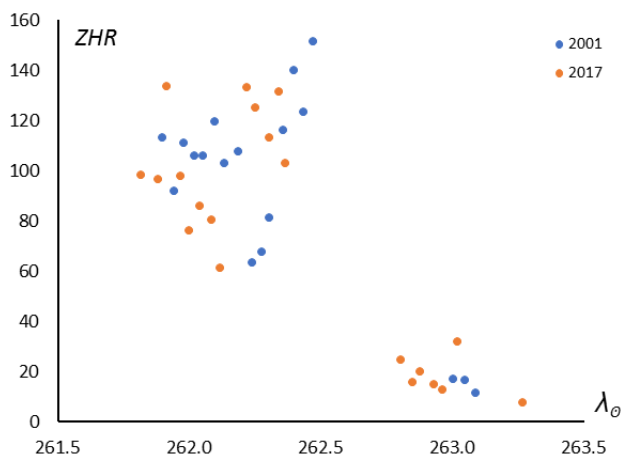

Figure 8 – Comparison between the ZHR curves from 2001 and 2017.

Again, the ZHR curves seem to have shifted relative to each other. Most of the time the ZHR from 2001 is slightly higher than 2017. Data from 2001 by *Robert Lunsford* and *Pierre Martin* has been added for comparison.

If we shift the ZHR curve from 2001 by 0.2 degrees in solar longitude, a different image is created. See *Figure 9* for that result. The result is remarkable; there is suddenly a reasonable agreement with each other! The second peak in 2017 was also seen in 2001 from the US. Based on the data, you could conclude that the 2017 curve shows a slightly lower level than in 2001.
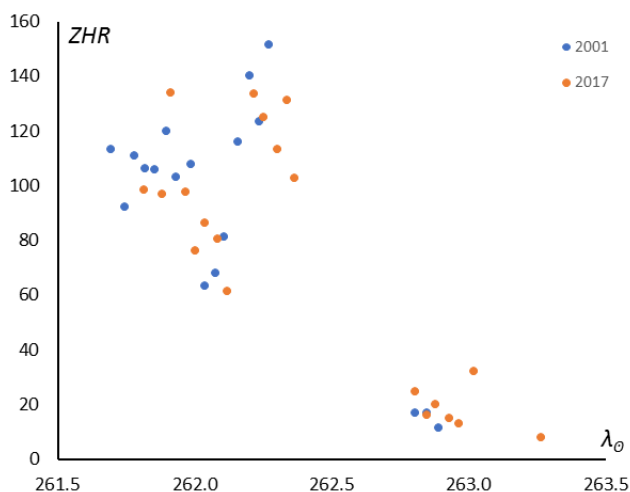

Figure 9 – The same graph as Figure 8, only the solar longitude of 2001 is shifted by 0.2 degrees.

2009–2017 (8 years)

Here too, it was checked whether North American data could be added to the 2009 ZHR curve. It is there but it is all very brief. Only *Wesley Stone* has a nice set of data available, but unfortunately he had varying weather conditions, which often means that too high sky coverage percentages were reported. So his data of that night could not be used.
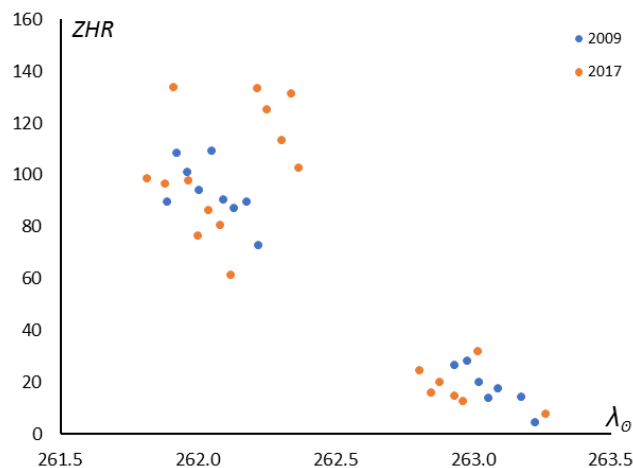

Figure 10 – ZHR comparison between the Geminids of 2009 and 2017.

The ZHR appears to be about 10% lower in 2017 compared with 2009. The points after $\lambda_\odot = 262.2°$ almost all appear outside the 2009 curve. If we apply the same method (shifting the solar longitude) as in the previous series 1985–2017 and 2001–2017, a different picture emerges. It also turns out that a shift forward of the 2009 curve by 0.1 degree (instead of the 0.2 degree of the previous two series) with respect to 2017 gives the best fit. The result is displayed in *Figure 11*. Again a striking resemblance appears. Just as with the comparison from the 2001–2017 series, the high activity in 2017 after $\lambda_\odot = 262.2°$ drops outside the 2009 observation window. The reason is because the 2017 data also contains data from the US.
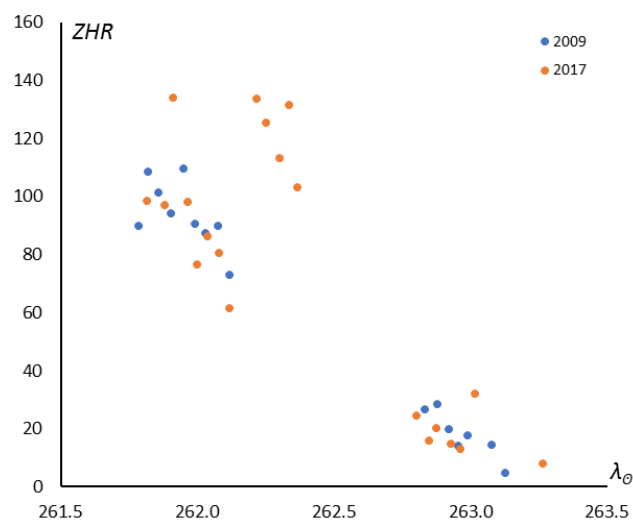

Figure 11 – The same figure as Figure 10. The solar longitude from 2009 has been moved forward by 0.1 degrees with respect to 2017.
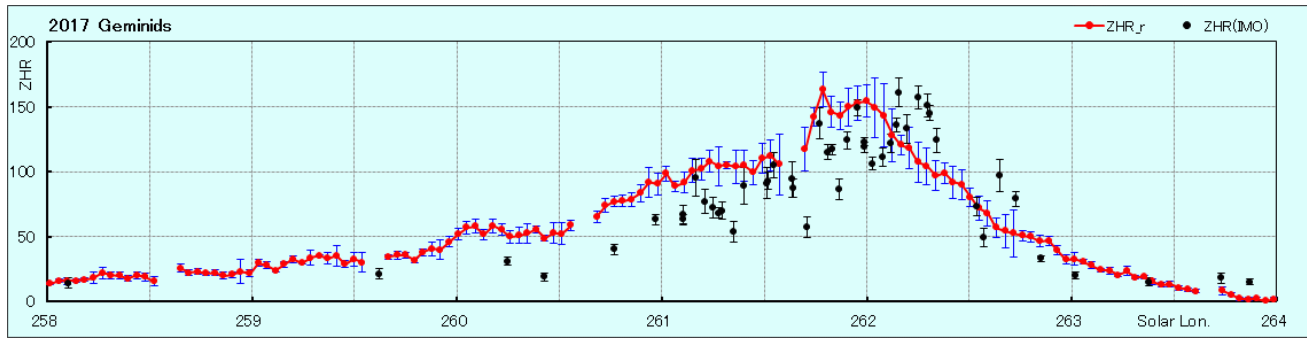
Figure 12 – Radio data Geminids 2017. There is no extra activity at $\lambda_{\odot}$ = 262.45 ± 0.005° (RMOB).

6   Some very cautious conclusions and recommendations

- This analysis clearly showed that there are two peaks, one around $\lambda_{\odot}$ = 261.9° and the second around $\lambda_{\odot}$ = 262.2°. In addition, there seems to be a shift in the time of the maximum in 2017 by 0.1 degree (= ~2.5 hours) earlier compared to 2009, 0.2 degree earlier compared to 2001 and 0.2 degree compared to 1985. That the ZHR profile varies in intensity (the height of the ZHR) is purely depending on the density of the dust trail, but the time in solar longitude is constant for all swarms over a longer period of time. If there is a real shift of ~0.1° after ~10 to 20 years then there must be a physical explanation for this. In the analysis of 2011, a shift of 0.1° and 0.05° is mentioned. In the case of the Geminids with a short orbital period, a shift or regression of the center of the swarm with respect to the orbit of the Earth could sometimes manifest itself in this observed shift. That must be consistent, and not move forward in one year and backwards in the next year. Between 2017 and 2009 are 8 years with a slide of the 2009 profile with 0.1° backwards in solar longitude, the profile of 2001 was shifted 0.2° backwards in solar longitude (16 years), but the profile of 1985 appears also to be shifted by only 0.2° in solar longitude during 32 years. If there is a regression of the core of the swarm then it is probably constant and slightly less than 0.1° between 2009 and 2017, also slightly less than 0.2° between 2001 and 2017 and just over 0.2° between 1985 and 2017. More good observing data obtained during the Geminids maximum in the coming years could provide more clarity here.

- It is interesting to find out if there is mass sorting at both peaks. This is certainly the case immediately after the second peak around $\lambda_{\odot}$ = 262.2°. It is unfortunate that the observations of 2017 are so fragmented; otherwise perhaps something could have been said about the first peak. There is a short period between the two peaks with considerably lower activity. This can easily be 40 to 50% lower than the peak activity. This seems to occur in all years in the series 1985–2001–2009–2017.

- A cautious comparison between 1985, 2001, 2009 and 2017 shows that the activity in 2017 was about 10 to 20% higher than in 1985, 10% lower than in 2001 and 5 to 10% lower than in 2009. The difference between 2001 and 2009 is slightly larger. However, the differences are small and mostly fall within the error margins. Unfortunately, the differences are too small to speak of a clear decrease in activity of the Geminids since 2001–2004.

- However it is very clear that based on visual observations, the maximum activity of the Geminids has NOT risen in the last 15 years. This in contrast to the claim in (Ryabova and Rendtel, 2018). Successful Geminid campaigns worldwide in 2018, 2020 and 2023 could perhaps provide a little more insight into this. The use of "moonlight data" is not recommended.

- Whether the parent body of the Geminids 3200 Phaethon caused extra activity in 2017 at $\lambda_{\odot}$ = 262.45 ± 0.005° (14 December 2017 12.1[h] UT) is very unlikely. Extra activity has not been observed by visual observers because there are no visual observations of around 14 December 2017 12.1[h] UT. The nearest dataset is from *Terrence Ross* of December 14, 2017 around 10[h] UT: they show no strange things, a ZHR of 110 was observed at that time with a magnitude distribution that looks normal. The radio data collected by the Japanese shows nothing strange around $\lambda_{\odot}$ = 262.45 ± 0.005° (see *Figure 12*). This curve is based on worldwide radio data collected by the RMOB[15].

- Again, this troublesome analysis has shown that only data from observers with a reliable C_p determination are eligible for use for a good ZHR analysis. It would be very nice if more observers would observe more often (preferably 15 hours effective or more) in the period from 25 July to the end of August from 0 to 4 hours local time. The more good data is used, the better the analyzes and results will be!

7   Plans for 2018–2020

A number of Dutch observers plan an observing session at the Pic-du-Midi, France, in 2018. Others plan a hit & run expedition to clear weather such as in 2007 and 2009. In 2019, an almost Full Moon will be disturbing. In 2020 there are plans for an observing expedition to Oman. If

---

[15] http://www.rmob.org/livedata/main.php

anyone wants to be kept informed about these plans or if someone wants to take part in a hit & run observing session, please contact the author of this article.

References

Jenniskens P. (1986). "De struktuur van het Geminidenmaximum". *Radiant*, **8**, 58–59.

Jobse K. (1986). "Geminiden 1985, 1600 visuele meteoren vanuit Puimichel". *Radiant*, **8**, 15–16.

Miskotte K., Johannink C., Vandeputte M. and Bus P. (2010). "Geminiden: 30 jaar waarnemingen (1980-2009)". *eRadiant*, **6**, 152–186.

Miskotte K., Johannink C., Vandeputte M. and Bus P. (2011). "Geminids: 30 years of observations (1980–2009)". *WGN, Journal of the IMO*, **39**, 167–186.

Ryabova G. and Rendtel J. (2018). "Increasing Geminid shower activity". *Monthly Notices of the Royal Astronomical Society: Letters*, **475**, L77–L80, https://doi.org/10.1093/mnrasl/slx205.

x Herculids (XHE-346)

Paul Roggemans[1] and Peter Cambell-Burns[2]

[1] **Pijnboomstraat 25, 2800 Mechelen, Belgium**
`paul.roggemans@gmail.com`

[2] **UKMON, Cavendish Gardens, Fleet, Hampshire, United Kingdom**
`peter@campbell-burns.com`

A small but remarkable number of orbits of the x Herculids were recorded by the CAMS BeNeLux network on 12 March 2018. An independent search was made to identify orbits of this shower. One photographic orbit obtained in 1954 and 6 radar orbits obtained between 1961 and 1969 qualify as possible members of this stream. For more recent data ~686000 public available video meteor orbits were searched for XHE orbits.

The 180 video meteors that fit the minimal similarity D criterion with D < 0.105 (Drummond criterion), radiated from R.A. 255.7° and Decl. +48.8° with a geocentric velocity of 34.4 km/s in a time lapse between 339° and 6° in solar longitude with a rather sharp peak around 351.5 ± 0.4°. The orbital elements match perfectly with previously published results. There is no indication for any periodicity in the shower displays from year to year. The XHE-meteors are remarkably rich in bright meteors and rather deficient in faint meteors and belong probably to an old remnant of a dust trail produced by a comet of the Jupiter-family. The distinct concentration of the orbits confirms this minor shower as an established meteor stream.

1 Introduction

In the night of 11–12 March 2018 a number of orbits were identified as belonging to the x Herculids (XHE-346) by the CAMS BeNeLux network. Although the number of orbits is not impressive, the radiants caught attention on the otherwise rather empty shower radiant maps around this time of the year.

Very little is known about this meanwhile established minor shower. The authors decided to search the publicly available orbit data in an attempt to document this minor shower.

Figure 1 – Screenshot of the CAMS radiant plot for the night of 2018 March 12 with the remarkable concentration of radiants identified as XHE (346) orbits.

2 XHE (346) history

A search for earlier recorded orbits that could be associated with this stream in the photographic meteor orbit catalogue with 4873 accurate photographic orbits obtained between 1936 and 2008 resulted in only one similar orbit. This meteor was photographed on 6 March 1954 (Jacchia et al., 1967) and fits with the XHE-reference orbit with a high threshold of $D_D < 0.04$.

The Harvard radar orbit catalogues 1961–1965 and 1968–1969 (Hawkins, 1963) contain only 6 orbits with $D_D < 0.105$ and 3 with $D_D < 0.08$.

The scarce amount of available orbital data explains why this meteor shower has never been detected before. The XHE (346) had to wait until sufficient numbers of video meteor orbits had become available to be detected. We did not check any single station based radiant analyses as the risk of contamination of the data with sporadics is far too high in single station video statistics for the XHE shower.

3 The available orbit data

With two major orbit datasets being recently updated, it was worthwhile to check if and what we can detect about the XHE (346) meteor shower. We have the following data, status as until March 2018, available for our search:

- EDMOND EU+world with 317830 orbits (until 2016). EDMOND collects data from different European networks which altogether operate 311 cameras (Kornos et al., 2014).
- SonotaCo with 257010 orbits (2007–2017). SonotaCo is an amateur video network with over 100 cameras in Japan (SonotaCo, 2009).

- CAMS with 111233 orbits (October 2010 – March 2013), (Jenniskens et al., 2011). For clarity, the CAMS BeNeLux orbits April 2013 – March 2018 are not included in this dataset because this data is still under embargo.

Altogether we can search among 686073 video meteor orbits.

4 Preliminary orbit selection

The triggers for this analysis were the 6 XHE orbits obtained by the CAMS BeNeLux network on 12 March 2018. The authors followed the procedure described in a previous similar analysis (Roggemans and Johannink, 2018) to identify possible XHE orbits. Based on the known parameters we can define a sub-dataset to limit the amount of orbits in time and space to a region where related orbits might be located.

In a first attempt orbits were selected in a period of 1 week before and after 12 March. The length of this interval was increased in small steps until no more extra candidate orbits were detected. All orbits within the following intervals were selected:

- Time interval: $335° < \lambda_{\Theta} < 8°$;
- Radiant area: $242° < \alpha < 273°$ and $+39° < \delta < +59°$;
- Velocity: $31.7 \text{ km/s} < v_g < 38.7 \text{ km/s}$.

In total 377 orbits occurred within these intervals. These 377 orbits were obtained from meteors that appeared in the sky in a way that any single station observer would associate these meteors as XHE shower members, coming from the right direction of the radiant with the right angular velocity expected for this shower. The purpose of analyzing the orbital data is to get an idea how many of these orbits are nothing else than sporadics that contaminate the radiant area and how many of these orbits have enough similarity to form a concentration that indicates the presence of a minor shower.

Although we used the previously known time, radiant position and velocity as bases to define our preselection of orbits, we will not use the orbit from previous research as parent orbit to detect XHE-candidates. The first step is to check to which extend the median values of the selected dataset compare to the literature values. If our dataset contains a concentration of orbits for the XHE shower, the median values should be comparable. We check this for the total dataset as well as for the sub datasets for CAMS, EDMOND and SonotaCo. The results are listed in *Table 1*. All combinations compare well to the orbit found in literature which is a first indication that a significant number of orbits of this shower are included. The median values listed also include the contamination by sporadics because no similarity criteria were applied yet.

We apply three discrimination criteria to evaluate the similarity between the individual orbits taking the median values as parent orbit. The D-criteria used are these of Southworth and Hawkins (1963), Drummond (1981) and Jopek (1993). We consider four different threshold levels of similarity:

- Low: $D_{SH} < 0.25$ & $D_D < 0.105$ & $D_H < 0.25$;
- Medium low: $D_{SH} < 0.2$ & $D_D < 0.08$ & $D_H < 0.2$;
- Medium high: $D_{SH} < 0.15$ & $D_D < 0.06$ & $D_H < 0.15$;
- High: $D_{SH} < 0.1$ & $D_D < 0.04$ & $D_H < 0.1$.

In *Table 2* we filter those orbits that fit the low threshold D-criteria to eliminate the obvious sporadic contamination from the sample. The median values for each set of orbits do not differ too much from *Table 1*, but the comparison is slightly better. In *Table 3* we compare the median values of the orbits according to the four levels of the D-criteria threshold. Again the resulting orbits for each of the levels of similarity show very little variation. Whether we consider the preselected dataset as a whole, or if we consider the different networks with or without D-criteria, all have about the same median values.

Table 1 – The median values for each sub-set of orbits, CAMS, SonotaCo and EDMOND, compared to the reference orbit from literature (Jenniskens et al., 2018).

	CAMS	SonotaCo	Edmond	All	Reference (2018)
α_g	256.7°	254.8°	258.8°	256.8°	257.8°
δ_g	+49.1°	+49.0°	+49.0°	+49.0°	+48.7°
v_g	35.6	34.9	34.5	34.8	34.7
a	3.17	2.76	2.70	2.75	2.74
q	0.983	0.979	0.985	0.983	0.982
e	0.692	0.647	0.636	0.645	0.642
ω	191.04°	195.02°	190.16°	192.07°	191.1°
Ω	350.87°	351.67°	351.74°	351.66°	352.4°
i	60.0°	59.1°	59.0°	59.1°	59.4°
N	42	128	207	377	86

Table 2 – The median values for each sub-set of orbits, CAMS, SonotaCo and EDMOND with $D_D < 0.105$, compared to the reference orbit from literature (Jenniskens et al., 2018).

	CAMS	SonotaCo	Edmond	All	Reference (2018)
α_g	254.8°	255.2°	257.2°	256.4°°	257.8°
δ_g	+48.7°	+48.8°	+48.8°	+48.8°	+48.7°
v_g	35.1	34.5	34.2	34.5	34.7
a	2.69	2.63	2.54	2.58	2.74
q	0.981	0.981	0.985	0.983	0.982
e	0.642	0.626	0.613	0.618	0.642
ω	195.01°	194.82°	192.31°	194.05°	191.1°
Ω	351.88°	351.75°	351.88°	351.86°	352.4°
i	60.6°	59.1°	59.0°	59.2°	59.4°
N	18	67	97	182	86

Table 3 – The median values for the selected orbits with four different threshold levels on the D-criteria, compared to the reference orbit from literature (Jenniskens et al., 2018).

	Low	Medium low	Medium high	High	Reference (2018)
α_g	256.4°	255.5°	254.8°	254.1°	257.8°
δ_g	+48.8°	+48.8°	+48.9°	+49.2°	+48.7°
v_g	34.5	34.5	34.5	34.6	34.7
a	2.58	2.64	2.66	2.68	2.74
q	0.983	0.981	0.980	0.979	0.982
e	0.618	0.627	0.631	0.635	0.642
ω	194.05°	194.49°	195.42°	196.19°	191.1°
Ω	351.86°	351.69°	351.47°	351.18°	352.4°
i	59.2°	59.3°	59.4°	59.1°	59.4°
N	182	137	89	47	86
S	52%	64%	76%	88%	

Table 3 shows the percentage (S) of orbits of the sample that fails to fulfill the D-criteria and must be considered as sporadic contamination of the radiant area. The remainder is an indication for the evidence of the presence of a dust concentration within the sample.

The presence of a cluster of very similar orbits in the dataset becomes very obvious in the graph of the inclination i (°) against the length of perihelion Π (°) (*Figure 2*).
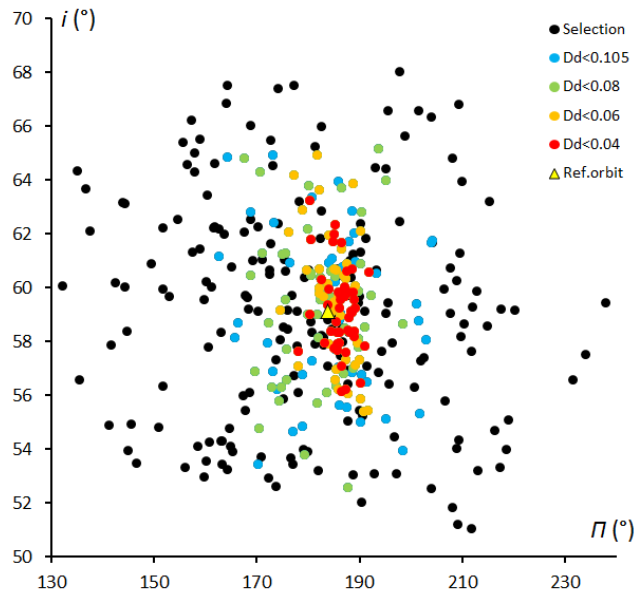

Figure 2 – The plot of inclination i (°) against the length of perihelion Π (°) for the 377 preselected orbits. The colors mark the different threshold levels of the D-criteria relative to the parent orbit defined by the median values of the entire dataset.

5   Final orbit selection

In the preliminary investigation we used the median values based on the entire dataset including the natural contamination by sporadics as a parent orbit to approach the cluster of similar orbits. In the final approach the median values for the 47 orbits that fit the high threshold D-criteria are taken as parent orbit to recalculate the individual D-criteria for each of the 377 selected orbits.

For reason of completeness we repeat the procedure explained in *section 4*, but based on the parent orbit obtained from the 47 orbits that fit the high threshold criteria.

Table 4 – The median values for each sub-set of orbits, CAMS, SonotaCo and EDMOND with $D_D < 0.105$ using the high threshold orbit from Table 3 as parent orbit. All compared to the reference orbit from literature (Jenniskens et al., 2018).

	CAMS	SonotaCo	Edmond	All	Reference (2018)
α_g	255.4°	254.8°	256.7°	255.7°	257.8°
δ_g	+48.6°	+48.8°	+48.8°	+48.8°	+48.7°
v_g	35.1	34.5	34.2	34.4	34.7
a	2.68	2.63	2.54	2.57	2.74
q	0.981	0.980	0.983	0.981	0.982
e	0.641	0.626	0.613	0.618	0.642
ω	195.17°	195.14°	193.29°	194.42°	191.1°
Ω	351.84°	351.70°	351.91°	351.80°	352.4°
i	60.6°	59.1°	59.0°	59.1°	59.4°
N	17	67	96	180	86

Table 5 – The median values for the selected orbits with four different threshold levels on the D-criteria using the high threshold orbit from Table 3 as parent orbit. All compared to the reference orbit from literature (Jenniskens et al., 2018).

	Low	Medium low	Medium high	High	Reference (2018)
α_g	255.7°	254.8°	254.2°	253.4°	257.8°
δ_g	+48.8°	+48.8°	+48.9°	+49.2°	48.7°
v_g	34.4	34.4	34.5	34.5	34.7
a	2.57	2.57	2.64	2.67	2.74
q	0.981	0.980	0.979	0.978	0.982
e	0.618	0.617	0.627	0.633	0.642
ω	194.42°	195.17°	196.13°	196.35°	191.1°
Ω	351.80°	351.65°	351.28°	351.05°	352.4°
i	59.1°	59.1°	59.2°	58.9°	59.4°
N	180	127	92	53	86
S	52%	66%	76%	86%	

Table 4 and 5 show that the final resulting orbit is only slightly different whether we look at different sub datasets or when we consider a higher or lower threshold level on the D-criteria. Regardless of the approach, we arrive at an orbit which matches closely with the value found in literature, except for a slight difference in the argument of perihelion. *Figure 3* shows the high concentration of orbits near the reference orbit with some dispersion in inclination. The black dots represent orbits that fail to fulfill the D-criteria and represent 52% of the sample as

sporadic contamination. The blue dots also display a rather large dispersion as their orbits just fulfill the weakest discrimination criteria to consider the degree of similarity with the parent orbit.
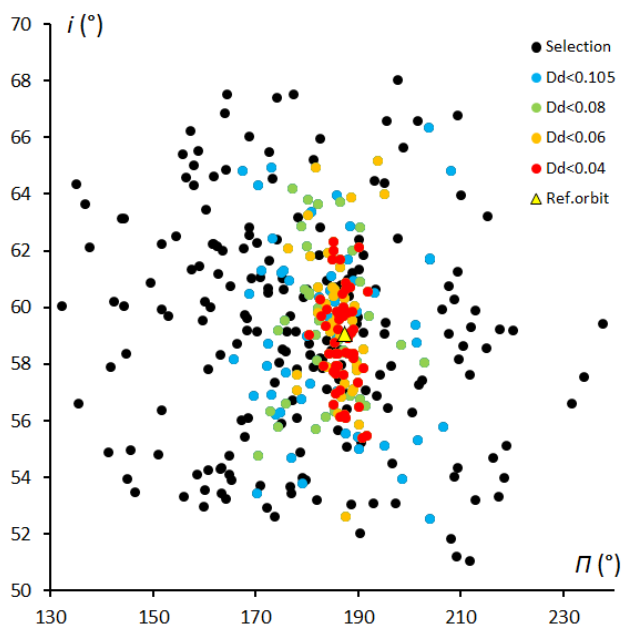

Figure 3 – The plot of inclination i (°) against the length of perihelion Π (°) for the 377 preselected orbits. The colors mark the different threshold levels of the D-criteria relative to the parent orbit based on the median values of the 47 orbits to fulfill the high threshold D-criteria.

6 Case study XHE-346: results

The final sample of 180 probable XHE-346 orbits includes 17 CAMS orbits (from 42), 96 EDMOND orbits (from 207) and 67 SonotaCo orbits (from 128). Although 48% of the preselected orbits qualified as probable XHE-346 members with the minimal threshold, only 14% fit the high threshold D-criteria, indicating a high contamination of the region with sporadic orbits.

The activity period and profile

The first XHE-346 orbit was registered at $\lambda_{\odot} = 339.5°$, the last at $\lambda_{\odot} = 5.3°$. This corresponds to an activity period from roughly 28 February until 26 March. The main activity takes place in the time interval $347° < \lambda_{\odot} < 358°$, or 8 March until 18 March, with the peak XHE activity on 12 March at $\lambda_{\odot} = 351.5±0.4°$ (*Figure 4*). There is no indication for any annual variation in XHE activity. The variation in number of orbits collected year by year reflects the total amount of orbits contributed by all the camera networks (see *Table 6*). Since no hourly rates can be determined for this kind of minor showers, the number of orbits collected for each degree in solar longitude provides an indication of the activity profile, showing the activity period as well as the solar longitude at which the largest number of orbits has been collected. The activity period to check for XHE-346 orbits can be defined as $\lambda_{\odot} > 339°$ and $\lambda_{\odot} < 6°$. This profile is given in *Figure 4*. Note the relative sharp peak at $\lambda_{\odot max} = 351.5±0.4°$, which occurs each year at about the 12th of March.

Table 6 – The number of XHE-346 orbits per year ($D_D < 0.105$).

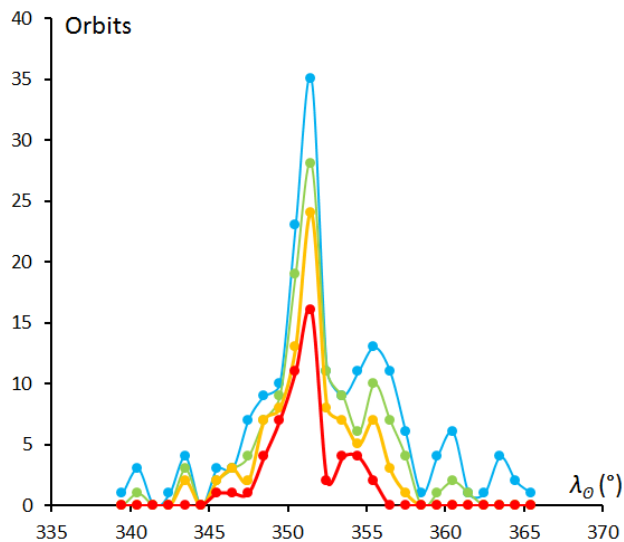| Year	Orbits	Year	Orbits
2006	0	2012	18
2007	6	2013	26
2008	4	2014	27
2009	17	2015	28
2010	7	2016	17
2011	23	2017	7

Figure 4 – The number of XHE-346 orbits collected per degree of solar longitude $\lambda_{\odot}$ during the period 2007–2017 with blue for $D_D < 0.105$, green for $D_D < 0.08$, orange for $D_D < 0.06$ and red for $D_D < 0.04$.

The radiant position, drift and diameter

With a radiant position at $\alpha = 355.7°$ and $\delta = +48.8°$, valid at $\lambda_{\odot} = 351.5°$ the radiant drift can be easily determined. The selection of radiant positions that fulfill the low threshold criteria displays a too large scatter, which may be an indication that this criterion is too weak to eliminate all sporadic outliers. The medium low and medium high threshold levels cover a relevant time span with an acceptable spread on the positions. The high threshold
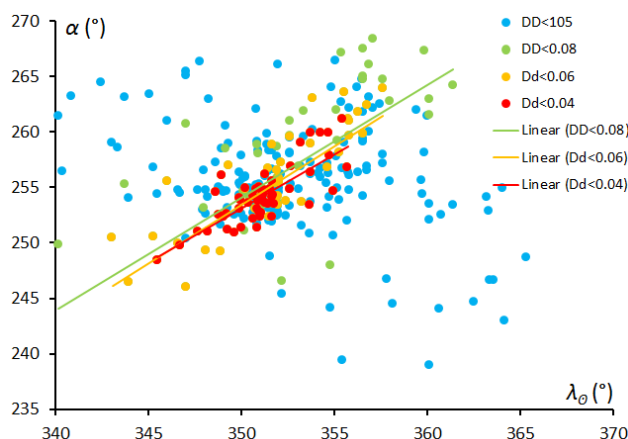

Figure 5 – Radiant drift in Right Ascension α against solar longitude $\lambda_{\odot}$. The different colors represent the 4 different levels of similarity.

level is less suitable as this represents a too short time span. As a compromise we use the medium high threshold ($D_D < 0.06$) position to obtain the radiant drift (see *Figures 5 and 6*). This results in the following radiant drift:

$$\Delta\alpha = 1.05°/\lambda_\odot \text{ and } \Delta\delta = -0.22°/\lambda_\odot.$$

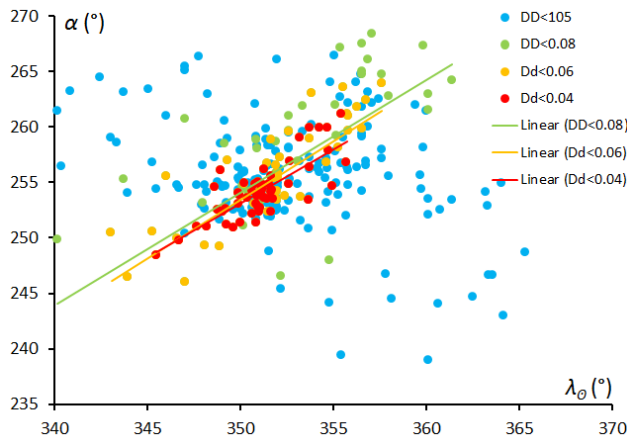*Figure 6* – Radiant drift in declination δ against solar longitude $\lambda_\odot$. The different colors represent the 4 different levels of similarity.

In order to get an idea of the size of the radiant we apply the radiant drift correction to get a plot of the radiant positions corrected for the daily motion (*Figure 8*). This shows a compact radiant slightly elongated in declination. Compared to the original, uncorrected radiant positions (*Figure 7*) the scatter of the radiants that failed to fulfill the D criteria increases considerably. Some radiants for orbits with a weak similarity get more diffused and may indicate that these orbits are sporadics that fit within the low threshold by pure chance. The higher the threshold level the more concentrated the radiant drift corrected positions become.
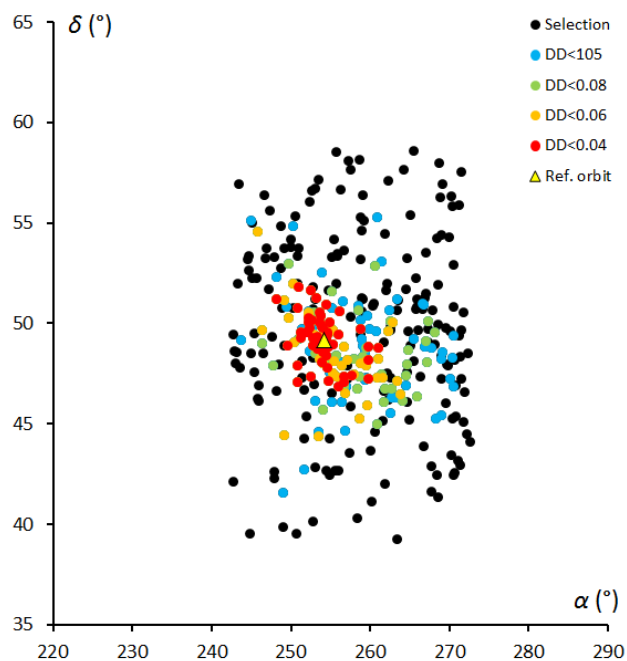

Figure 7 – Plot of the 377 radiant positions as selected. The different colors represent the 4 different levels of similarity according to different threshold levels in the D-criteria.
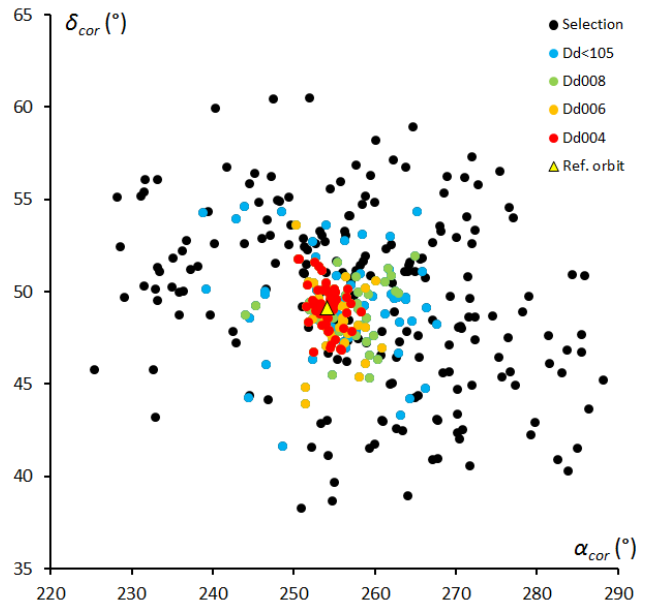

Figure 8 – Plot of the radiant drift corrected radiant positions. The different colors represent the 4 different levels of similarity.

Other shower characteristics

The x Herculids (346) are deficient in faint meteors and rich in medium bright meteors, which may indicate that this is a leftover of an old meteor stream. With a geocentric velocity v_g of 34.4 km/s, the XHE-346 are slightly faster than the Geminids (GEM-4) with 33.8 km/s and slower than the Quadrantids (QUA-10) with 40.7 km/s. The median value for the starting height with 96.2 ± 4.2 km and an ending height of 84.4 ± 6.0 km compares perfectly with the values found for the Geminids (Roggemans, 2017).

Dr. Peter Jenniskens (2016) classified this shower with the Jupiter-family comets although its inclination is rather high compared to most showers in this group.

The final orbits obtained in our analyses are listed in *Table 7* and compared to the only two relevant references available for the x Herculids so far. The results of this analysis match with the references. In order to visualize the distribution of the 53 individual orbits which fulfill the high threshold ($D_D < 0.04$) in space, we plot these orbits in *Figure 9* and compare these with the final result based on the median values plotted in red. The 3D view displays the scatter on the individual orbits. Seen from a position in the ecliptic plane the scatter at the aphelia becomes better visible on the orbits with an inclination of about 59° relative to the ecliptic plane (*Figure 10*). *Figure 11* presents a view as seen from a position in the orbital plane of the x Herculids and shows the scatter in inclination better.

It is obvious that the gravitational forces of planet Jupiter account to a large extent for the orbital evolution of the dust trail that once may have been released by a Jupiter family comet. The dispersion in inclination we noticed in *Figure 3* for instance is most likely the result of these gravitational forces.

Table – 7 The orbital data for the x Herculids (XHE-346) all J2000, the standard deviation σ is listed as ± where available.

| $\lambda_{\odot}$ (°)	α_g (°)	δ_g (°)	$\Delta\alpha$ (°)	$\Delta\delta$ (°)	v_g km/s	a AU	q AU	e	ω (°)	Ω (°)	i (°)	N	Source
350	253.0	+49.2	+0.48	-0.10	35.2	2.99	0.975	0.673	196.7	350.0	59.8	5	Jenniskens et al. (2016)
352.4	257.8	+48.7	–	–	34.7	2.74	0.982	0.642	191.1	352.4	59.4	86	Jenniskens et al. (2018)
351.8	255.7 ±5.7	+48.8 ±2.1	–	–	34.4 ±1.4	2.57 ±0.46	0.981 ±0.011	0.618 ±0.058	194.4 ±7.1	351.8 ±4.7	59.1 ±2.6	180	This analysis $D_D < 0.105$
351.6	254.8 ±4.7	+48.8 ±1.7	+1.02	–0.22	34.4 ±1.2	2.57 ±0.32	0.980 ±0.009	0.617 ±0.043	195.2 ±5.4	351.6 ±3.5	59.1 ±2.3	127	This analysis $D_D < 0.08$
351.3	254.2 ±3.6	+48.9 ±1.6	+1.05	–0.22	34.5 ±1.1	2.64 ±0.27	0.979 ±0.007	0.627 ±0.037	196.1 ±3.8	351.3 ±2.8	59.2 ±2.1	92	This analysis $D_D < 0.06$
351.1	253.9 ±2.6	+49.2 ±1.2	+0.97	–0.12	34.5 ±0.9	2.67 ±0.20	0.978 ±0.005	0.633 ±0.026	196.4 ±2.7	351.1 ±2.1	58.9 ±1.7	53	This analysis $D_D < 0.04$
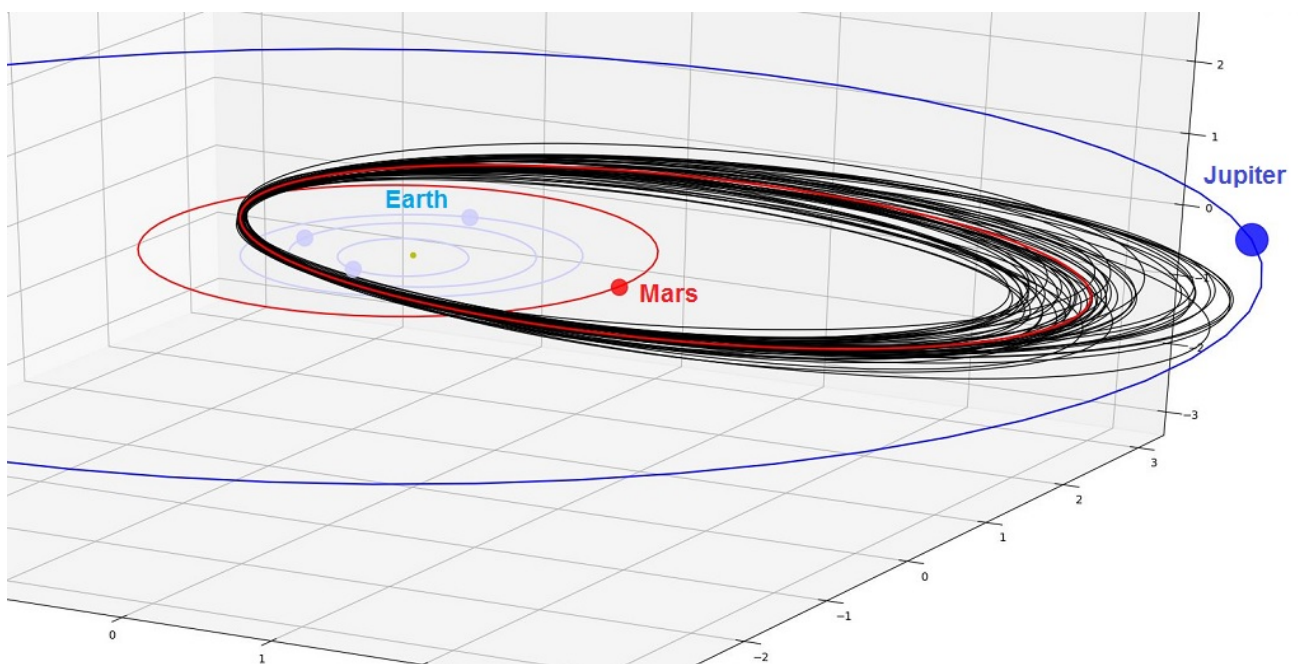
Figure 9 – A 3D view of the final 53 orbits that fulfill the high threshold D-criterion with $D_{SH} < 0.1$ & $D_D < 0.04$ & $D_H < 0.1$, with the final resulting orbit based on the median values of the orbital elements for the x Herculids (#346) in this case study. (Author Peter Cambell-Burns).
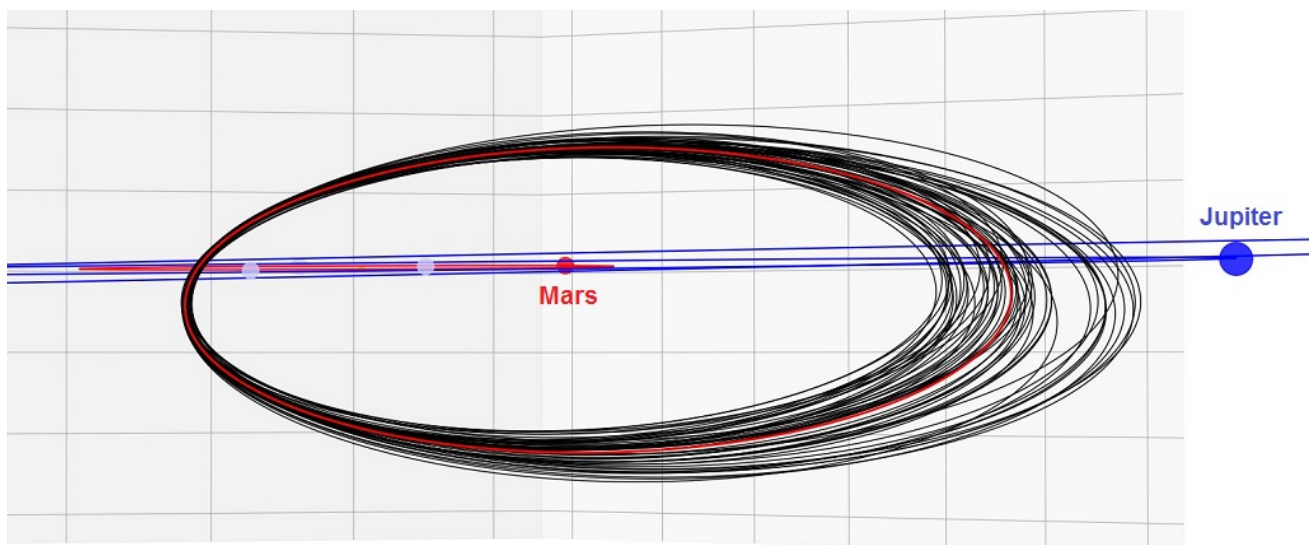

Figure 10 – A view as seen from a position in the ecliptic plane at the concentration of the 53 x Herculids orbits (black) and the final resulting orbit (red), with an inclination of 58.9 ± 1.7 ° relative to the ecliptic. (Author Peter Cambell-Burns).
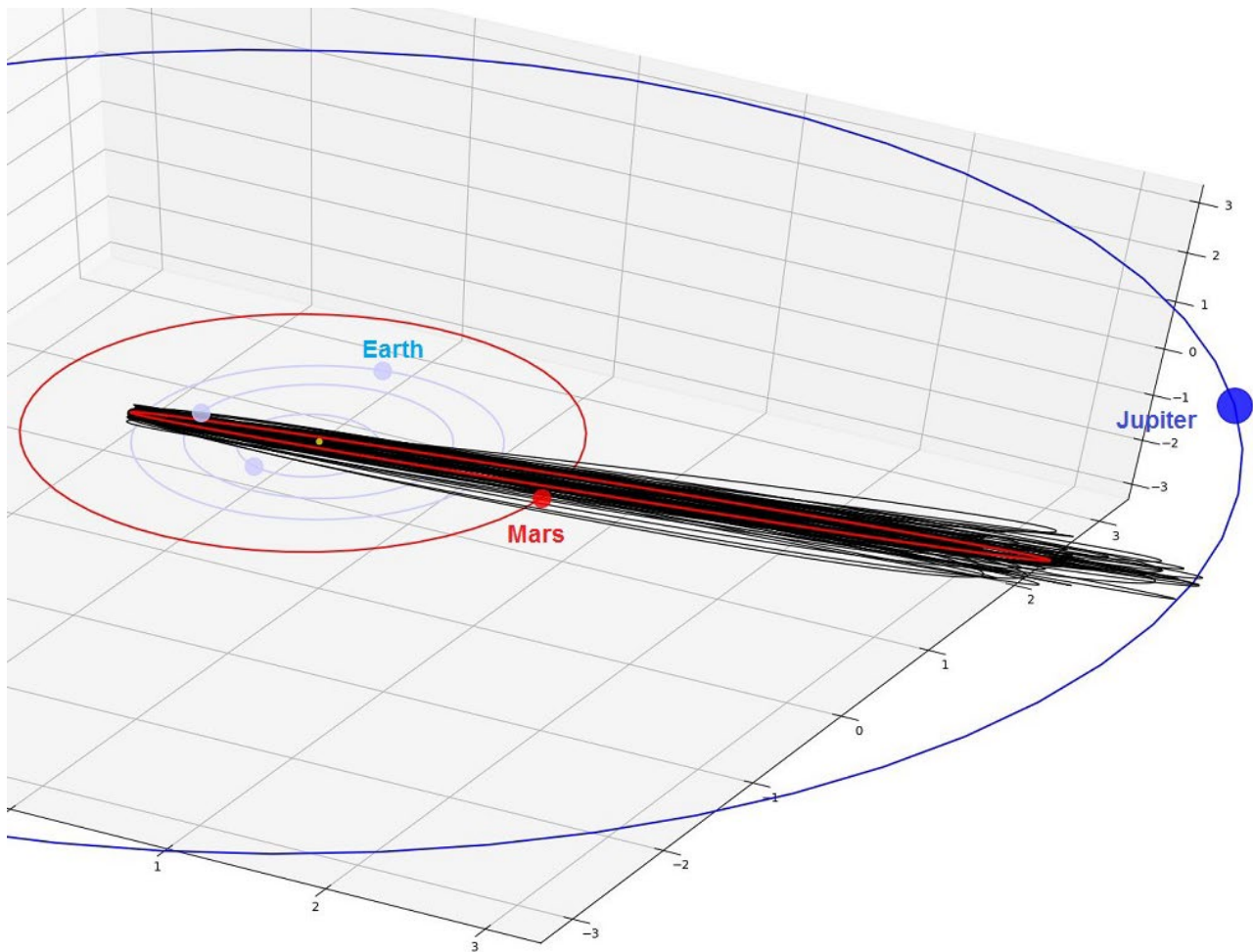
Figure 11 – View from a position in the orbital plane of the x Herculids meteor stream with the 53 x Herculids orbits (black) and the final resulting orbit (red) . (Author Peter Cambell-Burns).

7   Conclusion

A search on the orbital data from the major video camera networks worldwide, good for ~686000 orbits (status March 2018), resulted in 180 candidate XHE-orbits. 53 orbits fulfill the high threshold D-criteria of $D_D < 0.04$. An analysis of the available orbits proved the presence of a distinct cluster of similar orbits independently from previous stream searches. The resulting reference orbit compares very well with the previously published orbits.

Members of this shower have been detected every year since 2007 in a time span between 339° and 6° in solar longitude with a rather sharp maximum at about $\lambda_\Theta = 351.5\pm0.4°$. There is no indication of any periodicity in the stream activity. The abundant proportion of bright meteors and deficiency in faint meteors indicate that this is an old dust stream probably associated with a Jupiter-family comet.

Acknowledgment

References

Drummond J. D. (1981). "A test of comet and meteor shower associations". *Icarus*, **45**, 545–553.

Hawkins G. S. (1963). "The Harvard radio meteor project". *Smithsonian Contributions to Astrophysics*, **7**, 53–62.

Jacchia L., Verniani F. and Briggs R. E. (1967). "An Analysis of the Atmospheric Trajectories of 413 Precisely Reduced Photographic Meteors". *Smithsonian Contributions to Astrophysics*, **10**, 1–139.

Jenniskens P., Gural P. S., Grigsby B., Dynneson L., Koop M. and Holman D. (2011). "CAMS: Cameras for Allsky Meteor Surveillance to validate minor meteor showers". *Icarus*, **216**, 40–61.

Jenniskens P., Nénon Q., Albers J., Gural P.S., Haberman B., Holman D., Morales R., Grigsby B.J., Samuels D., Johannink C. (2016). "The established meteor showers as observed by CAMS". *Icarus*, **266**, 331–354.

Jenniskens P., Baggaley J., Crumpton I., Aldous P., Pokorny P., Janches D., Gural P.S., Samuels D., Albers J., Howell A., Johannink C., Breukers M.,

Odeh M., Moskovitz N., Collison J., and Ganjuag S. (2018). "A survey of southern hemisphere meteor showers". *Planetary Space Science*, **154**, 21–29.

Jopek T. J. (1993). "Remarks on the meteor orbital similarity D-criterion". *Icarus*, **106**, 603–607.

Kornoš L., Matlovič P., Rudawska R., Tóth J., Hajduková M. Jr., Koukal J., and Piffl R. (2014). "Confirmation and characterization of IAU temporary meteor showers in EDMOND database". In Jopek T. J., Rietmeijer F. J. M., Watanabe J., Williams I. P., editors, *Proceedings of the Meteoroids 2013 Conference*, Poznań, Poland, Aug. 26-30, 2013. A.M. University, pages 225–233.

Roggemans P. (2017). "Variation in heights of CAMS meteor trajectories". *eMetN*, **2**, 80–86.

Roggemans P. and Johannink C. (2018). "A search for December alpha Bootids (497)". *eMetN*, **3**, 64–72.

SonotaCo (2009). "A meteor shower catalog based on video observations in 2007-2008". *WGN, Journal of the International Meteor Organization*, **37**, 55–62.

Southworth R. R. and Hawkins G. S. (1963). "Statistics of meteor streams". *Smithson. Contrib. Astrophys.*, **7**, 261–286.

February Hydrids (FHY-1032)

Paul Roggemans[1] and Peter Cambell-Burns[2]

[1] **Pijnboomstraat 25, 2800 Mechelen, Belgium**
paul.roggemans@gmail.com

[2] **UKMON, Cavendish Gardens, Fleet, Hampshire, United Kingdom**
peter@campbell-burns.com

CAMS reported an outburst of an unknown minor stream on 14 February 2018, listed in the IAU working list of meteor showers as #1032 FCM ($\alpha = 124°$, $\delta = +2°$, $\lambda_\odot = 324°$, $v_g = 16.5$ km/s). This analysis shows that many similar orbits can be found in the time span and region in space around the reference orbit. The term 'outburst' is rather misleading as only few orbits were detected during several nights. A search through all public available orbit catalogues resulted in a significant number of similar orbits, but the region proves to be rich in unrelated similar sporadic meteors that fulfill low and medium low D-criteria. This case study on the possible February Hydrids did not result in a convincing evidence for the existence of this minor shower. Both the distribution of the number of similar orbits and the spreading in space indicate the possible presence of a diffuse minor shower without any distinct peak activity. This is a case of a barely detectable minor stream.

1   Introduction

February 2018 was an exceptional favorable month for the CAMS BeNeLux network with as many as 16 nights with more than 100 orbits. 13–14 February was the most successful night with 364 orbits. *Dr. Peter Jenniskens* drew the network coordinator's attention to a possible outburst for which the CAMS BeNeLux network had recorded some orbits. The new shower got listed as #1032 FCM ($\alpha = 124°$, $\delta = 2°$, $\lambda_\odot = 324°$, $v_g = 16.5$ km/s). More orbits of this shower were found in the period 9–16 February as well as in previous years.
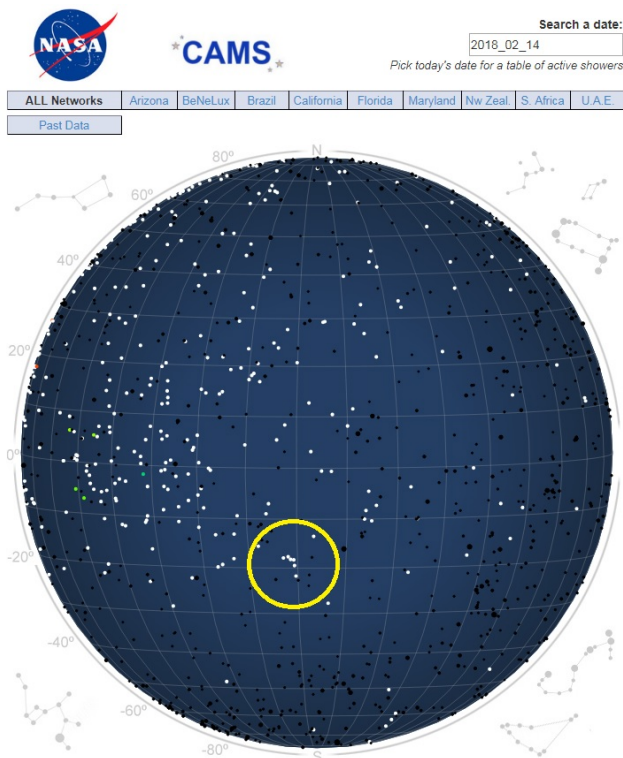

Figure 1 – The discovery of the February Hydrids (FHY-1032) with a few radiants around $\lambda = 198.7°$ and $\beta = –18.2°$ with $v_g \sim 16.4$ km/s.

The term outburst raises the expectation that suddenly a significant number of orbits were found to identify a distinct dust trail based on similar orbits. The reality is far less spectacular. The online CAMS tool[16] allows checking the results for all the CAMS networks. CAMS BeNeLux had the best conditions with 325 orbits on 13 February and 364 orbits on 14 February; the night of 15 February was clouded out. Only a few orbits were collected as candidate FHY-meteors. CAMS California collected 255 orbits on 13 Feb., 135 on 14 Feb. and 204 on 15 Feb. and had few extra candidates. CAMS United Arab Emirates had respectively 37, 40 and 36 orbits for the three nights and one candidate orbit. CAMS Arizona suffered bad weather and had only 9 obits on 14 February with 1 candidate FHY-orbit. The other CAMS networks had bad weather or did not work these nights.

Altogether, the evidence for a new meteor shower is rather thin and therefor the authors decided to search for more evidence in the publicly available meteor orbit catalogues.

2   The available orbit data

We have the following data, status as until April 2018, available for our search:

- EDMOND EU+world with 317830 orbits (until 2016). EDMOND collects data from different European networks which altogether operate 311 cameras (Kornos et al., 2014).
- SonotaCo with 257010 orbits (2007–2017). SonotaCo is an amateur video network with over 100 cameras in Japan (SonotaCo, 2009).
- CAMS with 111233 orbits (October 2010 – March 2013), (Jenniskens et al., 2011). For clarity, the CAMS orbits April 2013 – April 2018 are not included in this dataset because this data is still under embargo.

---

[16] http://cams.seti.org/FDL/index-cams.html

Altogether we can search among 686073 video meteor orbits.

3   Preliminary orbit selection

The authors followed the procedure described in a previous similar analysis (Roggemans and Johannink, 2018) to identify possible FHY orbits. Based on the known radiant position, velocity and date of activity, we can define a sub-dataset to limit the amount of orbits in time and space to a region where related orbits might be located.

Orbits were selected in a period of 15 days before and after 14 February. All orbits within the following intervals were selected:

- Time interval: $309° < \lambda_O < 340°$;
- Radiant area: $108° < \alpha < 139°$ and $-9° < \delta < +12°$;
- Velocity: 11 km/s $< v_g < 22$ km/s.

In total 461 orbits occurred within these intervals, 173 from SonotaCo, 158 from EDMOND and 130 from CAMS data. These 461 orbits were obtained from meteors that appeared in the sky in a way that any single station observer would associate these meteors as FHY shower members, coming from the right direction of the radiant with the right angular velocity expected for this shower. The purpose of analyzing the orbital data is to get an idea how many of these orbits are nothing other than sporadics that contaminate the radiant area and how many of these orbits have enough similarity to form a concentration that proves the presence of a minor shower.

The median values for these 461 orbits compare very well with the orbital parameters given by Jenniskens et al. (2018). The error margins σ represents the standard deviation:

- $\lambda_O = 321.4°$
- $\alpha = 126.5 \pm 8.0°$
- $\delta = +3.72.0 \pm 5.8°$
- $v_g = 16.9 \pm 2.9$ km/s
- $a = 2.4 \pm 3.0$ AU
- $q = 0.783 \pm 0.09$ AU
- $e = 0.674 \pm 0.08$
- $\omega = 61.4 \pm 13.9°$
- $\Omega = 141.4 \pm 7.8°$
- $i = 7.2 \pm 3.0°$

We apply three discrimination criteria to evaluate the similarity between the individual orbits taking the median values of the 461 selected orbits as parent orbit. The D-criteria used are these of Southworth and Hawkins (1963), Drummond (1981) and Jopek (1993). We consider four different threshold levels of similarity:

- Low: $D_{SH} < 0.25$ & $D_D < 0.105$ & $D_H < 0.25$;
- Medium low: $D_{SH} < 0.2$ & $D_D < 0.08$ & $D_H < 0.2$;
- Medium high: $D_{SH} < 0.15$ & $D_D < 0.06$ & $D_H < 0.15$;
- High: $D_{SH} < 0.1$ & $D_D < 0.04$ & $D_H < 0.1$.

315 orbits fulfill the D-criteria compared to the median values of our 461 orbits as parent orbit. If our dataset contains a concentration of orbits for the FHY shower, the median values should be comparable. The results are shown in *Table 1* and differ slightly from the reference orbit.

Table 1 – The median values for the selected orbits with four different threshold levels on the D-criteria, compared to the reference orbit from literature (Jenniskens et al., 2018).

	Low	Medium low	Medium high	High	Reference (2018)
λ_O	322.7°	322.5°	322.1°	321.4°	324.3°
α_g	125.9°	126.1°	125.8°	125.4°	123.9°
δ_g	+3.9°	+4.4°	+4.3°	+5.5°	+1.5°
v_g	16.9	16.9	16.9	16.9	16.4
a	2.42	2.43	2.43	2.42	2.68
q	0.785	0.786	0.787	0.780	0.812
e	0.676	0.678	0.677	0.675	0.697
ω	60.6°	60.6°	60.6°	61.3°	55.5°
Ω	142.7°	142.5°	142.1°	141.4°	144.3°
i	7.2°	7.0°	7.0°	6.9°	8.3°
N	315	221	126	44	17
S	*32%*	*52%*	*73%*	*90%*	

Table 1 shows the percentage (S) of orbits of the sample that fails to fulfill the D-criteria and must be considered as sporadic contamination of the radiant area. The remainder is an indication for the presence of a possible dust concentration within the sample.
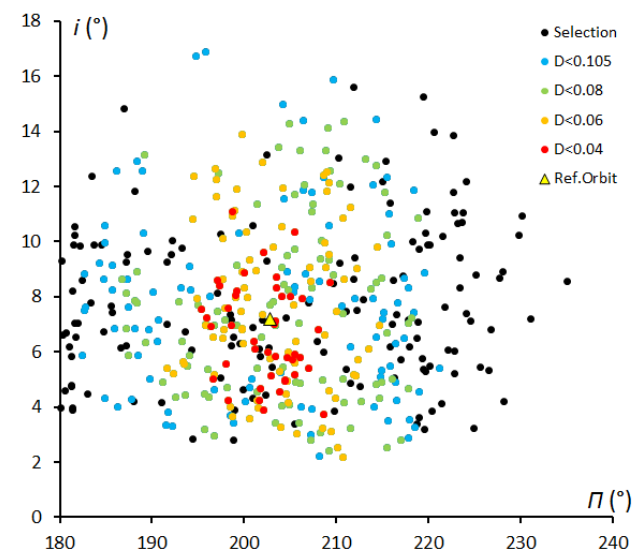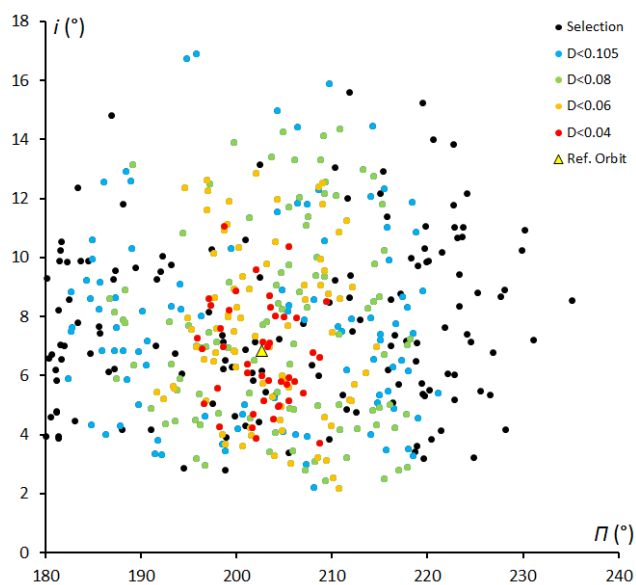

Figure 2 – The plot of inclination i (°) against the length of perihelion Π (°) for the 461 preselected orbits. The colors mark the different threshold levels of the D-criteria relative to the parent orbit defined by the median values of the entire dataset corresponding to the results in Table 1.

When we plot the graph for all 461 orbits with inclination *i* against length of perihelion *Π*, we see a rather dispersed picture (*Figure 2*). The spreading in length of perihelion is

rather large even for those orbits that fulfill the low, medium low and medium high threshold. Only orbits which fit the high threshold D-criteria show less dispersion but there is no real concentration of orbits. This could indicate that we are comparing sporadic orbits that fulfill the D-criteria by pure chance. Since we use the medium values of all selected orbits, this includes indeed some sporadic contamination.

In the next step we take the median values for the orbits that fulfill the high threshold D-criteria ($D_{SH} < 0.1$ & $D_D < 0.04$ & $D_H < 0.1$, *Table 1*) as parent orbit to recalculate the D-criteria for all 461 orbits of the dataset. The results are listed in *Table 2*. The median values for all orbits for each level of threshold on the D-criteria differ slightly from the reference orbit given by Jenniskens et al.

Table 2 – The median values for the selected orbits with four different threshold levels on the D-criteria, using the high threshold orbit from Table 1 as parent orbit, compared to the reference orbit from literature (Jenniskens et al., 2018).

	Low	Medium low	Medium high	High	Reference (2018)
$\lambda_\odot$	322.6°	322.4°	321.8°	321.1°	324.3°
α_g	126.0°	126.1°	125.6°	126.1°	123.9°
δ_g	+4.0°	+4.5°	+4.6°	+5.8°	+1.5°
v_g	16.9	16.9	16.9	16.9	16.4
a	2.42	2.42	2.46	2.43	2.68
q	0.785	0.785	0.787	0.779	0.812
e	0.676	0.678	0.680	0.675	0.697
ω	60.7°	60.8°	60.6°	61.5°	55.5°
Ω	142.6°	142.4°	141.8°	141.1°	144.3°
i	7.2°	7.0°	7.0°	6.6°	8.3°
N	317	221	123	43	17
S	*31%*	*52%*	*73%*	*91%*	

Figure 3 – The plot of inclination i (°) against the length of perihelion Π (°) for the 461 preselected orbits. The colors mark the different threshold levels of the D-criteria relative to the parent orbit defined by the median values of orbits which fulfill the high threshold D-criteria from Table 1.

Recalculating the D-criteria using the median values of the orbits that fulfill the high threshold criteria listed in *Table 1* as a parent orbit does not change much to *Figure 2*. Only a few more orbits fulfill the D-criteria and some dots change color. The result is shown in *Figure 3*.

At this point we can conclude that the region is rich in many similar orbits, but these may be unrelated sporadic orbits. Although the inclination *i* for all orbits is within 8° ± 4°, the spread in the length of perihelion is too large to conclude anything about the presence of a dust trail in this region. We look a bit further at the distribution of these orbits in time.

4   Case study FHY-1032: sporadic orbits?

Activity profile and periodicity
The dataset contains orbits for each year from 2007 until 2017 and in each of these years we find a significant number of similar orbits that fulfill the low threshold D-criteria. CAMS contributed only data to 2011, 2012 and 2013 while 2017 represents only SonotaCo orbits. *Figure 4* represents the proportion of similar orbits that respect the low threshold D-criteria for each year compared to the total number of orbits available for the interval 309° < $\lambda_\odot$ < 340°. In total 28149 orbits were collected during this time span and 317 or 1.1% of this total number of orbits fulfill the low threshold D-criteria for the FHY orbit. The variation in the percentage of orbits per year can be explained as normal statistical fluctuations, except for 2013 when, remarkably, many look-alike FHY-1032 orbits were found. It is not possible to conclude that the high number of 90 possible FHY-1032 orbits in 2013 represents some enhanced activity or rather a statistical fluctuation.
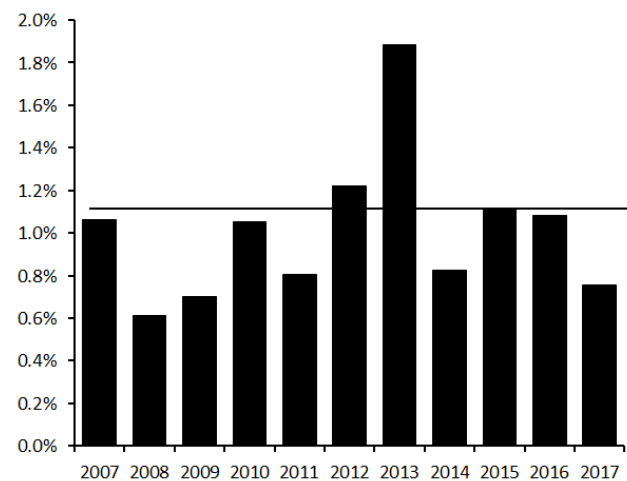

Figure 4 – The percentage of orbits per year that fulfill the low threshold of $D_D < 0.105$ relative to the total number of orbits obtained in the interval of 309° < $\lambda_\odot$ < 340°.

When we look at the time distribution of all the orbits that fulfill the D-criteria it becomes very obvious that we find these similar orbits at each degree of solar longitude (*Figure 5*). The profile does not look like a typical meteor shower activity profile with a shower maximum. There is a noticeable dip in the number of candidate FHY-1032 orbits at $\lambda_\odot = 324°$ with best numbers at $\lambda_\odot = 323°$ and

$\lambda_\Theta = 327°$. The relative high number or orbits that fulfill the D-criteria for each time slot in this interval may also indicate the presence of many look-alike sporadic orbits that fulfill D-criteria although not being related to any dust trail in this region.
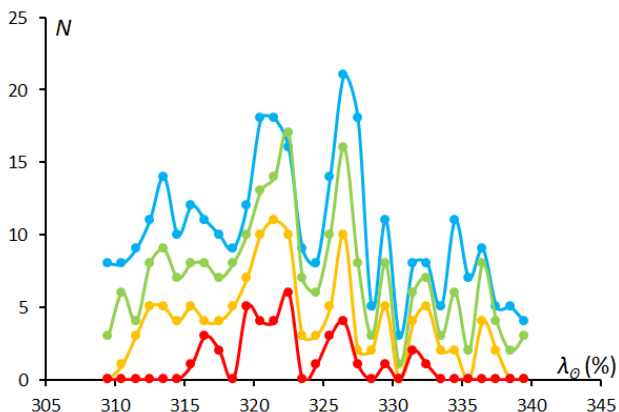

Figure 5 – The number of FHY-1032 candidate orbits collected per degree of solar longitude λ_Θ during the period 2007–2017 with blue for $D_D < 0.105$, green for $D_D < 0.08$, orange for $D_D < 0.06$ and red for $D_D < 0.04$.

The radiant position, drift and diameter
We try to detect a radiant drift relative to the reference position at $\alpha = 126.1°$ and $\delta = +4.5°$, valid at $\lambda_\Theta = 322.4°$.
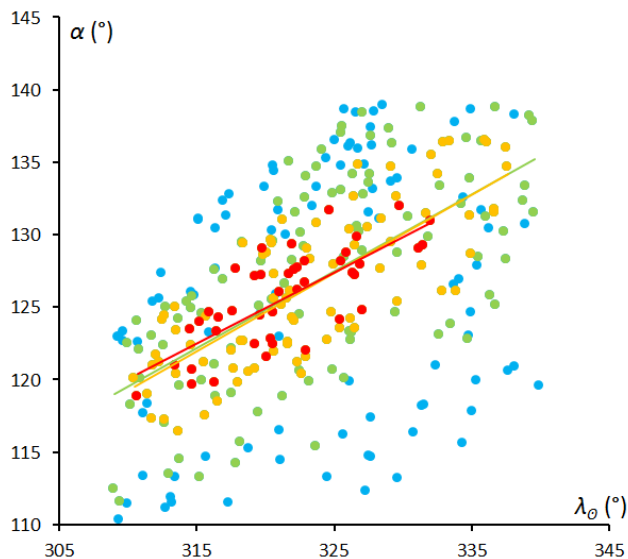
Figure 6 – Radiant drift in Right Ascension α against solar longitude λ_Θ. The different colors represent the 4 different levels of similarity.

It is obvious that the radiant positions that fulfill the low threshold criteria display a too large scatter. The medium low, medium high and high threshold levels cover a relevant time span and display an acceptable correlation. We use the high threshold ($D_D < 0.04$) data to obtain the radiant drift (see *Figures 6 and 7*). This results in the following radiant drift:

$$\Delta\alpha = 0.49°/\lambda_\Theta \quad \text{and} \quad \Delta\delta = -0.3°/\lambda_\Theta.$$
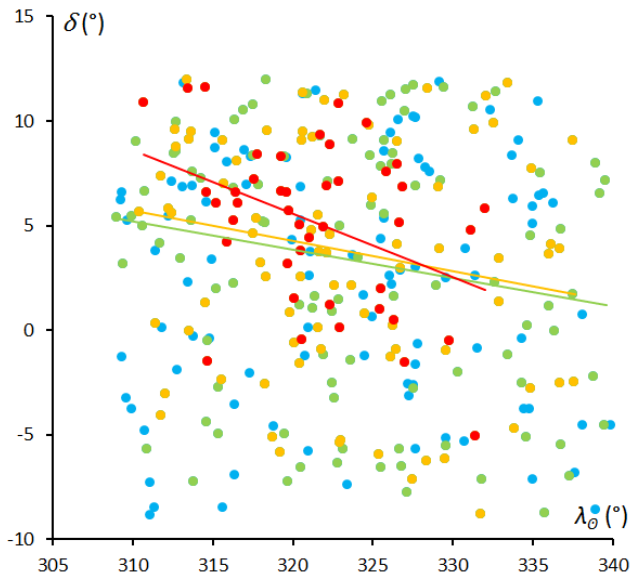
Figure 7 – Radiant drift in declination δ against solar longitude λ_Θ. The different colors represent the 4 different levels of similarity.
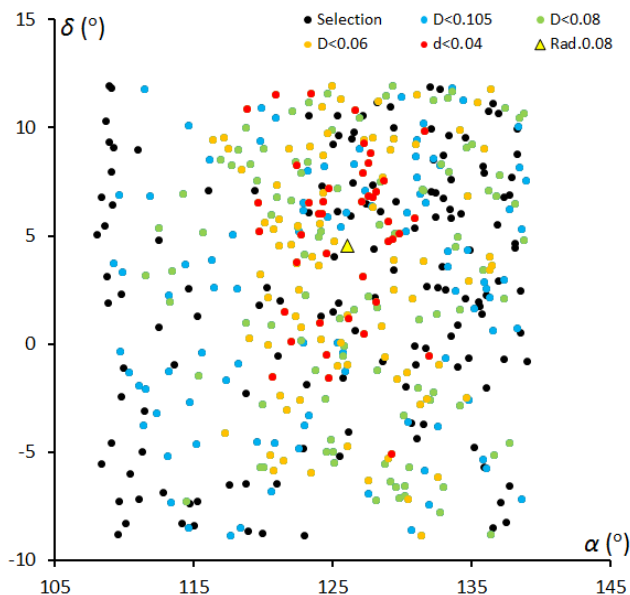

Figure 8 – Plot of the 461 uncorrected radiant positions as selected. The different colors represent the 4 different levels of similarity according to different threshold levels in the D-criteria.

The radiant distribution appears to be very diffuse (*Figure 8*). Some radiants of orbits that fail to fulfill any D-criteria appear close to the parent orbit position while orbits that fulfill the high threshold D-Criteria (red dots) appear much dispersed. This indicates we are in a region rich in unrelated but very similar sporadic orbits. Applying the radiant drift obtained from the high threshold D-criteria in *Figure 9*, we see on one hand the sporadic radiants (black dots) and some low threshold criteria radiants (blue dots) getting more dispersed while the medium high and high threshold criteria radiants (orange and red) contract towards the reference position, indicating that the radiant drift is valid for these orbits.
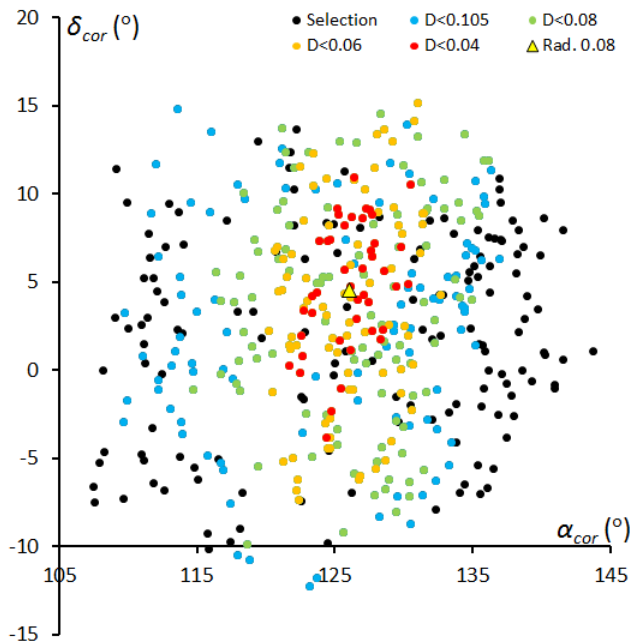
Figure 9 – Plot of the 461 radiant drift corrected radiant positions. The different colors represent the 4 different levels of similarity.

Other shower characteristics

The slow meteors have a median begin height of 90.0 ± 5.6 km and ending height of 79.4 ± 7.0 km. With a velocity of 16.9 km/s these are slower than the Draconids (DRA-9) with 97.7 ± 2.2 as starting height and 90.1 ± 3.4 as ending height (Roggemans, 2017). The Draconids are known to be relatively fresh cometary meteoroids which fail to penetrate deep into the atmosphere because of their fragile composition. The candidate February Hydrid meteors are only slightly slower than the Draconids but penetrate significant deeper into the atmosphere, perhaps a hint for a more compact meteoroid composition?
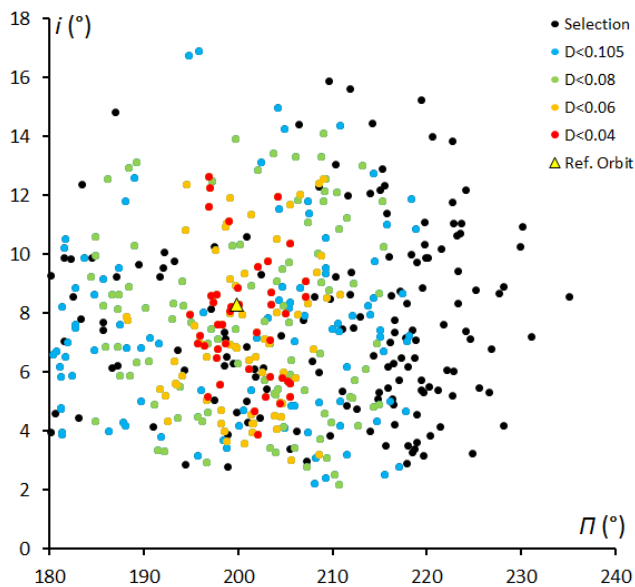
Figure 10 – The plot of inclination i (°) against the length of perihelion Π (°) for the 461 preselected orbits. The colors mark the different threshold levels of the D-criteria relative to the reference orbit in Table 3 taken as parent orbit.

The analysis does not prove a distinct concentration of orbits. A rather diffuse picture emerges of possibly related orbits embedded in a sporadic background rich in look-alike but unrelated sporadic orbits. To resolve such dispersed dust trail from the rich sporadic background is at the limit of detectability and tricky to distinguish possible shower members from similar sporadic orbits.

When we use the reference orbit given by Jenniskens et al. (2018) to compare the selected 461 orbits, recalculating the D-criteria, we obtain median values for the four threshold levels of D-criteria as listed in *Table 3*.

The median values for 43 high threshold orbits compare very well to the reference orbit as given by Jenniskens et al. (2018). The plot of inclination *i* against length of perihelion *Π* (*Figure 10*) does not show a distinct concentration, but a rather diffuse picture. The picture is about the same as what we obtained in *Figures 2 and 3*.

Table 3 – The median values for the selected orbits with four different threshold levels on the D-criteria, using the reference orbit given by Jenniskens et al. (2018), as parent orbit, compared to the reference orbit from literature (Jenniskens et al., 2018).

	Low	Medium low	Medium high	High	Reference (2018)
λ_O	322.6°	322.5°	322.4°	322.9°	324.3°
α_g	124.6°	124.6°	124.6°	124.6°	123.9°
δ_g	+3.7°	+3.8°	+4.0°	+3.7°	+1.5°
v_g	16.6	16.7	16.8	16.7	16.4
a	2.47	2.54	2.60	2.63	2.68
q	0.798	0.800	0.802	0.805	0.812
e	0.674	0.679	0.692	0.698	0.697
ω	58.1°	57.7°	57.5°	56.2°	55.5°
Ω	142.6°	142.5°	142.4°	142.9°	144.3°
i	7.2°	7.2°	7.1°	7.6°	8.3°
N	306	208	108	43	17
S	*34%*	*55%*	*77%*	*91%*	

Figure 11 shows the reference orbit published by Jenniskens et al. (2018) in red with the 43 orbits of our sample in grey that fulfill the high threshold D-criteria in *Table 3*. The final orbit that we obtain from our 461 selected orbits is shown in green and is situated well within the orbit given by Jenniskens et al. Also the orbit we found in *Table 2* (green in *Figure 11*) has 43 orbits that fulfill the high threshold D-criteria. The high threshold D-criteria orbits listed in *Table 3*, using the orbit given by Jenniskens et al. as parent orbit and those listed in *Table 2*, obtained from this analysis, have 20 orbits in common that fulfill the high D-criterion for both parent orbits! This paper indicates a diffuse meteor stream with more orbits further inside the reference orbits (smaller eccentricity and shorter perihelion and semi major axis).
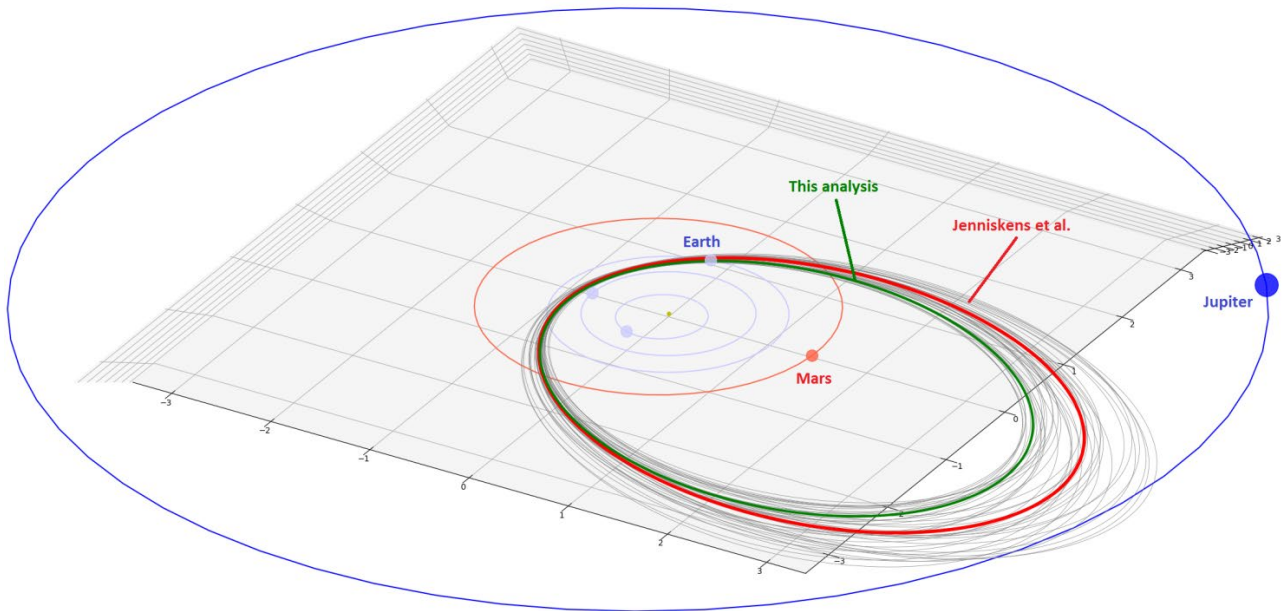
Figure 11 – The #1032-FHY orbit as listed in the IAU working list of meteor showers (red), the 43 orbits from the 461 selected orbits in this study which fulfill the high threshold D criteria (grey) with the red orbit as parent, compared to the orbit from Table 2 obtained from this analysis (in green). (Peter Campbell-Burns).

5   Conclusion

A search on the orbital data from the major video camera networks worldwide, good for ~686000 orbits (status April 2018), resulted in a collection of very similar orbits with a significant number of orbits that fulfill the high threshold D-criteria of $D_D < 0.04$. There is no distinct concentration but a rather diffuse trace of some weak shower embedded in a region strongly contaminated with similar sporadics orbits.

From this analysis we do not find convincing evidence to confirm the existence of the February Hydrids (FHY-1032). This study indicates that a weak and diffuse shower may be present in the data for the period 2007–2017. More attention is required in the future to assess the relevance of this discovered minor shower.

Acknowledgment

References

Drummond J. D. (1981). "A test of comet and meteor shower associations". *Icarus*, **45**, 545–553.

Jenniskens P., Gural P. S., Grigsby B., Dynneson L., Koop M. and Holman D. (2011). "CAMS: Cameras for Allsky Meteor Surveillance to validate minor meteor showers". *Icarus*, **216**, 40–61.

Jopek T. J. (1993). "Remarks on the meteor orbital similarity D-criterion". *Icarus*, **106**, 603–607.

Kornoš L., Matlovič P., Rudawska R., Tóth J., Hajduková M. Jr., Koukal J., and Piffl R. (2014). "Confirmation and characterization of IAU temporary meteor showers in EDMOND database". In Jopek T. J., Rietmeijer F. J. M., Watanabe J., Williams I. P., editors, *Proceedings of the Meteoroids 2013 Conference*, Poznań, Poland, Aug. 26-30, 2013. A.M. University, pages 225–233.

Roggemans P. (2017). "Variation in heights of CAMS meteor trajectories". *eMetN*, **2**, 80–86.

Roggemans P. and Johannink C. (2018). "A search for December alpha Bootids (497)". *eMetN*, **3**, 64–72.

Jenniskens P., Johannink C. and Moskovitz N. (2018). "February Hydrids outburst (IAU#1032, FHY)". *WGN, Journal of the International Meteor Organization,* **46**, 85–86.

SonotaCo (2009). "A meteor shower catalog based on video observations in 2007-2008". *WGN, Journal of the International Meteor Organization*, **37**, 55–62.

Southworth R. R. and Hawkins G. S. (1963). "Statistics of meteor streams". *Smithson. Contrib. Astrophys.*, **7**, 261–286.

Alpha Aquariids (AAQ-927)

Paul Roggemans[1] and Peter Cambell-Burns[2]

[1] Pijnboomstraat 25, 2800 Mechelen, Belgium
`paul.roggemans@gmail.com`

[2] UKMON, Cavendish Gardens, Fleet, Hampshire, United Kingdom
`peter@campbell-burns.com`

Japanese observers reported the discovery of a new minor shower listed as alpha Aquariids (927-AAQ) in the IAU Working list of meteor showers. A search in the orbit catalogues of the largest video camera networks resulted in a large number of similar orbits, with a significant number of orbits which fulfill the high threshold D-criteria. This analysis fails to find indications for the presence of a concentration of orbits that prove the existence of the alpha Aquariid meteor shower. The distribution of the orbits in time and space indicates the presence of a large number of similar but random distributed unrelated sporadic orbits in the ecliptic. Taking the physical properties into account (exceptional high beginning heights), no indication for any orbit concentration could be found. The shower discovery may be explained as a coincidence of unrelated sporadic orbits, unless other networks could produce evidence for the occurrence of similar orbits in 2017 with the same unusual beginning heights and ablation display as "melting meteors".

1   Introduction

In the night of 26 October 2017 the Japanese *SonotaCo* meteor network captured some meteors with a remarkable slow speed and similar luminosity profile[17]. *Chikara Shimodo* noticed a remarkable luminosity profile for a fireball, captured by 11 cameras at 9 stations of the *SonotaCo* network in Japan on 26 October 2017 at $14^h51^m48^s$ UT. The orbital elements for this fireball were computed as:

- $\lambda_\Omega = 213.1417°$
- $\alpha = 328.2 \pm 0.2°$
- $\delta = 1.8 \pm 0.2°$
- $v_g = 7.95 \pm 0.02$ km/s
- $a = 2.156 \pm 0.009$ AU
- $q = 0.9768 \pm 0.0003$ AU
- $e = 0.546 \pm 0.002$
- $\omega = 198.0 \pm 0.2°$
- $\Omega = 213.1369 \pm 0.0001°$
- $i = 2.94 \pm 0.04°$

Independent from this event *Yasuo Shiba* noticed a concentration of 4 meteors with similar radiants and velocities, including the fireball mentioned above. The data for these 4 meteors is listed in *Table 1*.

No known meteor shower could be associated with these radiant positions or with this orbit. In the period of 23 October until 1 November the *SonotaCo* network collected 812 orbits among which the above 4 mentioned meteors with a characteristic light curve and very slow velocity. The other nights were checked but there have been two typhoons over Japan in October 2017 leaving only few observable nights.

On the 1st of November 2017 *Yasuo Shiba* (*SonotaCo* Network) concluded that these meteors could indicate a

new unknown minor meteor shower with a radiant at the border of Aquarius and Pegasus. The new minor shower was reported to the IAU and a paper was sent to IMO for publication (Shiba et al., 2018). Based on the announcement of the publication about the new shower the discovery was included in the IAU Meteor Shower List with the identification AAQ (alpha Aquariids) and IAU number 927.

Table 1 – The four meteors on which the discovery of the AAQ-927 was based.

Date (UT)	λ_Ω (°)	α (°)	δ (°)	v_g (km/s)
2017.10.26 $12^h09^m04^s$	213.029	331.5±6.3	+0.2±9.0	7.5±4.3
2017.10.26 $14^h51^m48^s$	213.142	328.2±0.2	+1.8±0.2	7.95±0.02
2017.10.26 $15^h13^m18^s$	213.157	324.7±1.6	+0.1±0.7	8.1±0.4
2017.10.27 $10^h54^m07^s$	213.975	329.3±0.7	-8.1±11.4	7.4±3.7

All CAMS networks of the global CAMS project had collected 1184 orbits for 26 October, 66 of which were collected by the CAMS BeNeLux network. 1186 orbits were collected for 27 October, of which 166 orbits were registered by CAMS BeNeLux. In spite of the large numbers of orbits registered, no triggers went off to indicate any possible new meteor shower.

With the radiant position being near the ecliptic plane the newly announced meteor shower is embedded in a region that is very rich in sporadic meteoroids. The very slow velocity for meteors from any shower in this area close to the antapex causes a very large dispersion on the radiant size. Since the 2017 CAMS data fails to confirm any outburst, the authors searched all public available orbit data in an attempt to find more details for the alpha Aquariids (AAQ-927) meteor shower.

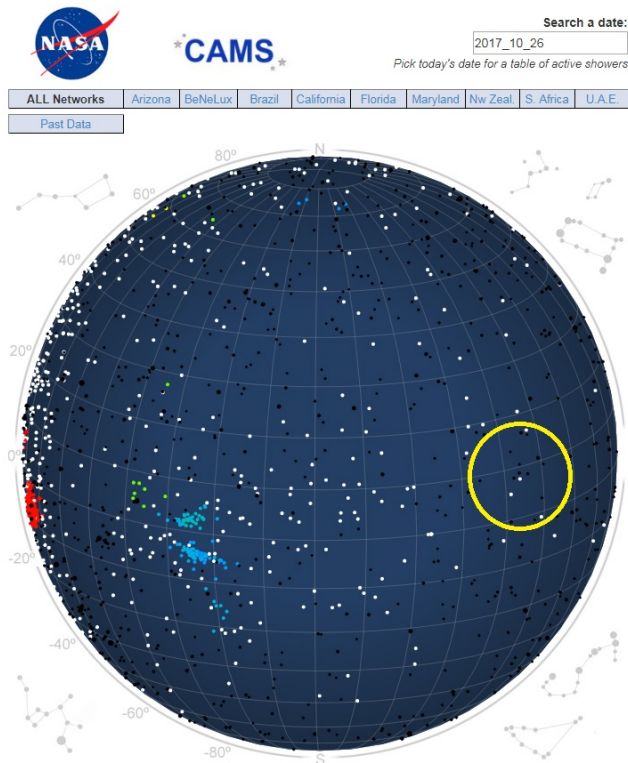[17] http://sonotaco.jp/forum/viewtopic.php?t=3977

Figure 1 – The radiant map for the night of 26 October for all CAMS networks (1184 orbits). The position of the AAQ-927 radiant is marked with a yellow circle.

2   The available orbit data

We have the following data, status as until April 2018, available for our search:

- EDMOND EU+world with 317830 orbits (until 2016). EDMOND collects data from different European networks which altogether operate 311 cameras (Kornos et al., 2014).
- SonotaCo with 257010 orbits (2007–2017). SonotaCo is an amateur video network with over 100 cameras in Japan (SonotaCo, 2009).
- CAMS with 111233 orbits (October 2010 – March 2013), (Jenniskens et al., 2011). For clarity, the CAMS orbits April 2013 – April 2018 are not included in this dataset because this data is still under embargo.

Altogether we can search among 686073 video meteor orbits.

3   Preliminary orbit selection

The authors followed the procedure described in a previous similar analysis (Roggemans and Johannink, 2018) to identify possible AAQ orbits. Based on the known radiant position, velocity and date of activity, we can define a sub-dataset to limit the amount of orbits in time and space to a region where related orbits might be located.

In a first attempt orbits were selected in a period of 10 days before and after 26 October. All orbits within the following intervals were selected:

- Time interval: $203° < \lambda_O < 223°$;
- Radiant area: $309° < \alpha < 338°$ and $-8° < \delta < +12°$;
- Velocity: 4 km/s $< v_g < 12$ km/s.

In total 75 orbits occurred within these intervals, 33 from SonotaCo, 23 from EDMOND and 19 from CAMS data. These 75 orbits were obtained from meteors that appeared in the sky in a way that any single station observer would associate these meteors as AAQ shower members, coming from the right direction of the radiant with the right angular velocity expected for this shower. The purpose of analyzing the orbital data is to get an idea how many of these orbits are nothing else than sporadics that contaminate the radiant area and how many of these orbits have enough similarity to form a concentration that indicates the presence of a minor shower.

The median values for these 75 orbits compare very well with the orbital parameters given by Yasuo Shiba. The error margins σ represents the standard deviation:

- $\lambda_O = 211.5°$
- $\alpha = 328.1 \pm 6.7°$
- $\delta = 2.0 \pm 5.4°$
- $v_g = 8.1 \pm 1.3$ km/s
- $a = 2.17 \pm 0.63$ AU
- $q = 0.9745 \pm 0.01$ AU
- $e = 0.550 \pm 0.09$
- $\omega = 199.1 \pm 5.9$ °
- $\Omega = 211.53 \pm 5.5°$
- $i = 2.91 \pm 1.3°$

61 of the 75 orbits fulfill the D criteria ($D_{SH} < 0.25$ & $D_D < 0.105$ & $D_H < 0.25$) using the median values listed above as parent orbit, 33 orbits fulfill the D criteria with the highest threshold ($D_{SH} < 0.1$ & $D_D < 0.04$ & $D_H < 0.1$).

This looks very promising for the presence of some meteor stream in this sample. Browsing the individual orbits in the sample, perfectly matching orbits appear at both limits of our selection, right after $\lambda_O = 203°$ and right before $\lambda_O = 223°$. This would indicate that more potential shower members are present beyond the time interval that we selected. Therefore a new, broader selection was made to resume the shower search procedure.

4   Final orbit selection

A new selection was made for a dataset of orbits within the following intervals:

- Time interval: $198° < \lambda_O < 228°$;
- Radiant area: $300° < \alpha < 359°$ and $-12° < \delta < +16°$;
- Velocity: 4 km/s $< v_g < 15$ km/s;
- Ecliptic latitude north of ecliptic $\beta > 0°$.

The time interval now covers 30 days, to compensate for the radiant drift and the typical large spread on any radiant for low velocity showers the radiant area was taken wider. This selection included orbits south of the ecliptic while we search a meteor shower north of the ecliptic, therefore

orbits with an ecliptic latitude β south of the ecliptic were rejected. The final sample contains 346 orbits, 133 from SonotaCo, 139 from EDMOND and 74 from CAMS.

We apply three discrimination criteria to evaluate the similarity between the individual orbits taking the median values of the 346 selected orbits as parent orbit. The D-criteria used are these of Southworth and Hawkins (1963), Drummond (1981) and Jopek (1993). We consider four different threshold levels of similarity:

- Low: $D_{SH} < 0.25$ & $D_D < 0.105$ & $D_H < 0.25$;
- Medium low: $D_{SH} < 0.2$ & $D_D < 0.08$ & $D_H < 0.2$;
- Medium high: $D_{SH} < 0.15$ & $D_D < 0.06$ & $D_H < 0.15$;
- High: $D_{SH} < 0.1$ & $D_D < 0.04$ & $D_H < 0.1$.

240 orbits fulfill the low threshold D-criteria with the median values of our 346 orbits as parent orbit. If our dataset contains a concentration of orbits of the AAQ shower, the median values should be comparable. The results are shown in *Table 2* and compare very well with the reference orbit.

Table 2 – The median values for the selected orbits with four different threshold levels on the D-criteria, compared to the reference orbit from literature (Shiba et al., 2018).

	Low	Medium low	Medium high	High	Reference (2018)
$\lambda_{\varnothing}$	209.7°	209.7°	209.3°	210.3°	213.1°
α_g	338.7°	336.2°	335.3°	335.3°	328.2°
δ_g	+4.4°	+3.7°	+3.8°	+2.6°	+1.8
v_g	9.3	9.0	9.1	9.0	8.0
a	2.29	2.29	2.31	2.30	2.16
q	0.957	0.961	0.962	0.963	0.977
e	0.587	0.582	0.585	0.582	0.546
ω	205.6°	204.1°	203.9°	204.0°	198.0°
Ω	209.7°	209.7°	209.3°	210.3°	213.1
i	3.0°	3.0°	3.2°	2.9°	2.9°
N	240	177	116	54	1 (4)
S	*31%*	*49%*	*66%*	*84%*	

In *Table 2* we select those orbits that fit the low threshold D-criteria to eliminate the obvious sporadic contamination from the sample. *Table 2* shows the percentage (S) of orbits of the sample that fails to fulfill the D-criteria and must be considered as sporadic contamination of the radiant area. The remainder is an indication for the possible presence of a dust concentration within the sample.

In the next step we take the median values for the orbits that fulfill the high threshold D-criteria ($D_{SH} < 0.1$ & $D_D < 0.04$ & $D_H < 0.1$) from *Table 2* as parent orbit to recalculate the D-criteria for all 346 orbits of the dataset. The results are listed in *Table 3*. The median values for all orbits for each level of threshold on the D-criteria compare very well with the reference orbit given by Shiba et al. 11 orbits fulfill the very high threshold of $D_D < 0.02$

representing very similar orbits. So far, we have strong indications for the presence of a meteor shower at this position in the solar system.

Table 3 – The median values for the selected orbits with four different threshold levels on the D-criteria, using the high threshold orbit from Table 2 as parent orbit, compared to the reference orbit from literature (Shiba et al., 2018).

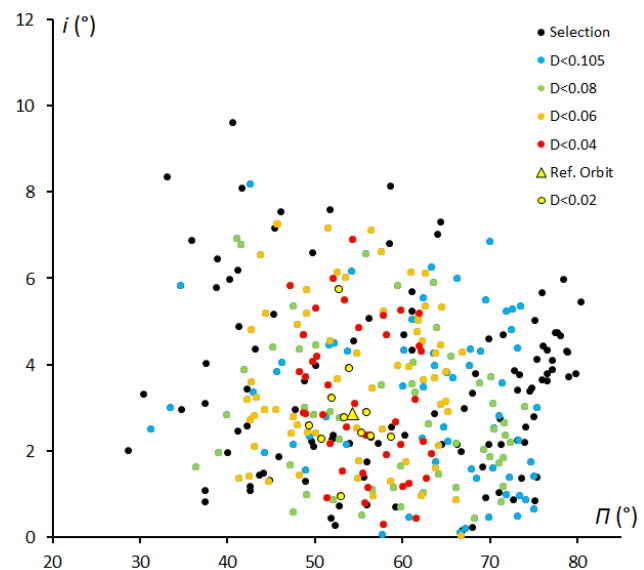|	Low	Medium low	Medium high	High	Reference (2018)
$\lambda_{\varnothing}$	209.8°	210.8°	209.5°	212.5°	213.1°
α_g	338.2°	335.7°	334.1°	333.7°	328.2°
δ_g	+4.0°	+3.1°	+3.1°	+2.2°	+1.8
v_g	9.2	8.9	9.0	8.9	8.0
a	2.26	2.25	2.29	2.25	2.16
q	0.960	0.963	0.965	0.965	0.977
e	0.584	0.578	0.581	0.574	0.546
ω	204.9°	203.8°	203.3°	202.8°	198.0°
Ω	209.8°	210.8°	209.5°	212.5°	213.1
i	3.0°	2.9°	3.2°	2.9°	2.9°
N	235	172	119	53	1 (4)
S	*32%*	*50%*	*66%*	*85%*	

Figure 2 – The plot of inclination i (°) against the length of perihelion Π (°) for the 346 preselected orbits. The colors mark the different threshold levels of the D-criteria relative to the parent orbit defined by the median values of the orbits that fulfill the high threshold D-criteria listed in Table 2.

The presence of a cluster of very similar orbits in the dataset should become very obvious in the graph of the inclination i (°) against the length of perihelion Π (°) (*Figure 2*). However a rather dispersed picture emerges with about the same dispersion on the points that represent orbits with low and medium low threshold D-criteria (blue and green dots in *Figure 2*) as for the orbits that fail for the D-criteria (black dots in *Figure 2*). Even for the medium high, high and very high threshold values there is no distinct concentration of points visible.

At this point we can conclude that the region is rich in many similar orbits, but these seem to be rather unrelated sporadic orbits. Although the inclination i for all orbits is within $4° ± 4°$, the spread in the length of perihelion is too large to conclude anything about the presence of a dust trail in this region. It would be appropriate to end the analyses at this point and to draw conclusions; however we look a bit further at the distribution of these orbits in time.

5   Case study AAQ-927: sporadic orbits?

The announcement of this possible minor shower has been based on very thin evidence, one fireball and three other meteors which appeared to come from the same radiant, while this radiant is situated close to the ecliptic not far from the antapex, a region rich in sporadic dust characterized by very slow velocity meteors. Meteors radiating from near the antapex must catch up with the Earth. The reference orbit given is valid for one single meteor which is not really representative for an entire stream. Altogether, the case of the AAQ-927 could be just spurious, based on a coincidence of few non-related sporadic meteors in the ecliptic region.

The authors (Shiba et al., 2018) mention the term 'outburst' although 3 meteors captured in one night and another similar orbit in the next night are rather few events to use the term 'outburst'. In a private communication Mr. *Yasuo Shiba* confirms the rich presence of similar but unrelated orbits. The main reason why these four meteors were considered were their physical characteristics, something that is not taken into account in the similarity criteria we use, which are purely geometrics. The four meteors appeared very unusual as 'melting meteors', with an unusual high beginning height for such very slow meteors, 10% above the expected beginning height. This is typical for very fresh fragile cometary dust such as for the Andromedids. Perhaps Earth crossed an isolated cloud of such meteoroids in 2017?

Activity profile and periodicity?

If the AAQ-927 are real and not a random coincidence of sporadics, it should have been detected by other networks in previous years, unless perhaps it was a periodic event only detectable in 2017? Only the SonotaCo dataset includes orbits for 2017. *Figure 3* represents the proportion of similar orbits that respect the low threshold D-criteria for each year compared to the total number of orbits available for the interval $198° < \lambda_{\Theta} < 228°$. In total 85731 orbits had been collected during this period. The CAMS network contributed only for 2010, 2011 and 2012 with a large number for 2011 and especially for 2012 (6770 orbits in 2012 for CAMS). No CAMS data was available from 2013 onwards. SonotaCo contributed its smallest number in 2013. A national camera network such as SonotaCo depends a lot on local weather circumstances which can cause large fluctuations on the number of meteors collected from year to year for a given period of time. *Figures 3* does not indicate any periodicity for the

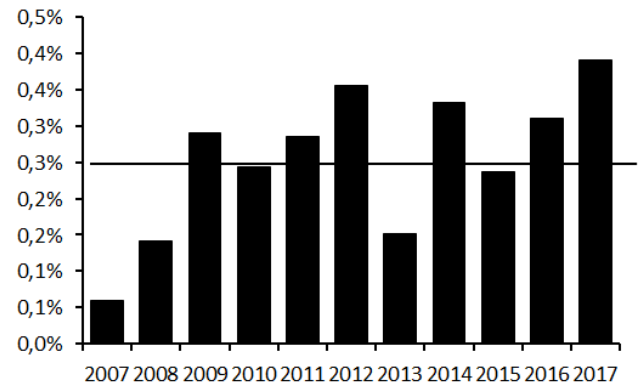suspected radiant, the variations are no more than the usual statistical fluctuations.

Figure 3 – The percentage of orbits per year that fulfill the low threshold of $D_D < 0.105$ relative to the total number of orbits obtained in the interval of $198° < \lambda_{\Theta} < 228°$.

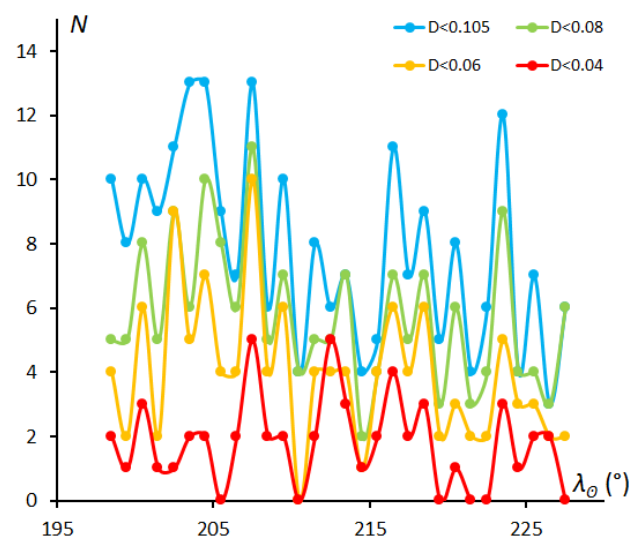*Figure 4* – The number of AAQ-927 look-alike orbits collected per degree of solar longitude λ_{Θ} during the period 2006–2017 with blue for $D_D < 0.105$, green for $D_D < 0.08$, orange for $D_D < 0.06$ and red for $D_D < 0.04$.

When we look at the time distribution of all the orbits that fulfill the D-criteria it becomes very obvious that we find these similar orbits at each degree of solar longitude (*Figure 4*). When extending the investigated period with another 10 days the same distribution is found. There is no trace of anything like a typical meteor shower activity profile with a shower maximum. *Figure 4* is a typical distribution for a number of unrelated sporadic look-alike orbits. This is an indication that the alpha Aquariids (AAQ-927) may appear as a result of a random coincidence of few similar sporadic orbits in a period of 2007–2017.

The radiant position, drift and diameter?

With a radiant position at $\alpha = 333.7°$ and $\delta = +2.2°$, valid at $\lambda_{\Theta} = 212.5°$ we try to detect a radiant drift. It is obvious that the radiant positions that fulfill the low and medium low threshold criteria display a too large scatter. The medium high and high threshold levels cover a relevant time span and display a weak correlation. We use the high

threshold (D_D < 0.04) radiant positions to obtain the radiant drift (see *Figures 5 and 6*). This results in the following radiant drift:

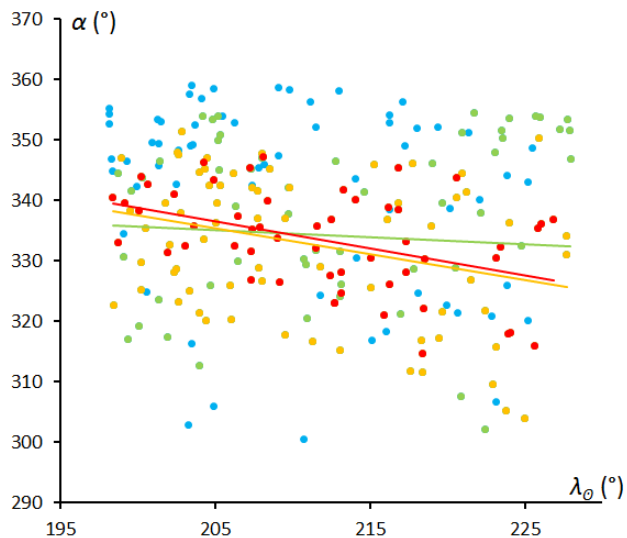$$\Delta\alpha = -0.45°/\lambda_\odot \quad \text{and} \quad \Delta\delta = +0.1°/\lambda_\odot.$$

Figure 5 – Radiant drift in Right Ascension α against solar longitude $\lambda_\odot$. The different colors represent the 4 different levels of similarity.
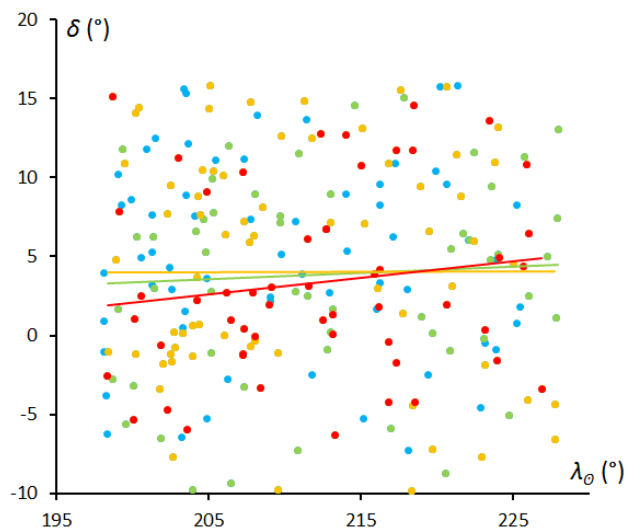

Figure 6 – Radiant drift in declination δ against solar longitude $\lambda_\odot$. The different colors represent the 4 different levels of similarity.

Instead of moving eastwards, the obtained radiant drifts westwards! We take it one step further to the drift corrected radiant positions. The plot of all the uncorrected radiant positions shows a large spread for all levels of threshold on the D-criteria (*Figure 7*). Such large spread is not unusual for meteor streams with such extreme slow velocity. The radiant drift which we derived proves to have no relevance since all radiant positions get randomly scattered for all threshold levels (*Figure 8*). A radiant is expected to drift eastwards, drifting westwards makes no sense and is the result of random distributed radiant points that belong to unrelated sporadics.
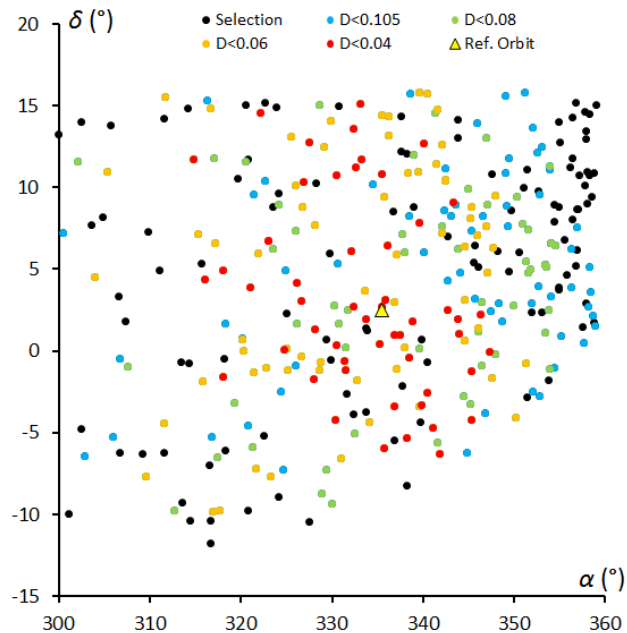
Figure 7 – Plot of the 346 uncorrected radiant positions as selected. The different colors represent the 4 different levels of similarity according to different threshold levels in the D-criteria.
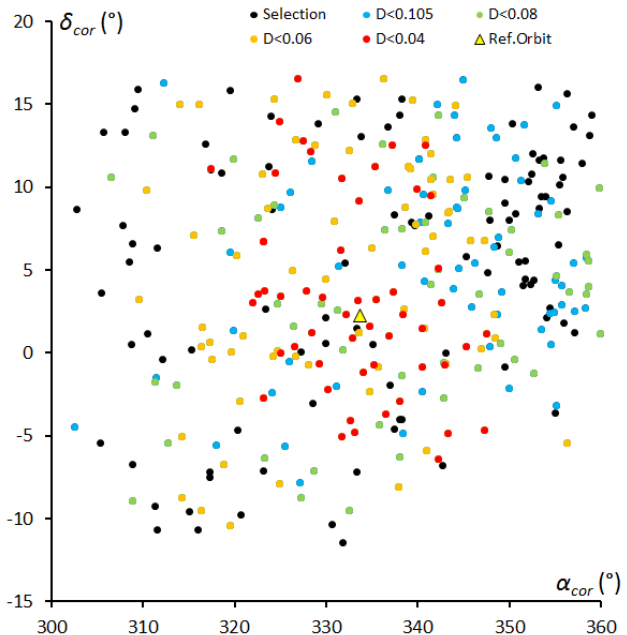
Figure 8 – Plot of the radiant drift corrected radiant positions. The different colors represent the 4 different levels of similarity.

We fail to find any evidence for a shower in past data. To remove all doubts we compute all D-criteria for the 346 orbits of our dataset using the reference orbit of the alpha Aquariids (AAQ-927) given by *Yasuo Shiba* as parent orbit. The results are given in *Table 4*.

Although the D-criteria identify a large number of very similar orbits no concentration appears in the graph of the inclination i (°) against the length of perihelion Π (°) with a too large spread in length of perihelion for all threshold levels of D-criteria (*Figure 9*).

Table 4 – The median values for the selected orbits with four different threshold levels on the D-criteria, using the reference orbit as parent orbit, compared to the reference orbit from literature (Shiba et al., 2018).

	Low	Medium low	Medium high	High	Reference (2018)
λ_O	210.8°	210.9°	211.7°	211.5°	213.1°
α_g	334.1°	332.4°	331.9°	329.9°	328.2°
δ_g	2.8°	2.4°	1.1°	1.0°	+1.8°
v_g	8.7	8.6°	8.4	8.1	8.0
a	2.18	2.17	2.17	2.16	2.16
q	0.965	0.967	0.969	0.972	0.977
e	0.564	0.555	0.551	0.550	0.546
ω	203.3°	202.5°	201.3°	200.3°	198.0°
Ω	210.8°	210.9°	211.7°	211.5°	213.1°
i	2.8°	2.8°	2.8°	2.8°	2.9°
N	213	163	108	61	1 (4)
S	*38%*	*53%*	*69%*	*82%*	
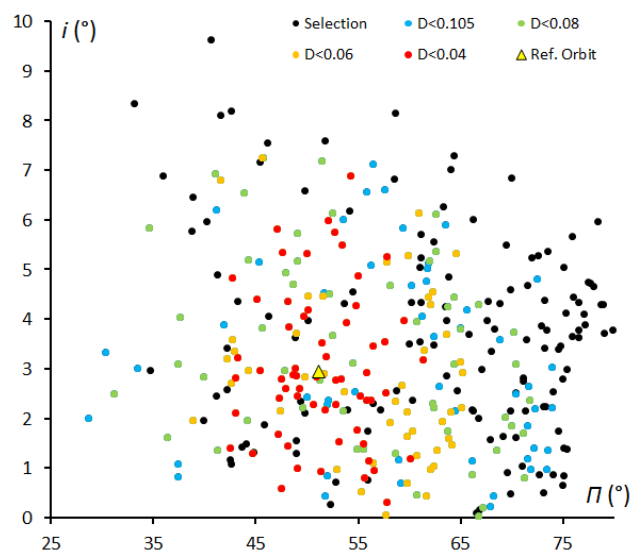
Figure 9 – The plot of inclination i (°) against the length of perihelion Π (°) for the 346 preselected orbits. The colors mark the different threshold levels of the D-criteria relative to the parent orbit defined by the orbit published by Shiba et al. (2018).

Other shower characteristics

These slow meteors have a median begin height of 78.8 ± 6.3 km and ending height of 69.0 ± 10.3km, comparing well to the Corvids (COR-63) with 79.1 ± 4.5 as starting height and 71.6 ± 6.5 as ending height (Roggemans, 2017). However the AAQ meteors on which the discovery is based are very different with beginning heights 10% above these values, combined with a very peculiar appearance as "melting meteors". In a private communication *Yasuo Shiba* clarified the description in his paper (Shiba et al., 2018): "*Alpha Aquariids were identified from data on only four meteors that were not only having analogous radiant positions with similar orbits, but producing similar luminous images stretching back and forth after half of the path. Recorded lengthened trails are not plasma emission left behind on the luminous track which is the so called 'train' and not fine pieces*

peele off from the meteoroid surface which is the so called 'tail'. But it was estimated that there is light from ablation by many fine, disintegrating meteoroids, occurring at an early stage in the low air density environment. As these 'dust ball' meteoroids give the appearance of melting away as they elongate and disintegrate, Mr. Bill Ward named this phenomenon 'melting meteor'. Melting meteors correlate with high beginning heights generally and agree with the characteristics of the four alpha Aquariid meteors."

Identification based on peculiar characteristics
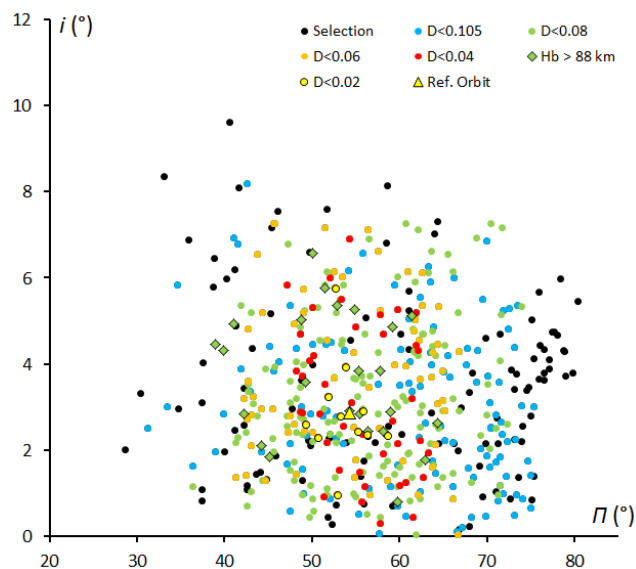
Figure 10 – The plot of inclination i (°) against the length of perihelion Π (°) for the 346 preselected orbits. The colors mark the different threshold levels of the D-criteria relative to the parent orbit defined by the median values of the entire dataset corresponding to the results in Table 2. The green diamonds represent orbits for meteors ablating 10% or more above the median value for this velocity class.

Looking at the physical aspects, we have no possibility to visualize the appearance of the video recordings of past video observations. These may be very depending on the visualization technics used, and to some extent the look could be an artifact depending on the software to visualize the image. However we can make a query on the beginning height and see if we have AAQ lookalikes with significant above average beginning heights. The result of this selection is shown in *Figure 10* for orbits with $D_D < 0.08$ and beginning heights +10% above the median value for beginning heights. Also the candidate AAQ meteors with exceptional high beginning heights (green diamonds) do not show any concentration that could identify a meteor shower. The spread in longitude of perihelion *Π* is too large.

An isolated meteoroid cloud?

The appearance of these slow meteors may recall the case of the Corvids which were only observed by Cuno Hoffmeister in South West Africa between 1937 June 25 and July 2 with a distinct maximum of 13 Corvids per hour on June 26 (Hoffmeister, 1948). This radiant was at the zenith at the start of the night in Southwest Africa and

the numbers of Corvids observed allowed establishing the radiant drift and the activity profile. The appearance of the Corvids in 1937 was of a complete different magnitude than the alpha Aquariids (927) in 2017. Neither before 1937, nor after that year any high activity of these Corvids has been detected, therefore is the 1937 Corvid activity considered having been caused by an isolated meteoroid cloud.

In our time, 80 years later with many video meteor networks active around the globe, it is very unlikely that an event like the Corvids would pass unnoticed. Looking at the time of the meteors on which the discovery of the AAQ (927) is based, the time lapse between the four meteors is rather large which means it was not a very short duration outburst. During the time of the discovery several other video networks were active in the world. The CAMS

networks collected as many as 2370 orbits during the two nights concerned, 26 and 27 October. The map with the radiant positions of these many orbits does not indicate anything of an outburst not even some weak activity from the radiant area (*Figure 1*). If an outburst occurred or even if at least some low activity could have been detected, it should be possibly confirmed by the other active networks. The absence of any hint for alpha Aquariid activity in the 2017 data of other networks requires some skepticism.

Taking into account that this region is rich in similar but unrelated orbits, the very low number of events on which the discovery is based and the absence of an independent confirmation, may indicate the AAQ-927 shower was based on a random coincidence of few lookalike sporadic meteors.
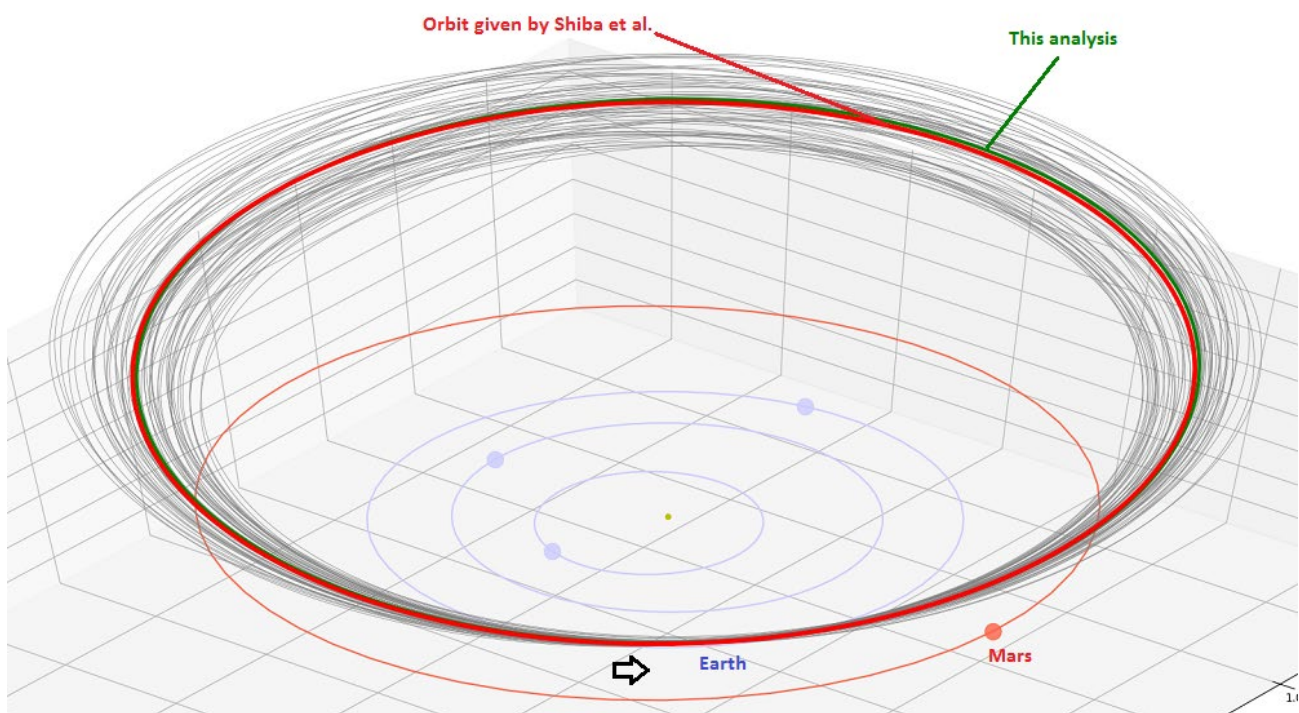
Figure 11 – The orbit of Shiba et al. as listed in the IAU working list of meteor showers (red) and the 61 orbits of our selection that fulfill the high threshold D-criteria with the red orbit as parent orbit. The orbit in green is median of the high threshold orbits. Note how particles on this type of orbits must catch up with the Earth, coming right from behind the Earth on its orbit around the Sun.

6 Conclusion

A search on the orbital data from the major video camera networks worldwide, good for ~686000 orbits (status April 2018), resulted in a collection of very similar orbits with a significant number of orbits that fulfill the high threshold D-criteria of $D_D < 0.04$. However no evidence could be found to prove a dust concentration. The radiant distribution is like a pure random distribution of sporadic orbits. The dispersion of the orbits in time and in space is typical for the rich sporadic dust distribution which produces meteors that radiate from the ecliptic region.

From this analysis we cannot confirm the existence of the alpha Aquariids (AAQ-927) in the orbit data for 2007-

2017. Also the candidate orbits with exceptional high beginning heights do not indicate any concentration.

The authors invite other networks to visually browse their results for meteors from this radiant area with exceptional high beginning heights for the nights 25-26-27-28 October 2017. If the Earth travelled through an isolated cloud of fragile meteoroids, other active networks should have recorded members of this AAQ meteor shower. A visual verification of the meteor images checking for the "melting meteor" shape may be the ultimate way to find more evidence for the existence of the recently reported possible new meteor shower. Attention should be paid to the orbit and radiant position, as well as to the beginning height and the visual appearance of these slow meteors.

Acknowledgment

References

Drummond J. D. (1981). "A test of comet and meteor shower associations". *Icarus*, **45**, 545–553.

Hoffmeister C. (1948). "Meteorströme". Verlag Werden und Wirken Weimar.

Jenniskens P., Gural P. S., Grigsby B., Dynneson L., Koop M. and Holman D. (2011). "CAMS: Cameras for Allsky Meteor Surveillance to validate minor meteor showers". *Icarus*, **216**, 40–61.

Jopek T. J. (1993). "Remarks on the meteor orbital similarity D-criterion". *Icarus*, **106**, 603–607.

Kornoš L., Matlovič P., Rudawska R., Tóth J., Hajduková M. Jr., Koukal J., and Piffl R. (2014). "Confirmation and characterization of IAU temporary meteor showers in EDMOND database". In Jopek T. J., Rietmeijer F. J. M., Watanabe J., Williams I. P., editors, *Proceedings of the Meteoroids 2013 Conference*, Poznań, Poland, Aug. 26-30, 2013. A.M. University, pages 225–233.

Roggemans P. (2017). "Variation in heights of CAMS meteor trajectories". *eMetN*, **2**, 80–86.

Roggemans P. and Johannink C. (2018). "A search for December alpha Bootids (497)". *eMetN*, **3**, 64–72.

Shiba Y., Shimoda C., Maeda K., SonotaCo, Sekiguchi T., Yoneguchi K., Kawakami H., Miyoshi T., Yamakawa H., Okamoto S., Muroishi H., Masuzawa T., Kamimura T. (2018). "A new meteor shower Alpha Aquariids(#927:AAQ)". *WGN, Journal of the International Meteor Organization,* **46**, 79–81.

SonotaCo (2009). "A meteor shower catalog based on video observations in 2007-2008". *WGN, Journal of the International Meteor Organization*, **37**, 55–62.

Southworth R. R. and Hawkins G. S. (1963). "Statistics of meteor streams". *Smithson. Contrib. Astrophys.*, **7**, 261–286.

Eta Lyrids (ELY-145)

Paul Roggemans[1] and Peter Cambell-Burns[2]

[1] Pijnboomstraat 25, 2800 Mechelen, Belgium
paul.roggemans@gmail.com

[2] UKMON, Cavendish Gardens, Fleet, Hampshire, United Kingdom
peter@campbell-burns.com

Two years in a row the eta Lyrids (#145-ELY) caught the attention of the CAMS BeNeLux camera network with surprisingly large numbers of orbits collected for this stream. An independent search was made on the data of ~686000 public available video meteor orbits. The results confirm earlier studies with a clear activity profile between solar longitude 45° and 53° with a sharp peak at 49.5±0.2°. No mention of this shower could be found before the passage of the parent comet C/1983 H1 (IRAS-Araki-Alcock) in 1983. In recent years the shower tends to surprise observers with some low but distinct activity. Outbursts are not excluded in the future, observers are recommended to keep an eye on this shower.

1   Introduction

Last year, the CAMS BeNeLux network had clear nights 9–10–11 May 2017. On the nights 26 orbits were identified as η-Lyrids (#145 ELY) which was sufficient to warrant an analysis (Johannink and Miskotte, 2017). The question arose whether or not the shower displayed greater than usual activity in 2017, or that the strong ELY presence was just the result of favorable weather around 10 May? Also in May 2018, the weather was very favorable and the η-Lyrids (#145 ELY) caught again the attention of the observers. This shower requires attention.

2   ELY (145) history

A search for historic records from this shower proved negative, this stream was not identified in any old meteor shower list. Gary Kronk did not mention this shower in his book (Kronk, 1988) and nowhere anything indicates that the shower was noticed by anyone.

Jack Drummond (1983) mentioned possible meteor activity on May 10.0 (λ_O = 49.1°) from a radiant at α = 289° and δ = +44° (Marsden, 1983a) associated with comet C/1983 H1 (IRAS-Araki-Alcock). His own observations confirmed a definite minor meteor shower associated with the comet, with hourly rates of 2 to 5 meteors per hour on nights of May 9–10–11 (Marsden, 1983b). A call if anyone noticed meteor activity from comet IRAS-Araki-Alcock (1983d) in WGN (Roggemans, 1983) remained without response. This comet is actually the parent comet of the η-Lyrids. The IAU working list of meteor showers does not mention any parent body for the shower at this moment. The orbit of the parent comet is listed in *Table 3*.

Johannink and Miskotte (2017) recall that Peter Jenniskens drew attention in an article in Radiant in 1985 to possible meteors from C/1983 H1 (IRAS-Araki-Alcock), expected to occur around 9 May (Jenniskens, 1985). A search for visual observations of this shower in the archives of the

Dutch Meteor Society resulted in visual data for this shower for 1982 and 1983. The shower caught attention again in 2000, 2001 and 2008 when favorable weather allowed more visual observations. The successful CAMS registrations in May 2017 and now again in May 2018 indicate that this shower may bring nice surprises to the observers.
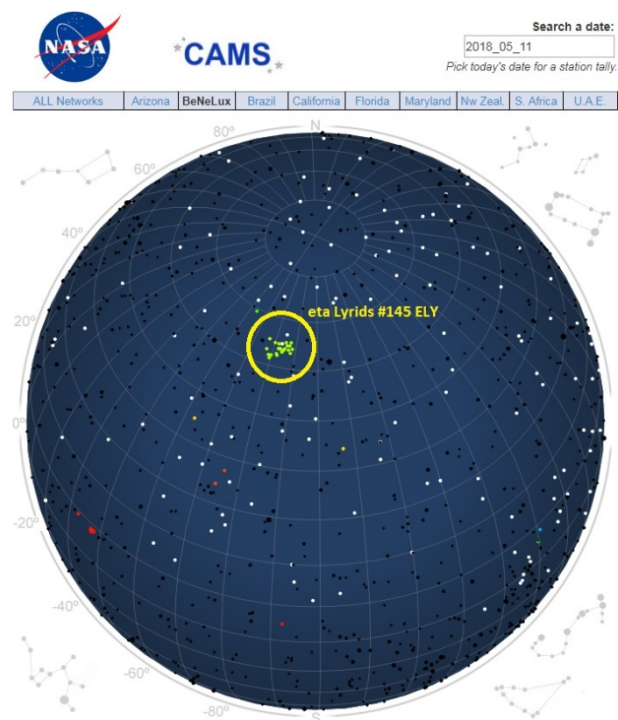
Figure 1 – Screenshot of the CAMS radiant plot for the night of 2018 May 11 with the remarkable concentration of radiants identified as #145 ELY orbits.

The photographic meteor orbit catalogue with 4873 accurate photographic orbits obtained between 1936 and 2008 resulted in only four possible η-Lyrid orbits, in 1956, 1961, 1964 and 2007. The Harvard radar orbit catalogues 1961–1965 and 1968–1969 (Hawkins, 1963) contain only few orbits with a low threshold of D_D < 0.105.

Having no solid evidence for the activity of the η-Lyrids before the passage of its parent comet, the question arises if we are observing dust particles from this very long (970 years) periodic comet that have spread behind the comet and which may sooner or later produce enhanced activity when Earth passes through some denser dust trails left by this comet?

At this point it is useful to take a look at the available orbital data collected in past 10 years.

3   The available orbit data

With two major orbit datasets being recently updated, it was worthwhile to check if and what we can detect about the #145 ELY or η-Lyrids meteor shower. We have the following data, status as until May 2018, available for our search:

- EDMOND EU+world with 317830 orbits (until 2016). EDMOND collects data from different European networks which altogether operate 311 cameras (Kornos et al., 2014).
- SonotaCo with 257010 orbits (2007–2017). SonotaCo is an amateur video network with over 100 cameras in Japan (SonotaCo, 2009).
- CAMS with 111233 orbits (October 2010 – March 2013), (Jenniskens et al., 2011). For clarity, the CAMS BeNeLux orbits April 2013 – March 2018 are not included in this dataset because this data is still under embargo.

Altogether we can search among 686073 video meteor orbits.

4   Orbit selection

All orbits within the following intervals were selected:

- Time interval: $38° < \lambda_O < 62°$;
- Radiant area: $276° < \alpha < 306°$ & $+33.9° < \delta < +53.9°$;
- Velocity: 38.8 km/s $< v_g < 48.8$ km/s.

Table 1 – The median values for each sub-set of orbits, CAMS, SonotaCo and EDMOND, all combined orbits and the final parent orbit derived for $D_D < 0.04$.

	CAMS	SonotaCo	Edmond	All	Final parent
λ_O	49.9°	49.5°	49.6°	49.6°	49.9°
α_g	291.3°	291.1°	291.4°	291.3°	290.5°
δ_g	+43.4°	+43.0°	+43.4°	+43.3°	+43.5°
v_g	43.5	43.8	43.0	43.3	43.6
a	11.9	8.2	7.1	7.9	14.0
q	0.999	1.000	1.000	1.000	0.999
e	0.916	0.923	0.893	0.909	0.929
ω	191.2°	190.5°	191.0°	190.9°	191.9°
Ω	49.9°	49.5°	49.6°	49.6°	49.9°
i	74.0°	74.4°	73.6°	73.9°	74.0°
N	167	353	518	1038	193

In total 1038 orbits were selected within these intervals. When we calculate the median values for each of the contributing networks, the results compare very well (*Table 1*). We use the median values of the complete selection as first approach parent orbit to compute the D-criteria. The median values for those orbits that fulfill the high threshold D-criteria are taken as final parent orbit.

We apply three discrimination criteria to evaluate the similarity between the individual orbits and the final parent orbit from *Table 1*. The D-criteria used are these of Southworth and Hawkins (1963), Drummond (1981) and Jopek (1993). We consider four different threshold levels of similarity:

- Low: $D_{SH} < 0.25$ & $D_D < 0.105$ & $D_H < 0.25$;
- Medium low: $D_{SH} < 0.2$ & $D_D < 0.08$ & $D_H < 0.2$;
- Medium high: $D_{SH} < 0.15$ & $D_D < 0.06$ & $D_H < 0.15$;
- High: $D_{SH} < 0.1$ & $D_D < 0.04$ & $D_H < 0.1$.

Table 2 – The median values for the selected orbits with four different threshold levels on the D-criteria, compared to the reference orbit from literature (Jenniskens et al., 2018).

	Low	Medium low	Medium high	High	Reference (2018)
λ_O	49.8°	49.8°	49.9°	49.9°	50.1°
α_g	290.7°	290.6°	290.4°	290.2°	291.1°
δ_g	+43.5°	+43.5°	+43.6°	+43.5°	+43.9°
v_g	43.7	43.8	43.8	43.8	43.8
a	10.8	12.3	13.6	18.1	17.8
q	1.000	1.000	1.000	0.999	1.001
e	0.931	0.937	0.946	0.946	0.944
ω	191.5°	191.6°	191.8°	192.4°	190.8°
Ω	49.8°	49.8°	49.9°	49.9°	50.1°
i	74.2°	74.2°	74.2°	74.2°	74.2°
N	543	423	333	199	237
S	*48%*	*59%*	*68%*	*81%*	
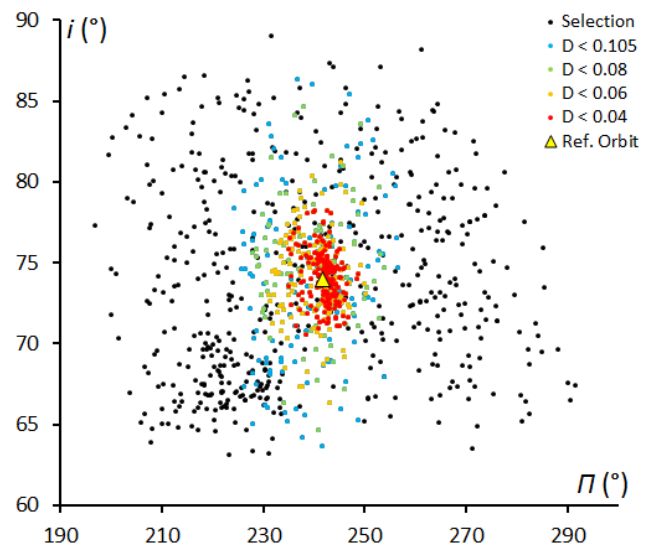
Figure 2 – The plot of inclination i (°) against the length of perihelion Π (°) for the 1038 preselected possible ELY-orbits. The colors mark the different threshold levels of the D-criteria relative to the final parent orbit listed in Table 1.

In *Table 2* we compare the median values of the orbits according to the four levels of the D-criteria threshold. The resulting orbits for each of the levels of similarity show very little variation. The results are in perfect agreement with the most recent values from literature (Jenniskens et al., 2018).

Table 2 shows the percentage (*S*) of orbits of the sample that fail to fulfill the D-criteria and must be considered as sporadic contamination of the radiant area. The presence of a cluster of very similar orbits in the dataset becomes very obvious in the graph of the inclination *i* (°) against the length of perihelion *Π* (°) (*Figure 2*).

5 Case study ELY-145: results

The final sample of 543 probable ELY-orbits represents 52% of the preselected orbits that fulfill the minimal threshold. With other words, one on two meteors that look like an ELY meteor for an observer has an orbit that is similar to the eta Lyrids shower while the other is a sporadic lookalike. It is no surprise that meteors from this minor shower catch the attention of visual meteor observers around the shower maximum.

The activity period and profile

There is no indication for any annual variation in ELY activity. The variation in number of orbits collected year by year reflects the total amount of orbits contributed by all the camera networks (see *Figure 3*). On average 2.3% of the total available orbits in the interval $38° < \lambda_O < 62°$ have an orbit similar to the eta Lyrids meteor shower. The variations from year to year can be explained as statistical fluctuations.
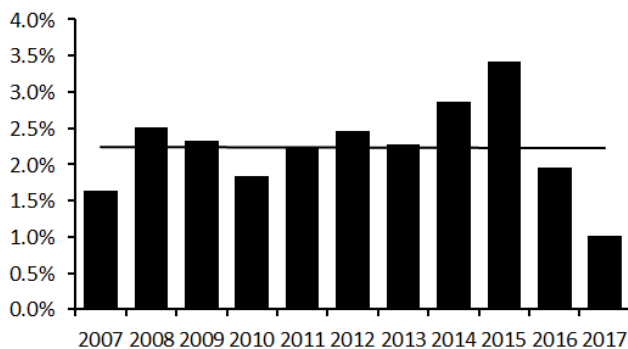
Figure 3 – The percentage of ELY orbits per year ($D_D < 0.105$) relative to the total number of orbits obtained.

The first #145 ELY orbit was registered at $\lambda_O = 38.3°$, the last at $\lambda_O = 61.6°$ with the lowest threshold *D*-Criteria. The main activity takes place in the time interval $45° < \lambda_O < 53°$, or 6 May until 14 May, with the peak ELY activity on 10 May at $\lambda_O = 49.5±0.2°$ (*Figure 4*) This is in good agreement with single station video camera work by Molau & Rendtel (2009) who obtained an activity interval of 45° to 52° with a peak at 50°, confirmed later in 2013 by the same camera network of IMO (Molau et al., 2013). Since it is difficult to obtain hourly rates for this kind of minor showers, the number of orbits collected for each degree in solar longitude provides an indication of the

activity profile, showing the activity period as well as the solar longitude at which the largest number of orbits has been collected. The small number of similar orbits detected before $\lambda_O = 46°$ and after $\lambda_O = 54°$, may be real eta Lyrids that got dispersed from the main dust trail but may be also unrelated sporadics that fulfill the low threshold D-criteria by pure chance.
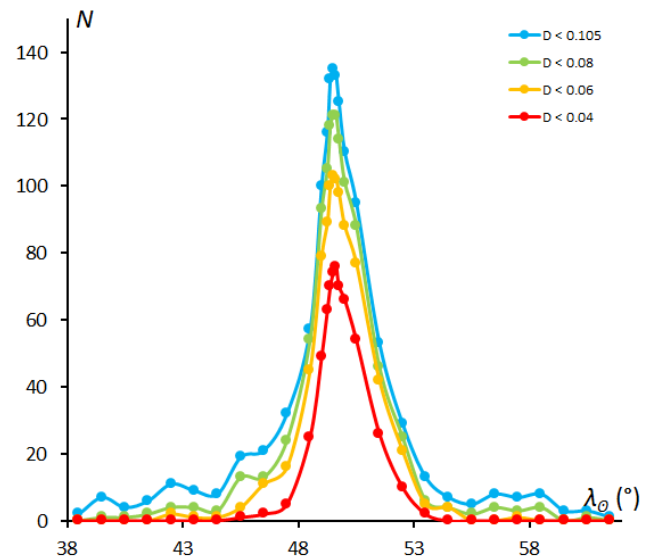
Figure 4 – The number of eta Lyrids orbits collected per degree of solar longitude λ_O during the period 2007–2017 with blue for $D_D < 0.105$, green for $D_D < 0.08$, orange for $D_D < 0.06$ and red for $D_D < 0.04$.

The radiant position, drift and diameter

With a radiant position at $\alpha = 290.5°$ and $\delta = +43.5°$, valid at $\lambda_O = 49.9°$ the radiant drift can be determined. The medium low and medium high threshold levels cover a relevant time span with an acceptable spread on the positions. The high threshold level is less suitable as this represents a rather short time span. As a compromise we use the medium low threshold ($D_D < 0.08$) positions to obtain the most likely radiant drift (see *Figures 5 and 6*). This results in the following radiant drift:

$$\Delta\alpha = 0.56°/\lambda_O \text{ and } \Delta\delta = +0.07°/\lambda_O.$$

This compares well to the values found in Jenniskens et al. (2016).

In order to get an idea of the size of the radiant we apply the radiant drift correction to get a plot of the radiant positions corrected for the daily motion (*Figure 8*). This shows a compact radiant slightly elongated in declination. Compared to the original, uncorrected radiant positions (*Figure 7*) the scatter of the radiants that failed to fulfill the D criteria increases considerably. Some radiants for orbits with a weak similarity get more diffused and may indicate that these orbits are sporadics that fit within the low threshold by pure chance. The higher the threshold level the more concentrated the radiant drift corrected positions become. Another way to consider the radiant size is to plot the ecliptic coordinates as the ecliptic latitude β against the Sun centered longitude $\lambda - \lambda_O$. Also here the radiant size appears to be rather compact.
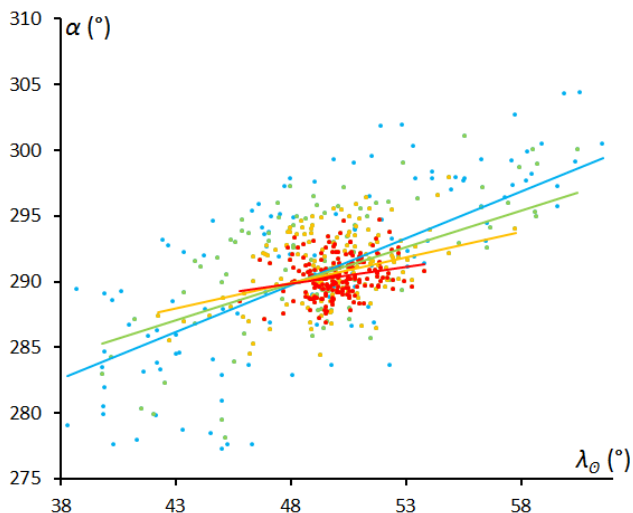
Figure 5 – Radiant drift in Right Ascension α against solar longitude λ_Θ. The different colors represent the 4 different levels of similarity.
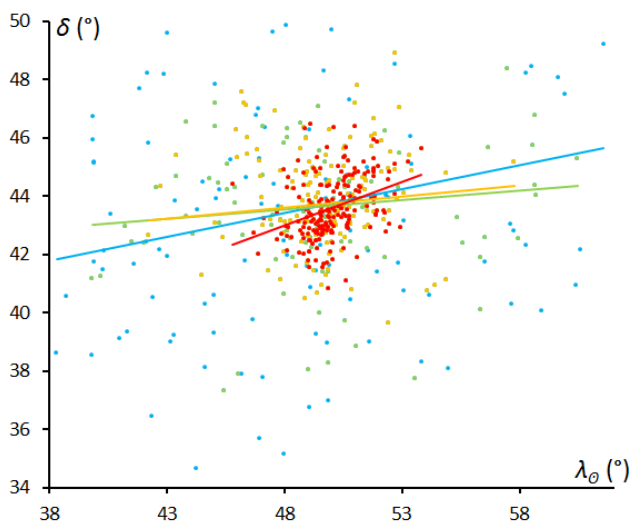

Figure 8 – Plot of the radiant drift corrected radiant positions. The different colors represent the 4 different levels of similarity.

Figure 6 – Radiant drift in declination δ against solar longitude λ_Θ. The different colors represent the 4 different levels of similarity.
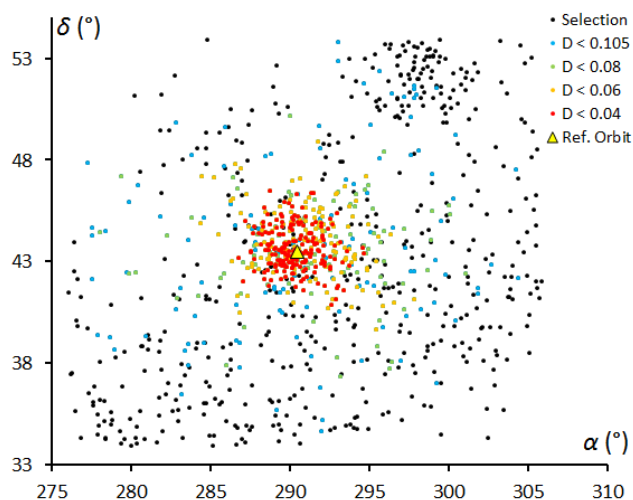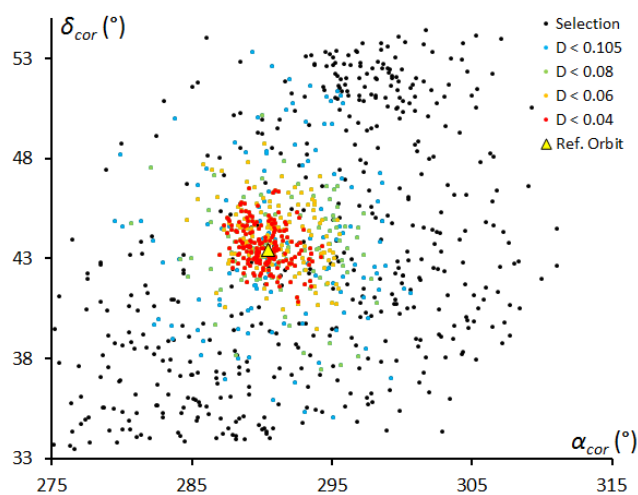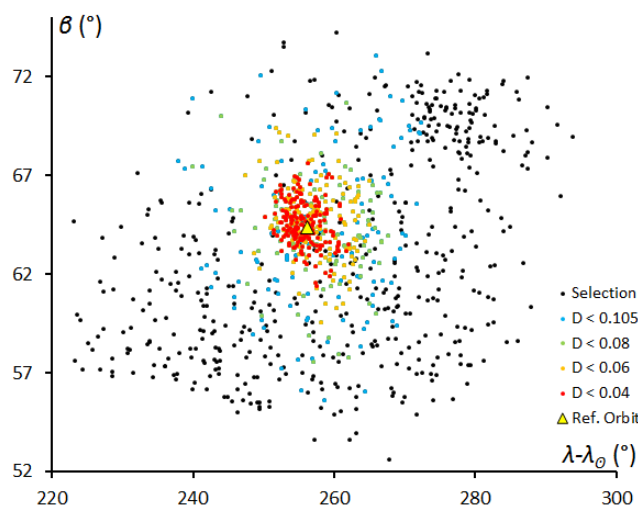

Figure 9 – Plot of the ecliptic latitude β against the Sun centered longitude $\lambda - \lambda_\Theta$. The different colors represent the 4 different levels of similarity.

Other shower characteristics

The eta Lyrids (ELY-145) are rich in bright meteors. With a geocentric velocity v_g of 43.8 km/s, the ELYs are slightly slower than the April Lyrids (LYR-6) with 46.7 km/s and faster than the Quadrantids (QUA-10) with 40.7 km/s. The median value for the starting height with 104.1 ± 4.4 km and an ending height of 90.3 ± 5.9 km compares perfectly with the values found from earlier work with 105.5±3.3 and 92.1±4.7 (Roggemans, 2017).

Dr. Peter Jenniskens (Jenniskens et al., 2016) classified this shower with the established long-period comet showers. This type of meteor shower tend to display activity during a limited period of time, during 10° or less degrees of solar longitude and have a rather compact radiant, characteristics that prove valid for the eta Lyrids and appear from *Figures 4, 8 and 9*. Unexpected outbursts happened for various other meteor streams of this type, but not yet for the η-Lyrids (ELY-145) so far. *Figure 10* shows the different orbits listed in Table 3 in a 3D view. The eta Lyrids are produced by dust trails that were left behind by the parent comet, inside the comet orbit.

Figure 7 – Plot of the 377 radiant positions as selected. The different colors represent the 4 different levels of similarity according to different threshold levels in the D-criteria.
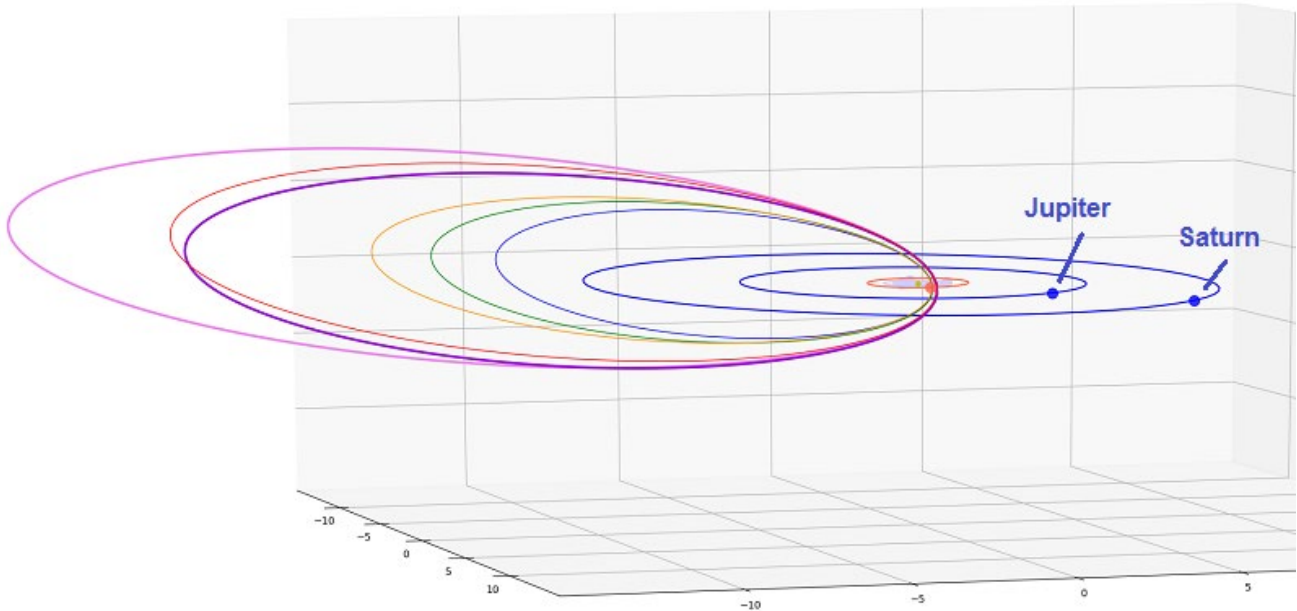
Figure 10 – The eta Lyrid orbits listed in Table 3, with the reference orbits of Jenniskens et al. (2018) in dark purple, Jenniskens et al. (2016) in light purple and the results of this analysis with blue for $D_D < 0.105$, green for $D_D < 0.08$, orange for $D_D < 0.06$ and red for $D_D < 0.04$.

Table – 3 The orbital data for the η-Lyrids (ELY-145) all J2000, the standard deviation σ is listed as ± where available. The orbit of the parent comet C/1983 H1 (IRAS-Araki-Alcock) is also given.

$\lambda_\odot$ (°)	α_g (°)	δ_g (°)	$\Delta\alpha$ (°)	$\Delta\delta$ (°)	v_g km/s	a AU	q AU	e	ω (°)	Ω (°)	i (°)	N	Source
49.0	289.9	+43.4	+0.56	+0.14	43.7	21.4	0.999	0.954	192.3	50.1	74.1	39	Jenniskens et al. (2016)
50.1	291.1	+43.9	–	–	43.9	17.8	1.001	0.944	190.8	50.1	74.2	237	Jenniskens et al. (2018)
49.8 ±4.0	290.7 ±2.5	+43.5	+0.72	+0.16	43.7 ±1.7	10.8	1.000 ±0.009	0.931 ±0.073	191.5 ±5.0	49.8	74.2 ±3.3	543	This analysis $D_D < 0.105$
49.8 ±2.9	290.6 ±1.6	+43.5	+0.56	+0.07	43.8 ±1.3	12.3	1.000 ±0.006	0.937 ±0.061	191.6 ±3.6	49.8 ±2.6	74.2 ±2.5	423	This analysis $D_D < 0.08$
49.9 ±2.1	290.4 ±1.4	+43.6	+0.39	+0.08	43.8 ±1.1	13.6	1.000 ±0.004	0.946 ±0.052	191.8 ±2.8	49.9 ±1.8	74.2 ±2.1	333	This analysis $D_D < 0.06$
49.9 ±1.5	290.2 ±1.1	+43.5	+0.26	+0.30	43.8 ±0.8	18.1	0.999 ±0.004	0.946 ±0.035	192.4 ±2.1	49.9 ±1.2	74.2 ±1.6	199	This analysis $D_D < 0.04$
						98.0	0.991	0.990	192.9	49.1	73.3		C/1983 H1

6   Conclusion

A search on the orbital data from the major video camera networks worldwide, good for ~686000 orbits (status May 2018), resulted in 543 candidate ELY-orbits. 199 orbits fulfill the high threshold D-criteria of $D_D < 0.04$. An analysis of the available orbits proved the presence of a distinct cluster of similar orbits independently from previous stream searches. The resulting reference orbit compares very well with the previously published orbits.

Members of this shower have been detected every year since 2007 in a time span between 45° and 53° in solar longitude with a rather sharp maximum at about $\lambda_\odot = 49.5\pm0.2°$. There is no indication of any periodicity in the stream activity. This minor shower displays an activity with statistical relevant hourly rates around its maximum to be observed by experienced visual observers. This type of shower associated with long periodic comets may sooner or later surprise observers with an outburst when Earth encounters a more dense dust trail released by this comet. Alertness around 10 May for eta Lyrid activity is highly recommended.

Acknowledgment

References

Drummond J. D. (1981). "A test of comet and meteor shower associations". *Icarus*, **45**, 545–553.

Hawkins G. S. (1963). "The Harvard radio meteor project". *Smithsonian Contributions to Astrophysics*, **7**, 53–62.

Jenniskens P. (1985). "Meteoren van 1983-d ?". *Radiant*, **7**, 31–33.

Jenniskens P., Gural P. S., Grigsby B., Dynneson L., Koop M. and Holman D. (2011). "CAMS: Cameras for Allsky Meteor Surveillance to validate minor meteor showers". *Icarus*, **216**, 40–61.

Jenniskens P., Nénon Q., Albers J., Gural P.S., Haberman B., Holman D., Morales R., Grigsby B.J., Samuels D., Johannink C. (2016). "The established meteor showers as observed by CAMS". *Icarus*, **266**, 331–354.

Jenniskens P., Baggaley J., Crumpton I., Aldous P., Pokorny P., Janches D., Gural P.S., Samuels D., Albers J., Howell A., Johannink C., Breukers M., Odeh M., Moskovitz N., Collison J., and Ganjuag S. (2018). "A survey of southern hemisphere meteor showers". *Planetary Space Science*, **154**, 21–29.

Johannink C. and Miskotte K. (2017). "The remainders of an old acquaintance: Eta Lyrids from comet IRAS-Araki-Alcock (C/1983 H1)". *eMetN*, **2**, 88–91.

Jopek T. J. (1993). "Remarks on the meteor orbital similarity D-criterion". *Icarus*, **106**, 603–607.

Kornoš L., Matlovič P., Rudawska R., Tóth J., Hajduková M. Jr., Koukal J., and Piffl R. (2014). "Confirmation and characterization of IAU temporary meteor showers in EDMOND database".

In Jopek T. J., Rietmeijer F. J. M., Watanabe J., Williams I. P., editors, *Proceedings of the Meteoroids 2013 Conference*, Poznań, Poland, Aug. 26-30, 2013. A.M. University, pages 225–233.

Kronk G. (1988). "Meteorshowers A descriptive Catalog". Enslow Publishers, Inc. Hillside, U.S.A.

Marsden B. (1983a). "Comet IRAS-Araki-Alcock (1983d)." *IAU Circular* N°. 3805 (1983 March 9).

Marsden B. (1983b). *IAU Circular* N°. 3817.

Molau S. and Rendtel J. (2009). "A comprehensive list of meteor showers obtained from 10 years of observations with the IMO Video Meteor network". *WGN, Journal of the International Meteor Organization*, **37**, 98–121.

Molau S., Kac J., Berko E., Crivello S., Stomeo E., Igaz A., Barentsen G., Goncalves R. (2013). "Results of the IMO Video Meteor Network — May 2013". *WGN, Journal of the International Meteor Organization*, **41**, 133–138.

Roggemans P. (1983). "Comet IRAS". *WGN*, **11**, 109.

Roggemans P. (2017). "Variation in heights of CAMS meteor trajectories". *eMetN*, **2**, 80–86.

Roggemans P. and Johannink C. (2018). "A search for December alpha Bootids (497)". *eMetN*, **3**, 64–72.

SonotaCo (2009). "A meteor shower catalog based on video observations in 2007-2008". *WGN, Journal of the International Meteor Organization*, **37**, 55–62.

Southworth R. R. and Hawkins G. S. (1963). "Statistics of meteor streams". *Smithson. Contrib. Astrophys.*, **7**, 261–286.

The Leonids during the off-season period
Part 1 – 2017: a small outburst!

Koen Miskotte

Dutch Meteor Society
k.miskotte@upcmail.nl

A comprehensive analysis of the Leonids 2017 is presented based on visual observational data sent to the International Meteor Organization and to the author. During the night of 16 on 17 November, some increased activity of the Leonids with bright meteors has been observed over Europe. Also during the night of 19 on 20 November, possible increased activity of the Leonids was observed over North America. This article focusses on these two possible small outbursts of the Leonids observed by Kai Frode Gaarder from Norway and George Gliba from the U.S.

1   Introduction

It is already 15 years ago since we were able to observe the last major outburst of the Leonids. In the period after 2002 there have been a few smaller outbursts, such as in 2006, 2008 and 2009. Then the activity level calmed down. But every now and then the Leonids show some surprises. Also in 2017, on 17 November 2017 the author received an enthusiastic Facebook message from the Norwegian observer Kai Gaarder:

"*I had great fun watching the Leonids tonight! I got 3.5 hours of observations, and both activity level and magnitude distribution changed a lot during the watch. First half of the period many bright Leonids were seen, and there was a complete lack of faint meteors. Then things suddenly changed. The bright meteors disappeared, and the faint ones started to show up. A short time activity level was quite good, before activity dropped to almost nothing at the end of the watch with the radiant high in the sky*".

A more detailed report of his observations has been described in MeteorNews (Gaarder, 2018). His message remained in my mind, especially after capturing two bright Leonids in the night of 18 on 19 November 2017 with my all-sky camera: these were two Leonids of resp. –8 and –3. The brightest Leonid was also extensively recorded by other all-sky and CAMS systems in the BeNeLux (Roggemans et al., 2018a, 2018b). Has there been something strange going on here?

The question remained unanswered for a long time due to other issues, until I received an email in early April from the American observer George Gliba about a nice Leonid activity on November 20. His observation is described in detail in "The Valley Skywatcher of the Chagrin Valley Astronomical Society[18]".

He wrote: "*I was rewarded by seeing what was probably part of an older dust trail that was not predicted. I was also able to get in a good hour with clear LM = 6.5 skies. From 9:42 to 10:42 UT I was able to see 11 Leonids. The average Leonid was a relatively bright 1.6 magnitude and left a train. I also saw 3 NTA, 3 STA, 1 NOO, 1 AMO, and 9 SPO meteors. There were also seen a beautiful -2, a very nice -1, and two good 0 magnitude Leonids. It was cold out with a 6° F wind chill, but it was well worth it. I'm glad I didn't go back to sleep after I put that last log on the fire (which I almost did)*".

As a result of both reports, I decided to make an analysis of the Leonids 2017. The interesting results are described in this report.

2   Collecting the data
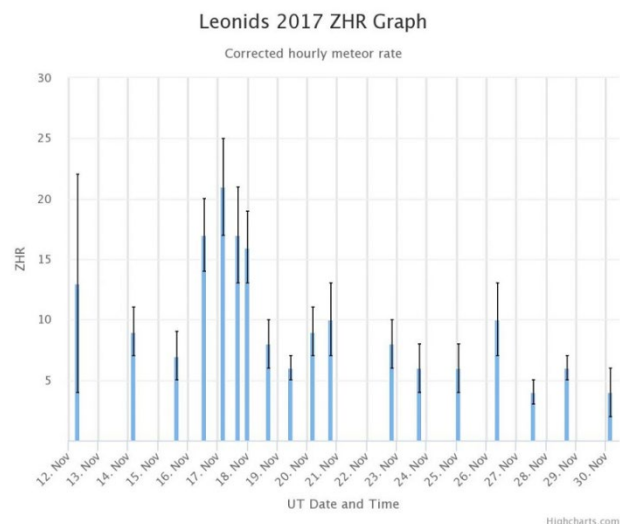
Figure 1 – ZHR Leonids 2017 "on the fly" profile on the IMO website.

Unfortunately, there is very little data available from the Leonids 2017. The IMO site shows that 21 observers submitted data with observations made between 12 and 30 November. A total of 272 Leonids were reported. *Figure 1*

---

shows the "on the fly" curve based on data reported to IMO.

It is clearly visible that the highest activity according to this curve occurred in the night of 16 on 17 November over Europe. Furthermore, it also appears that this is only the data of Kai Gaarder from Norway, the weather for most European meteor observers having been bad that night. The author also obtained data from observers who did not report to IMO.

After the data was stored in the ZHR spreadsheet it turned out that there is hardly overlap between the observations. That is very unfortunate, because that is the only way to check if there are some outliers. The fact that few observers were active in November 2017 may have to do with the fact that we are now in the off season period for the Leonids and that the weather hardly cooperated in 2017.

The data included in the ZHR spreadsheet with the following known requirements: the limiting magnitude should not be less than rounded off to 5.9, the minimum radiant height is 25 degrees and only data from observers with a known C_p determination are used. In the end, 306 Leonids were used for ZHR calculations. This number is higher than reported to IMO, because some observers only sent data to the author.

3 Leonids 2017: Zenithal Hourly Rate

The ZHR was determined using the method of Peter Jenniskens as described in Miskotte & Johannink (2005a; 2005b) with gamma being set to 1.0 instead of 1.4 in order to make a comparison with the IMO curve. Because very little data was available, no reliable calculation could be made for the population index r. Therefore, a value of 2.50 (Rendtel, 2016) has been assumed. The result is presented in *Figure 2*.
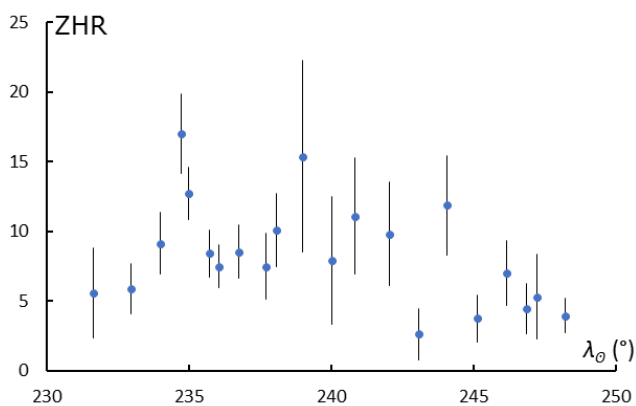
Figure 2 – ZHR Leonids in 2017, based on 306 Leonids, zenith exponent γ = 1.0 and population index r = 2.5.

According to the IMO 2017 Meteor Shower Calendar (Rendtel, 2017) the nodal maximum of the Leonids was predicted at $\lambda_O = 235.27°$ (17 November 2017 at 16:30 UT) with a ZHR of 10. This time is very unfavorable because the maximum was above the Pacific Ocean.

Indeed and unfortunately there is no data available for the period November 17, 2017, between 10:00 and 20:05 UT.

The maximum activity of the Leonids as found in *Figure 2* is visible on November 17 above Europe ($\lambda_O = 234.8°$). This is entirely and solely based on data from Kai Gaarder. Furthermore, a relatively high activity is visible near $\lambda_O = 239°$, but this ZHR point has a large deviation and is probably an outlier caused by a relatively low radiant level (30 degrees in this case) and this is data from one single observer. The points after $\lambda_O = 239.0°$ also have the same problems.

Furthermore, it is emphasized again that the ZHR graph was compiled on the basis of few data. *Figure 3* is the same graph as *Figure 2*, but now the colors of the ZHR points indicate how many count periods have been used for that particular ZHR point. This gives us a little insight into how reliable the ZHR points are. It is clear that a ZHR point based on 3 or (better) more periods is more reliable than a ZHR point based on only 1 period.
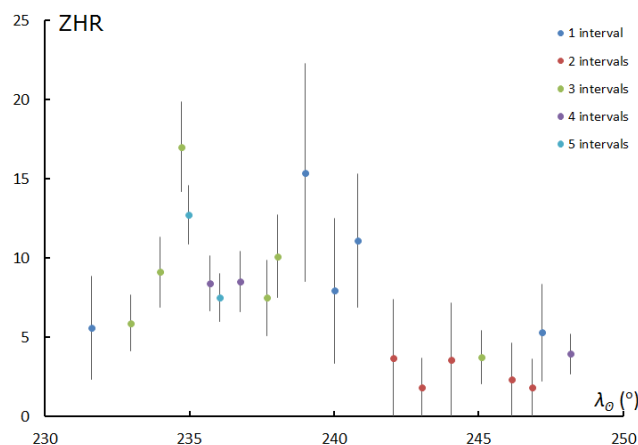
Figure 3 – The same graph as in Figure 2, but now the ZHR points are in different colors to indicate the number of periods used for each ZHR point, using zenith exponent γ = 1.0 and population index r = 2.5.
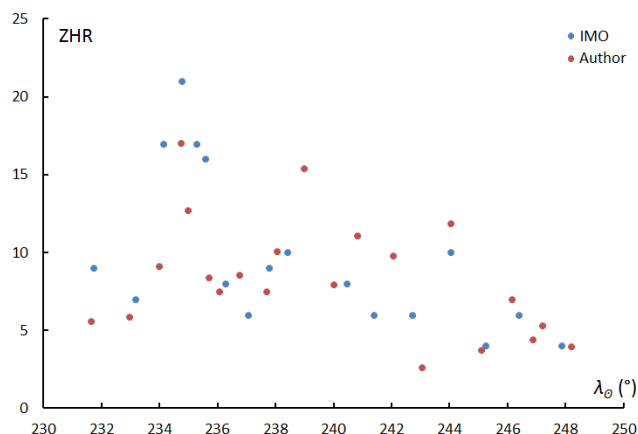
Figure 4 – Comparison between the ZHR curve of the author and the on the fly curve of the IMO, using a zenith exponent γ = 1.0 and population index r = 2.5.

In *Figure 4* a comparison with the on the fly curve of the IMO is presented. Note, the parameters of the IMO curve are different from those used by the author. The most

important is that IMO uses a minimum limiting magnitude of 5.0 compared to the 5.9 used by the author. As a result, part of the data that is used in the IMO curve is not used. In addition, the C_p's of the observers are also taken into account. As a result, the ZHR values of this analysis are slightly lower than those of the IMO.

4   The observations of Kai Gaarder

Because Kai mentioned in his report (2018); "*a lot of bright Leonids and later more weak Leonids*", the author extensively analyzed his data once again. His data is summarized in *Tables 1 and 2*.

Table 1 – Magnitude distribution of Leonids by Kai Gaarder on 17 November 2017 between 01:45 and 05:15 UT.

Date	Period UT	SHO	-3	-2	-1	0	1	2	3	4	5	Total	Lm	m
17/11/2017	01:45-02:50	LEO	~	~	2	3	1	1	2	1	~	10	6.15	1.10
17/11/2017	02:50-03:55	LEO	1	1	1	~	~	3	3	1	1	11	6.15	1.64
17/11/2017	03:55-05:15	LEO	~	1	~	~	~	2	2	7	3	15	6.13	3.40

Table 2 – ZHR Leonids 17 November 2017 based on hourly counts.

Year	Month	Day	t/m	Lm	$\lambda_\odot$	ZHR	Dev
2017	11	17	2.29	6.15	234.678	17.35	5.49
2017	11	17	3.375	6.15	234.723	16.78	5.06
2017	11	17	4.58	6.13	234.774	16.93	4.37

The magnitude distribution and the (uncorrected) average magnitude are striking. These drop by 2 magnitudes in the last hour. This is indeed a strange phenomenon. Kai Gaarder also reports in his report that the last bright Leonid of –2 appears almost immediately at the beginning of his last period, followed by an increase of weak Leonids. This activity also decreases at the end of his session.
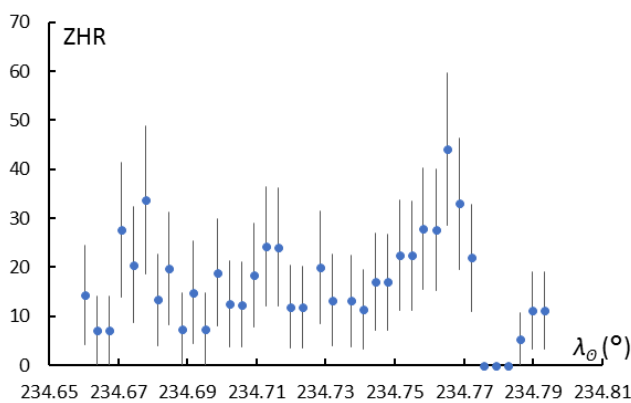
Figure 5 – ZHR Leonids November 17, 2017 based on visual data from Kai Gaarder.

A ZHR of 17 during his observational window is rather high, also taking into account that the maximum would take place 14 hours later with a maximum ZHR expected to be around 10. *Table 2* also shows that there appears to be a constant ZHR with a ZHR of 17 for the entire period. Because Kai Gaarder's report mentioned rapid changing activity, it was decided to do a ZHR analysis in much smaller intervals. At the request of the author, Kai sent his data in 5 minutes intervals. From his 5 minute counts 15

minute counts were made and these were used for ZHR calculations. A ZHR determination is then made every 5 minutes and based on the 15-minute counts. As *r* value, 2.00 was now adopted, this because of the bright Leonids. The result is very interesting despite the fact that this is a small amount of data! The result is shown in *Figure 5*.

A cautious conclusion is that there seems to be a maximum around $\lambda_\odot = 234.68°$ (November 17, 2017 02:18 UT) with a ZHR of 34 (~15). This peak consists of mostly bright Leonids (magnitude between –2 and +3). A second peak is found at $\lambda_\odot = 234.77°$ (November 17, 2017 04:22 UT) with a ZHR of 43 and which consists of more weak Leonids (magnitudes between +2 and +5.). Between the two peaks, the ZHR is variable between 8 and 23 with still bright Leonids, but this activity decreases rapidly as the 2nd peak approaches. After the second peak, the activity collapses rapidly. Attention: the amount of data is not that big and may have a negative effect on this analysis.

A possible cause for this small outburst has been given by Mikhail Maslov (Rendtel, 2016; Maslov, 2007): an old dust trail of comet 55P Tempel-Tuttle from 1300. The maximum he predicted on 16 November 17:07 UT ($\lambda_\odot = 234.292°$) with a ZHR of 10 and bright meteors. It seems that Kai Gaarder has observed (part of) this outburst, although his observation session begins 6 hours later. The occurrence of the peak with weaker meteors does not fit with Maslov's story. It is not clear how wide this expected peak would be, nothing is mentioned in the 2017 Meteor Shower Calendar (Rendtel, 2016) or in a Maslov publication from 2007 (Maslov, 2007). Also in the book by Peter Jenniskens (2006) there is nothing to be found for 2017, not for expected dust trails and not for any filament.

If we look at the well-known radio graphs of the Japanese based on worldwide radio data from the RMOB (*Figure 6*), we indeed see the highest (radio) activity of the Leonids close to Maslov's time in 2017. The peak observed by Kai Gaarder is somewhat later than the radio peak. The radio data is converted to a visual ZHR, but it is not clear how this is done exactly.

The nearest visual observation at the time of Maslov's prediction for the 1300 dust trail is next to that of Kai Gaarder, as well as that of Terrence Ross (Texas, USA) from November 16, 2017 from 07:53 to 10:00 UT ($\lambda_\odot = 233.905°$ to 233.994°), which is 7 hours earlier. It is striking that half of the 8 observed Leonids are of magnitude 0 and –1.

5   The observations of George Gliba

In the early morning of November 20, 2017, George Gliba witnessed nice Leonid activity from Mathias, West Virginia, US. He counted 11 Leonids between 09:42 and 10:42 UT (resulting in a ZHR of 13), including a number of bright Leonids. This took place around $\lambda_\odot = 238.038°$. The Japanese radio profile (*Figure 6*) hardly shows any Leonid activity around that solar longitude.
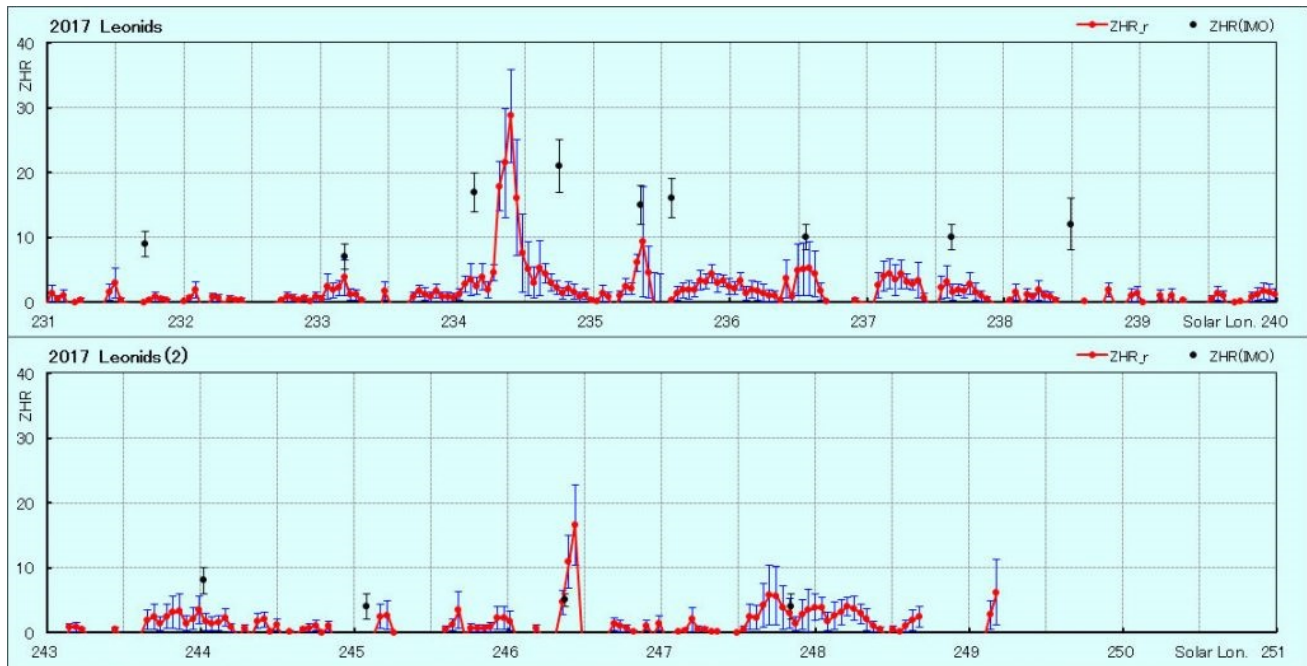
Figure 6 – Activity curve of the Leonids 2017 based on radio data from the RMOB.

Subsequently, we looked in detail at data from other observers who were active in the same night, e.g. Robert Lunsford (from El Cajon, California, US) and Terrence Ross (from Alpine, Texas, US). *Table 3* gives an overview of their data (including the data of George Gliba).

Table 3 – Data from 3 observers for the night November 20, 2017 (UT).

Date	Period UT	Obs	-4	-3	-2	-1	0	1	2	3	4	5	Tot	lm
20/11/2017	08:16-09:30	ROSTE	1				1		3	1	1		7	6.36
20/11/2017	09:42-10:42	GLIBA			1	1	2						11	6.50
20/11/2017	11:00-13:00	LUNRO						1	2	2	1		6	5.69

Table 4 – Individual ZHR values on November 20, 2017 (US only).

Jaar	Maand	Dag	t/m	Lm	Obs	λ	ZHR	Dev
2017	11	20	8.88	6.36	ROSTE	237.982	12.67	4.79
2017	11	20	10.2	6.50	GLIBA	238.038	12.19	3.68
2017	11	20	12.5	5.89	LUNRO	238.135	8.00	4.00

Altogether, the observational data shows a hint of increased activity, especially taking into account that it was observed on November 20. Neither in the article by Maslov (2007) nor in the book by Peter Jenniskens (2006) have we found anything that may have caused this possible outburst.

6   Conclusions and recommendations

The Leonids of 2017 have been moderately observed. The nodal maximum expected to fall above the Pacific has not been observed. The observation of Kai Gaarder for the night of 16/17 November 2017 shows an increased activity with nice bright Leonids up to -3. According to Maslov (Rendtel, 2016; Maslov, 2007), the cause could be an old dust trail from comet 55P Tempel-Tuttle from 1300. The radio data from RMOB matches better with the prediction of Maslov than the observations of Kai Gaarder.

There may also have been some increased activity observed by George Gliba and Terrence Ross on November 20, 2017 at ~ 10 UT. A possible explanation for this is not yet known. The activity is not confirmed by the RMOB radio data. It is known that enhanced Leonid activity has been observed more often around and after 20 November. A good example is 22 on 23 November 2015 when some activity was observed from a dust trail from 636. The observations of Gliba and Ross therefore clearly show that the period (far) after the Leonid maximum may still be full of unexpected surprises. The modelers should take a look at old dust traces of comet 55P Tempel-Tuttle after November 18th.

Therefore it is advisable for observers to continue observing (far) after the Leonid's maximum. Go observing from a dark location where the limiting magnitude is at least 5.9. Watch preferably in the last hours of the night when the Leonid radiant is high. Also ensure that there is sufficient sporadic data from the period 25 July to the end of August between 0 and 4 am local time. Then a reliable C_p can be calculated and the analysis becomes more robust.

Acknowledgments

References

Gaarder K. F. (2018). "Leonids 2017 from Norway – A bright surprise!". *eMetN*, **3**, 28–30.

Jenniskens P. (1994). "Meteor Stream activity 1. The annual streams". *Astron. & Astrophys.* **287**, 990–1013.

Jenniskens P. (2006). Meteor showers and their Parent Comets. Cambridge Univ. Press., 790 pages.

Maslov M. (2007). "Leonid predictions for the period 2001-2100". *WGN, Journal of the International Meteor Organization*, **35**, 5–12.

Miskotte K. and Johannink C. (2005a). "Analyse Perseïden 2004". *eRadiant*, **1**, 9–12.

Miskotte K. and Johannink C. (2005b). "Analyse Geminiden 2004". *eRadiant*, **1**, 14–19.

Roggemans P., Johannink C., Biets J. M., Breukers M., Haas R. and Jobse K (2018a). "Leonid fireball above the BeNeLux 2017 November 19, 02h29m UT". *eMetN*, **3**, 21–25.

Roggemans P., Johannink C., Biets J. M., Breukers M., Haas R. and Jobse K (2018b). "Heldere Leonide vuurbol boven de BeNeLux (19 november 02:29 UT)". *eRadiant*, **12**, 130–139.

Rendtel J. (2016). "2017 Meteor Shower Calendar". IMO.

Radiometeors – 2017 and first quarter 2018

Felix Verbelen

Vereniging voor Sterrenkunde & Volkssterrenwacht MIRA, Grimbergen, Belgium
`felix.verbelen@skynet.be`

An overview of the radio observations during the year 2017 is given as well as for January, February and March 2018.

1   Introduction

An overview of the radio observations for 2017 is presented together with the monthly results for the months of January, February and March 2018, all observed at Kampenhout (BE) on the frequency of our VVS-beacon (49.99 MHz).

The hourly numbers, for echoes shorter than 1 minute, are weighted averages derived from:

$$N(h) = \frac{n(h-1)}{4} + \frac{n(h)}{2} + \frac{n(h+1)}{4}$$

If you are interested in the actual figures, please send me an e-mail.

2   Annual report for 2017

The graphs show the daily totals (*Figure 1 and 2*) of "all" reflections counted automatically and of manually counted "overdense" reflections, overdense reflections longer than 10 seconds and longer than 1 minute.

Figure 1 – The daily totals of "all" reflections counted automatically and of manually counted "overdense" reflections as observed here at Kampenhout (BE) on the frequency of our VVS-beacon (49.99 MHz) during 2017.
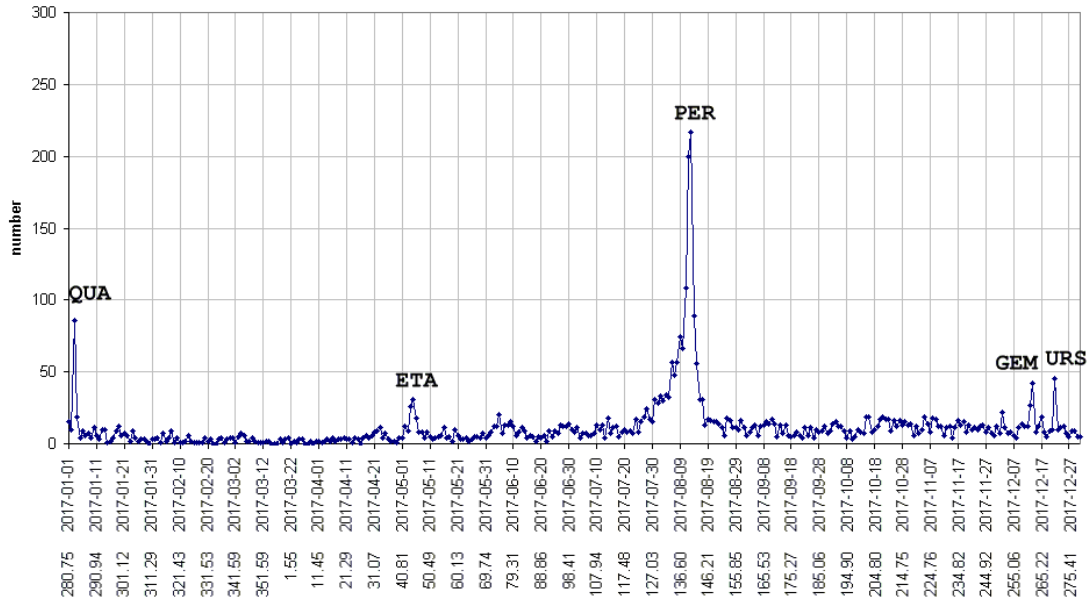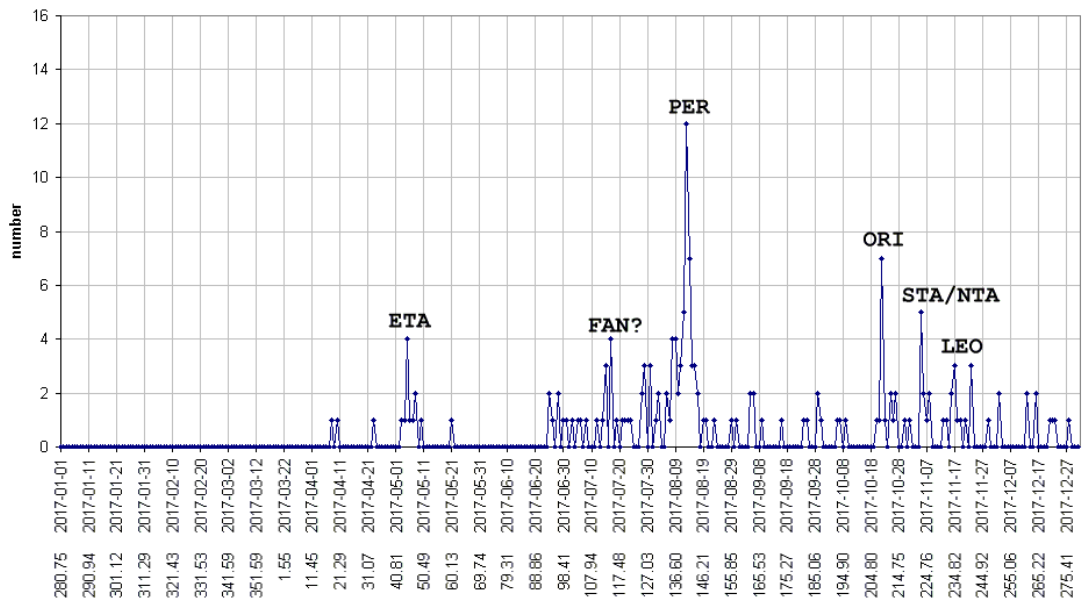
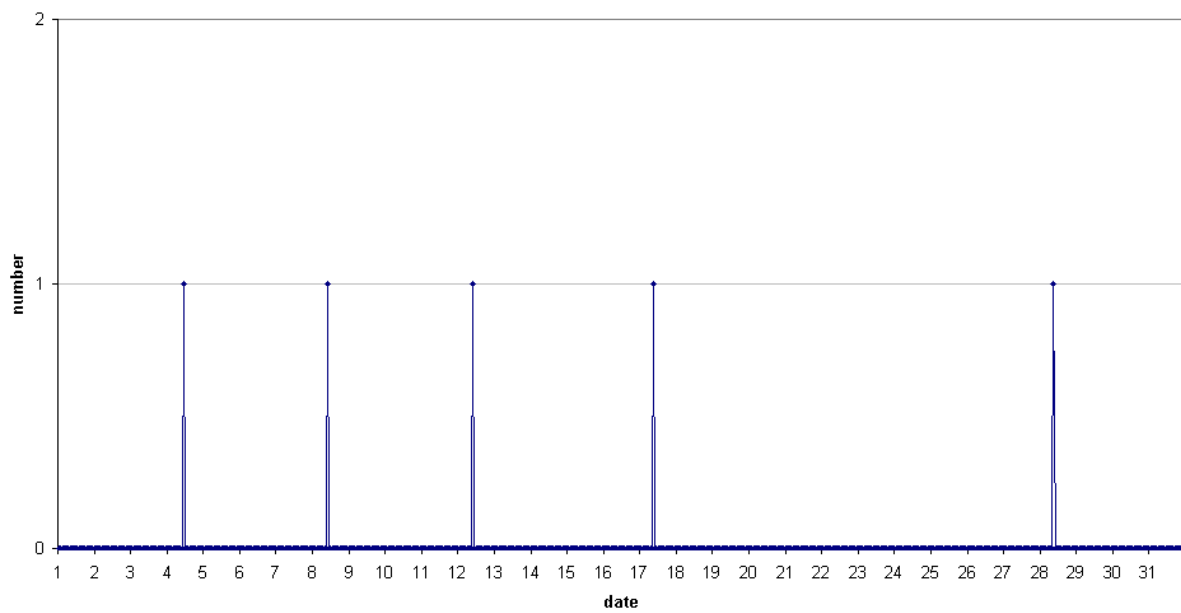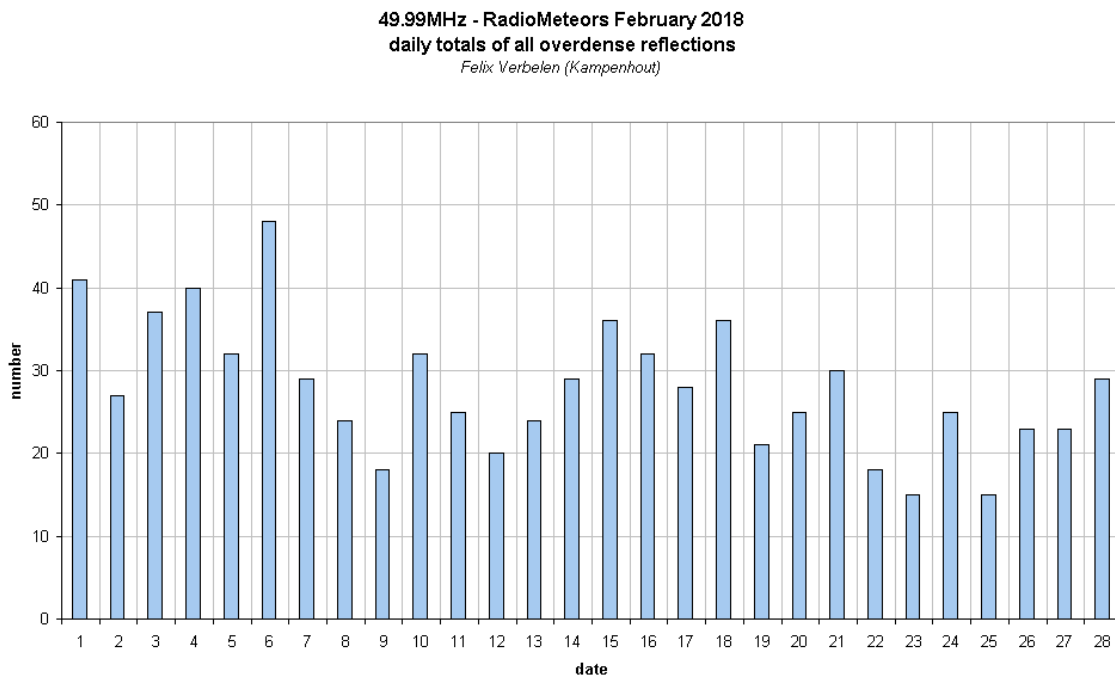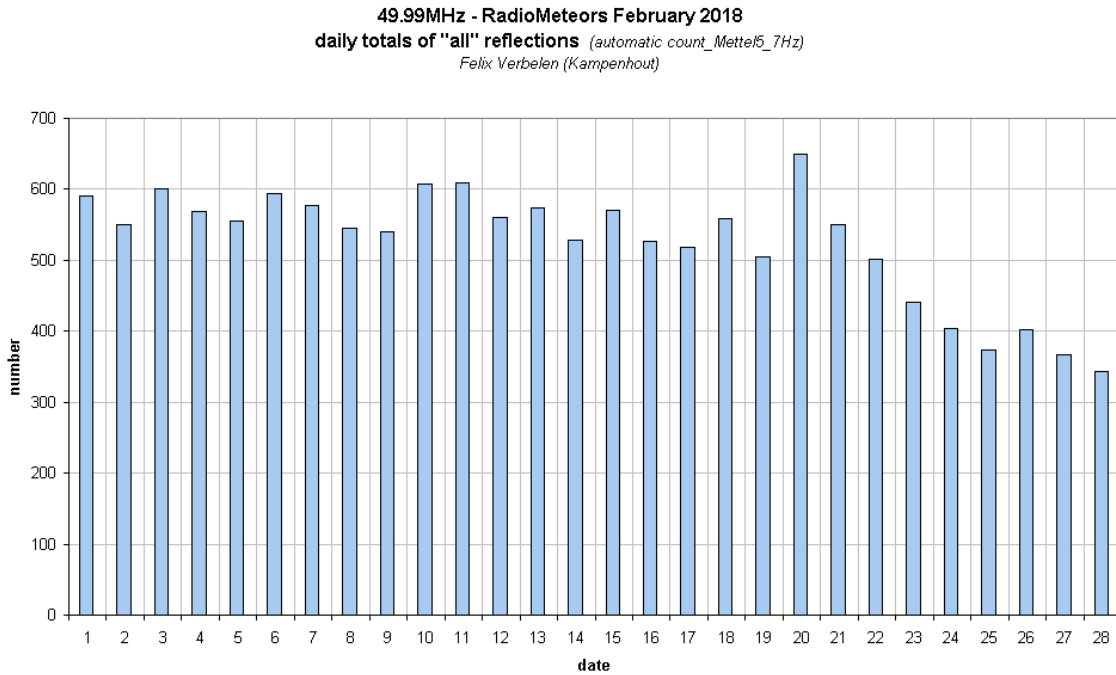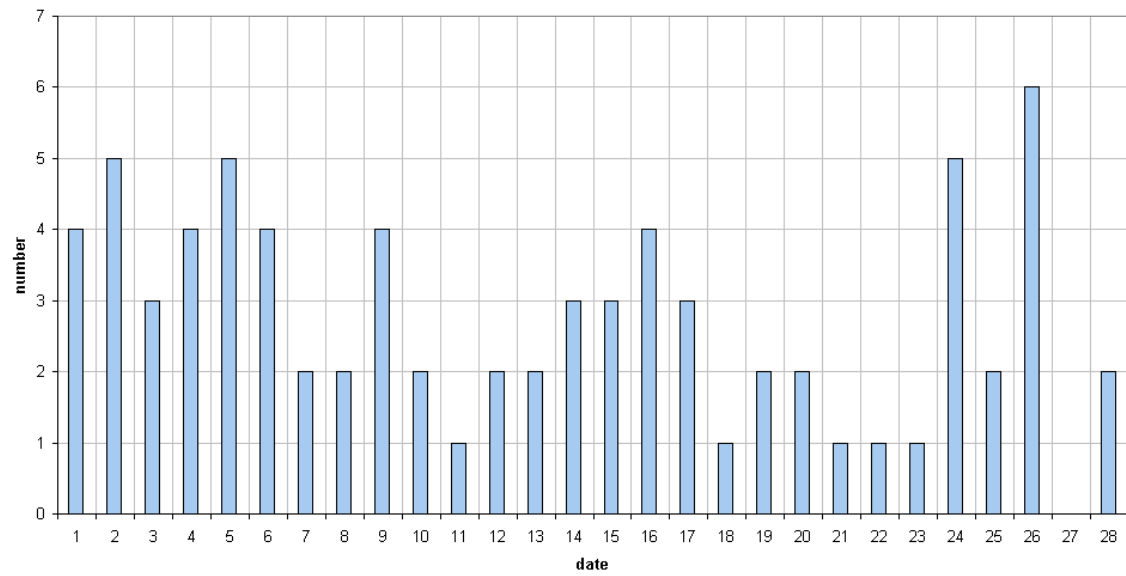*Figure 2* – The daily totals of manually counted overdense reflections longer than 10 seconds and longer than 1 minute., as observed here at Kampenhout (BE) on the frequency of our VVS-beacon (49.99 MHz) during 2017.

3   Radiometeors January 2018

The graphs show both the daily totals (*Figure 3 and 4*) and the hourly numbers (*Figure 5 and 6*) of "all" reflections counted automatically, and of manually counted "overdense" reflections, overdense reflections longer than 10 seconds and longer than 1 minute.

Figure 3 – The daily totals of "all" reflections counted automatically and of manually counted "overdense" reflections, as observed here at Kampenhout (BE) on the frequency of our VVS-beacon (49.99 MHz) during January 2018.

49.99MHz - RadioMeteors January 2018
daily totals of reflections longer than 10 seconds
Felix Verbelen (Kampenhout)
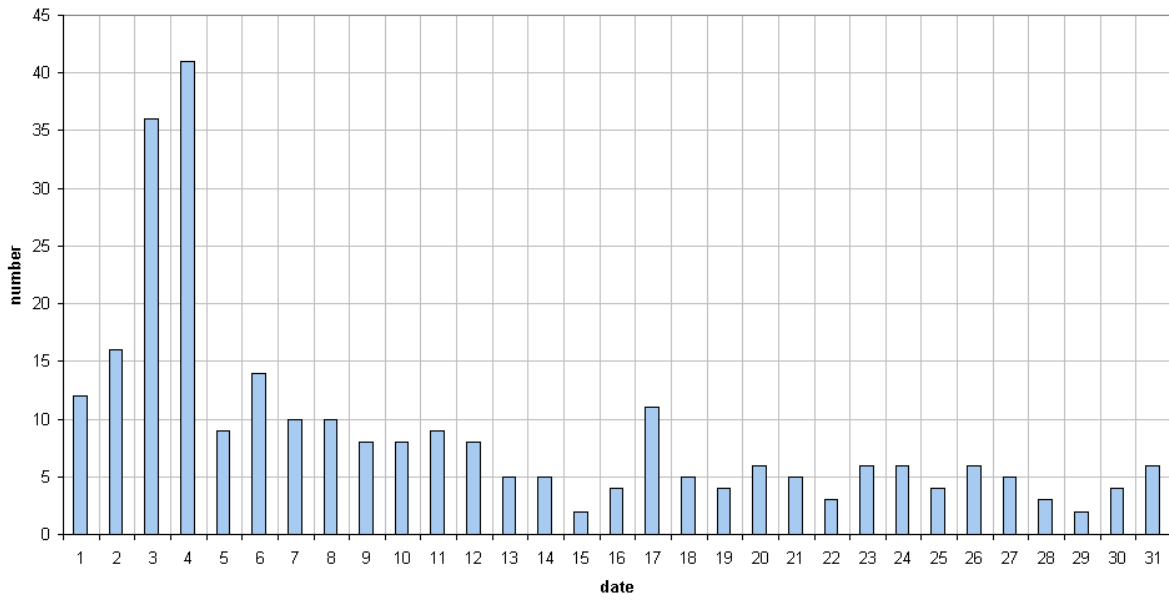
49.99MHz - RadioMeteors January 2018
daily totals of reflections longer than 1 minute
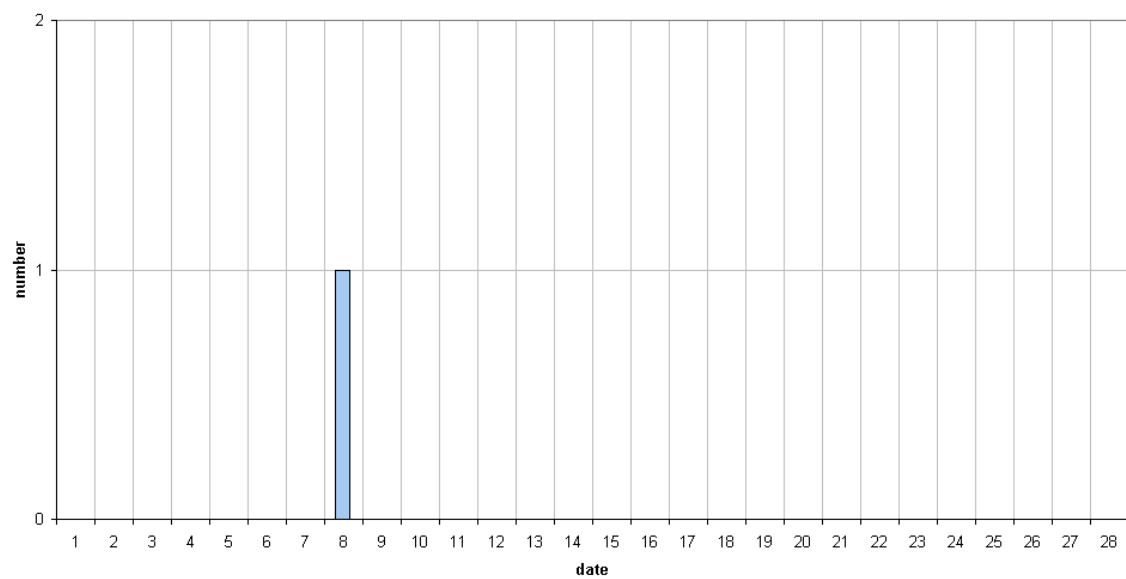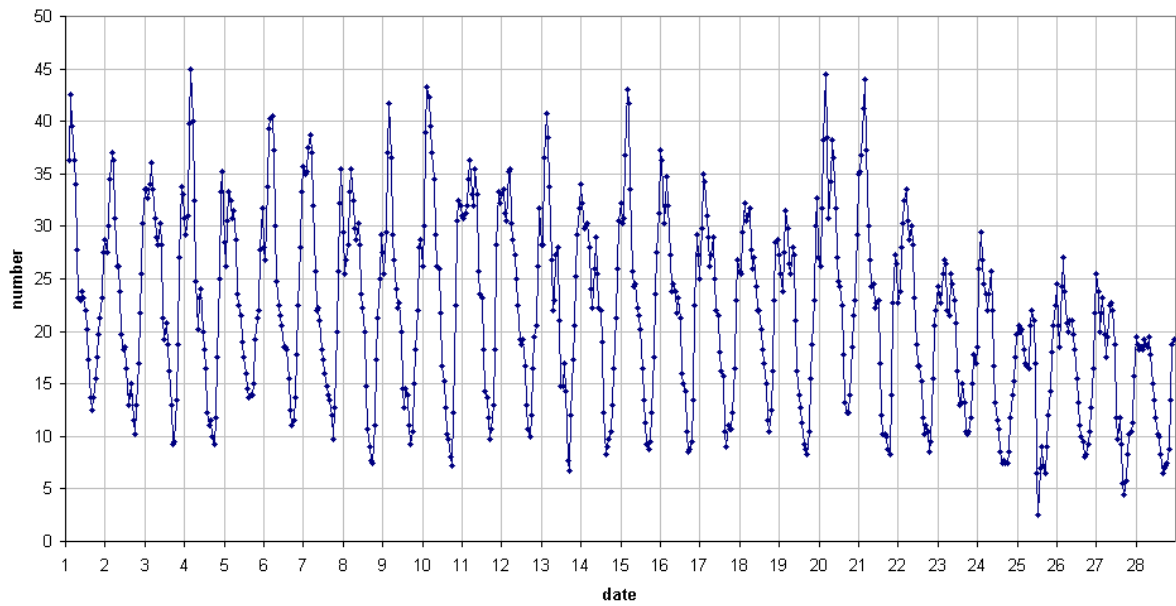*Felix Verbelen (Kampenhout)*
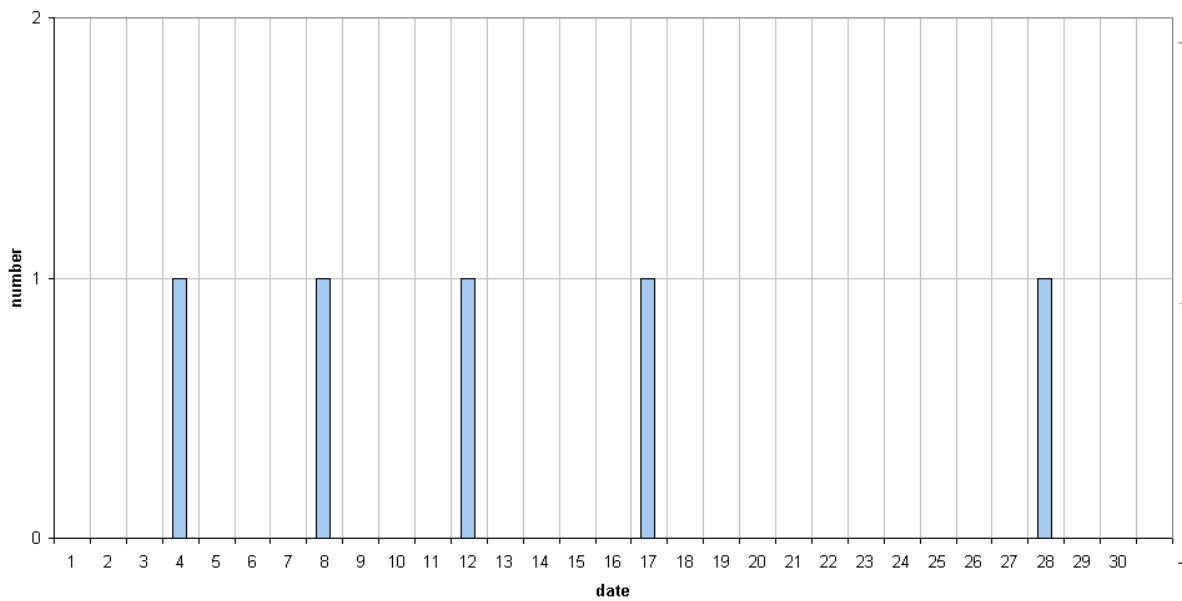
Figure 4 – The daily totals of overdense reflections longer than 10 seconds and longer than 1 minute, as observed here at Kampenhout (BE) on the frequency of our VVS-beacon (49.99 MHz) during January 2018.
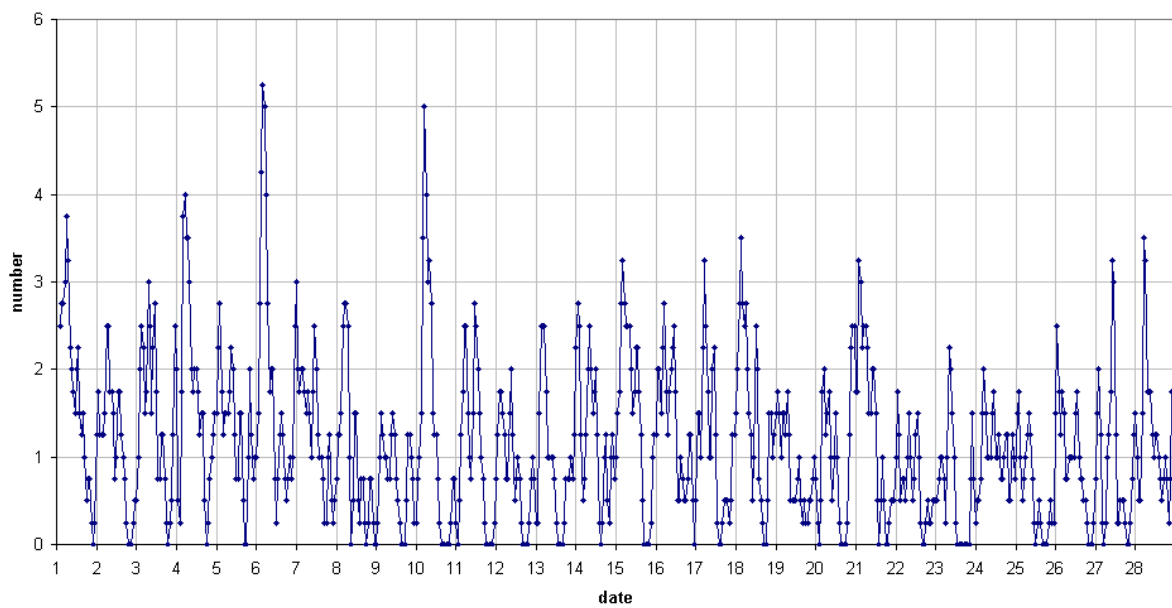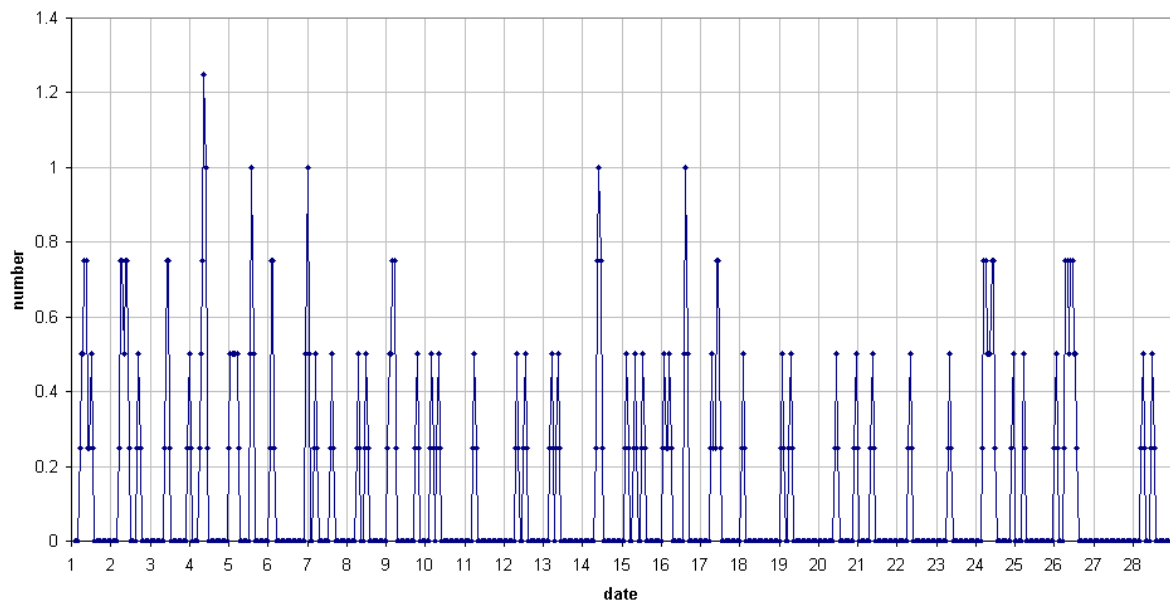
Figure 5 – The hourly numbers of "all" reflections counted automatically and the weighted average of manually counted "overdense" reflections, as observed here at Kampenhout (BE) on the frequency of our VVS-beacon (49.99 MHz) during January 2018.
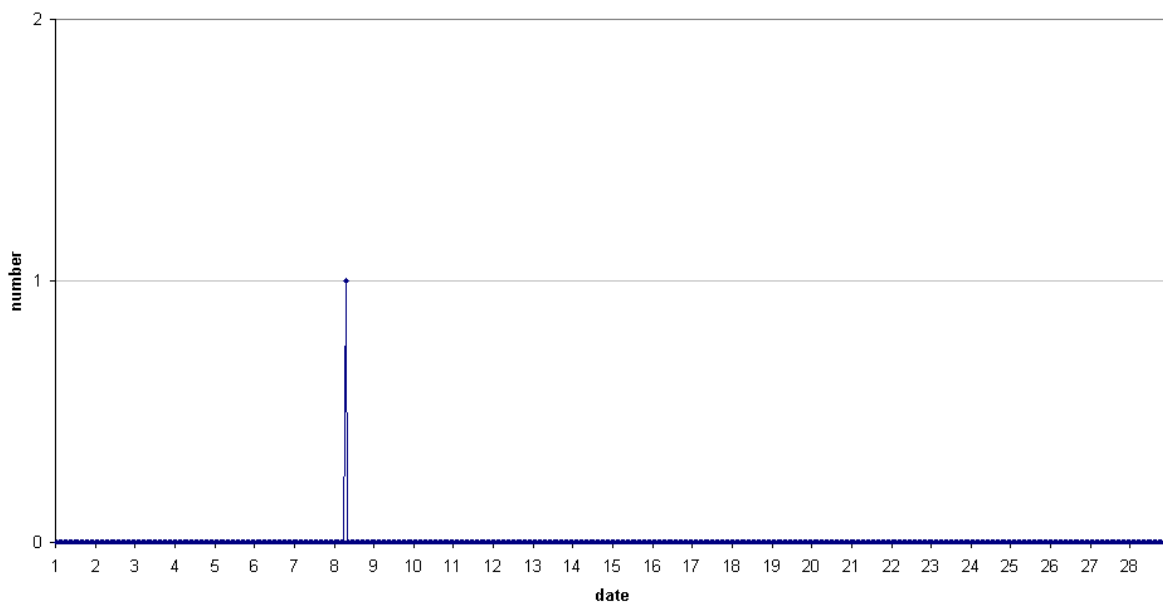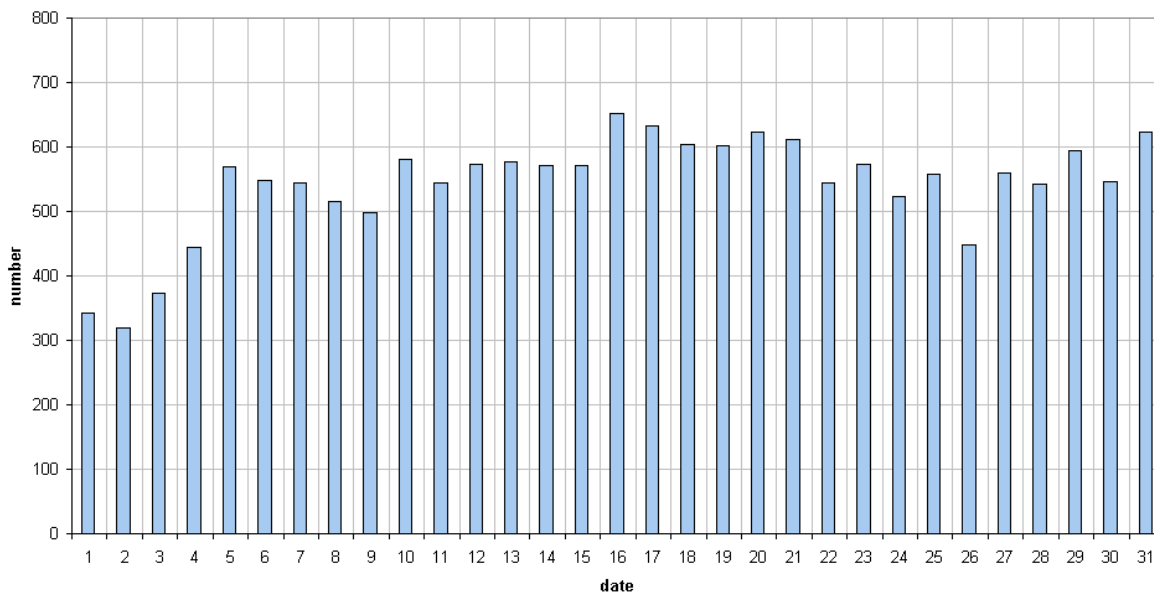
Figure 6 – The hourly numbers of overdense reflections longer than 10 seconds and longer than 1 minute, as observed here at Kampenhout (BE) on the frequency of our VVS-beacon (49.99 MHz) during January 2018.

4   Radiometeors February 2018

The graphs show both the daily totals (*Figure 7 and 8*) and the hourly numbers (*Figure 9 and 10*) of "all" reflections counted automatically, and of manually counted "overdense" reflections, overdense reflections longer than 10 seconds and longer than 1 minute.

49.99MHz - RadioMeteors February 2018
daily totals of "all" reflections *(automatic count_Mettel5_7Hz)*
Felix Verbelen (Kampenhout)

49.99MHz - RadioMeteors February 2018
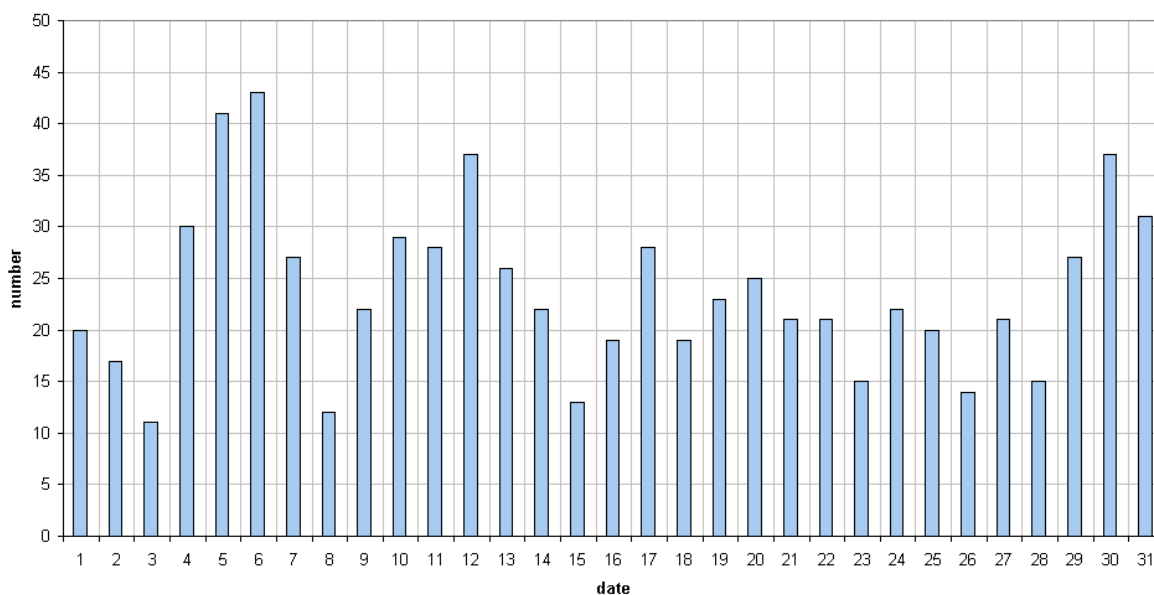**daily totals of all overdense reflections**
Felix Verbelen (Kampenhout)

Figure 7 – The daily totals of "all" reflections counted automatically and of manually counted "overdense" reflections, as observed here at Kampenhout (BE) on the frequency of our VVS-beacon (49.99 MHz) during February 2018.

49.99MHz - RadioMeteors February 2018
daily totals of reflections longer than 10 seconds
Felix Verbelen (Kampenhout)

49.99MHz - RadioMeteors February 2018
daily totals of reflections longer than 1 minute
Felix Verbelen (Kampenhout)

Figure 8 – The daily totals of overdense reflections longer than 10 seconds and longer than 1 minute, as observed here at Kampenhout (BE) on the frequency of our VVS-beacon (49.99 MHz) during February 2018.

49.99 MHz - RadioMeteors February 2018
number of "all" refections per hour (weighted average) *(automatic count_Mettel5_7Hz)*
Felix Verbelen (Kampenhout)

49.99MHz - RadioMeteors February 2018
number of overdense reflections per hour (weighted average)
Felix Verbelen (Kampenhout)

Figure 9 – The hourly numbers of "all" reflections counted automatically and the weighted average of manually counted "overdense" reflections, as observed here at Kampenhout (BE) on the frequency of our VVS-beacon (49.99 MHz) during February 2018.

49.99MHz - RadioMeteors February 2018
number of reflections >10 seconds per hour (weighted average)
Felix Verbelen (Kampenhout)

49.99MHz - RadioMeteors February 2018
hourly totals of overdense reflections longer than 1 minute
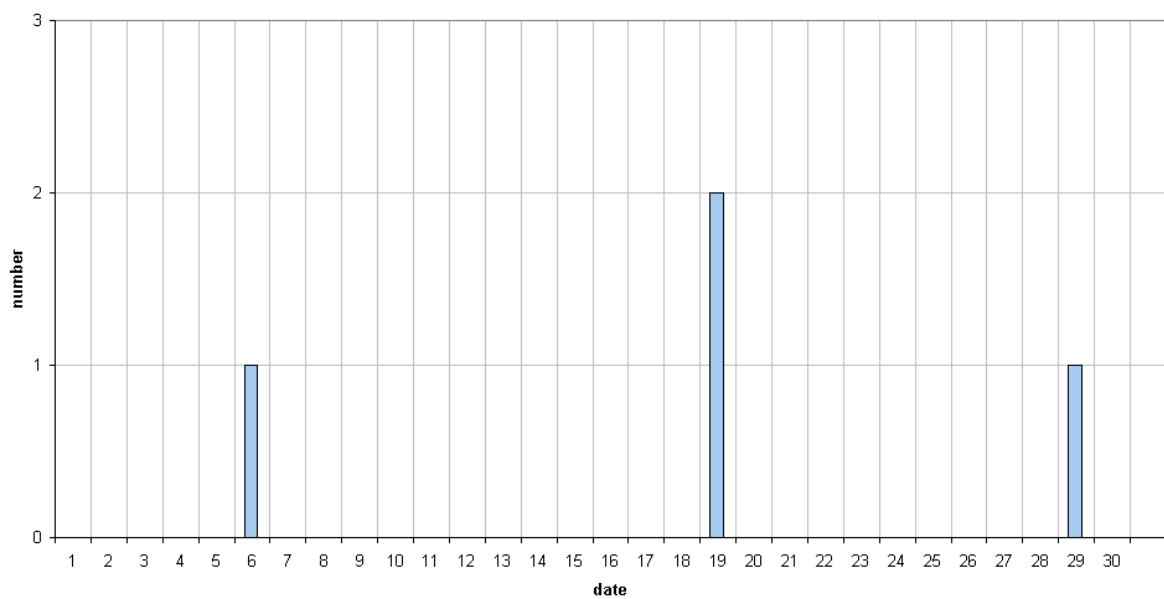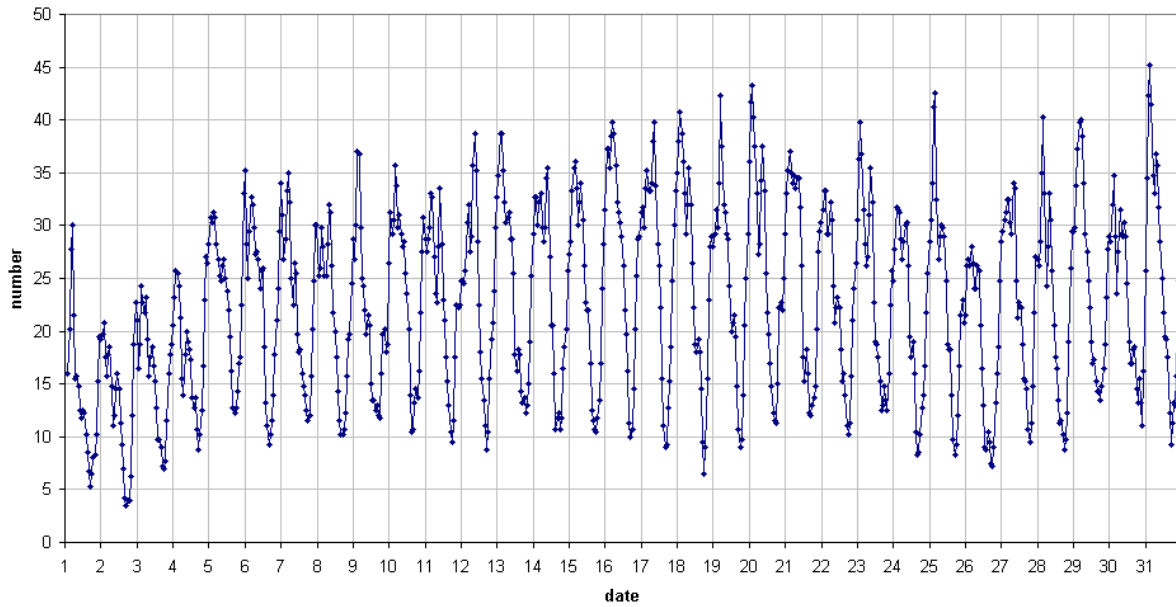*Felix Verbelen (Kampenhout/BE)*

Figure 10 – The hourly numbers of overdense reflections longer than 10 seconds and longer than 1 minute, as observed here at Kampenhout (BE) on the frequency of our VVS-beacon (49.99 MHz) during February 2018.

5   Radiometeors March 2018

The graphs show both the daily totals (*Figure 11 and 12*) and the hourly numbers (*Figure 13 and 14*) of "all" reflections counted automatically, and of manually counted "overdense" reflections, overdense reflections longer than 10 seconds and longer than 1 minute.

Figure 11 – The daily totals of "all" reflections counted automatically and of manually counted "overdense" reflections, as observed here at Kampenhout (BE) on the frequency of our VVS-beacon (49.99 MHz) during March 2018.

49.99MHz - RadioMeteors March 2018
daily totals of reflections longer than 10 seconds
Felix Verbelen (Kampenhout)

49.99MHz - RadioMeteors March 2018
daily totals of reflections longer than 1 minute
Felix Verbelen (Kampenhout)

Figure 12 – The daily totals of overdense reflections longer than 10 seconds and longer than 1 minute, as observed here at Kampenhout (BE) on the frequency of our VVS-beacon (49.99 MHz) during March 2018.

49.99 MHz - RadioMeteors March 2018
number of "all" refections per hour (weighted average) *(automatic count_Mettel5_7Hz)*
Felix Verbelen (Kampenhout)

49.99MHz - RadioMeteors March 2018
number of overdense reflections per hour (weighted average)
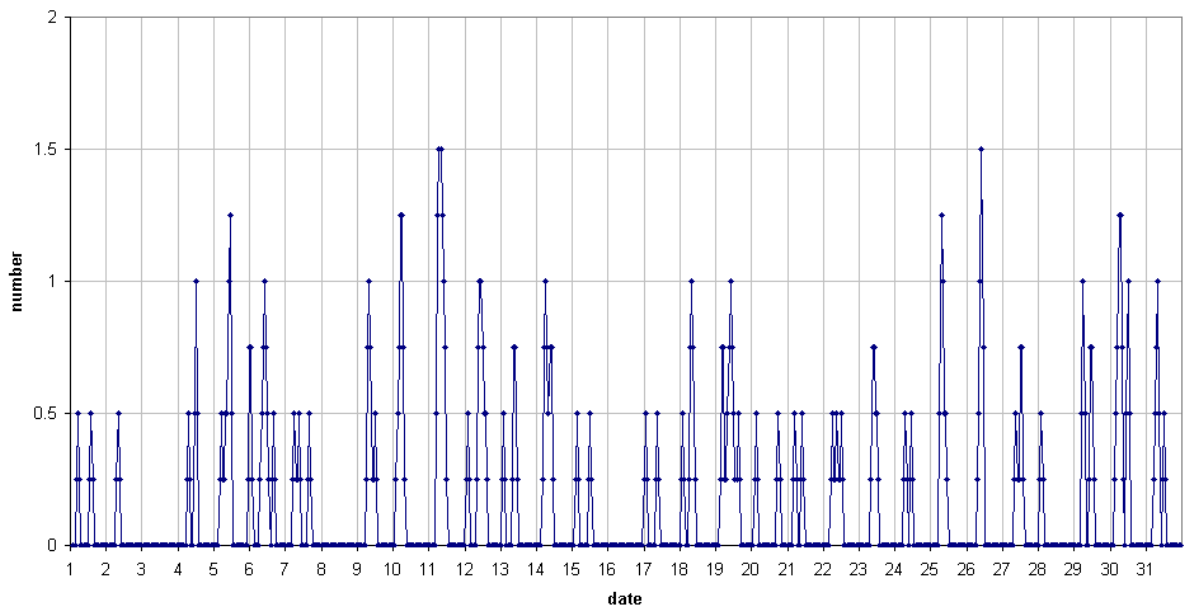*Felix Verbelen (Kampenhout)*
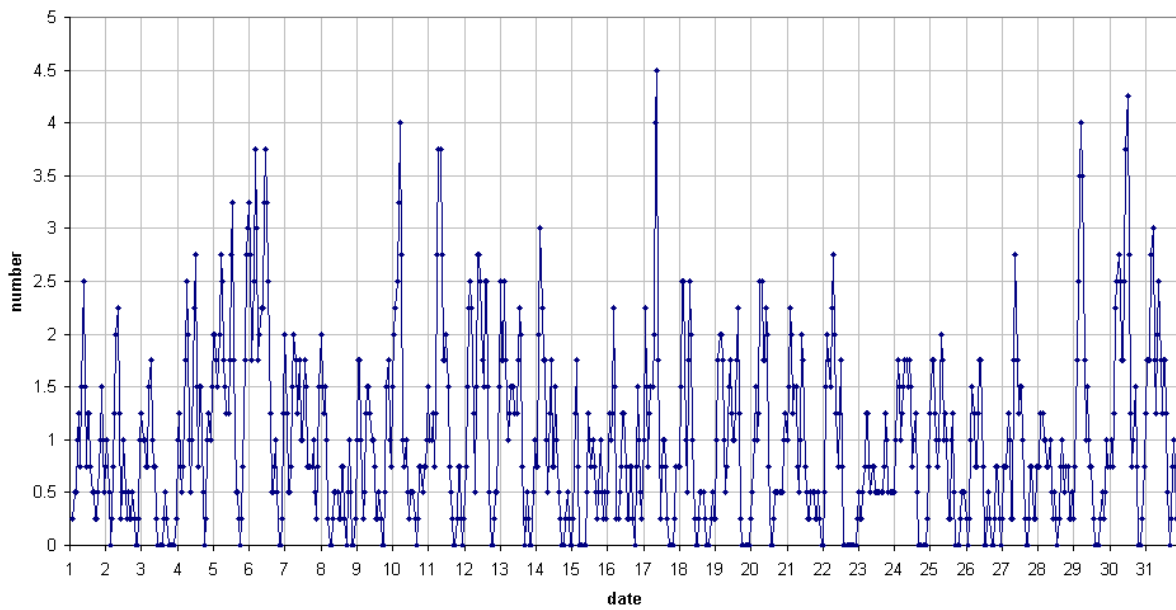
Figure 13 – The hourly numbers of "all" reflections counted automatically and the weighted average of manually counted "overdense" reflections, as observed here at Kampenhout (BE) on the frequency of our VVS-beacon (49.99 MHz) during March 2018.

49.99MHz - RadioMeteors March 2018
number of reflections >10 seconds per hour (weighted average)
Felix Verbelen (Kampenhout)

49.99MHz - RadioMeteors March 2018
hourly totals of overdense reflections longer than 1 minute
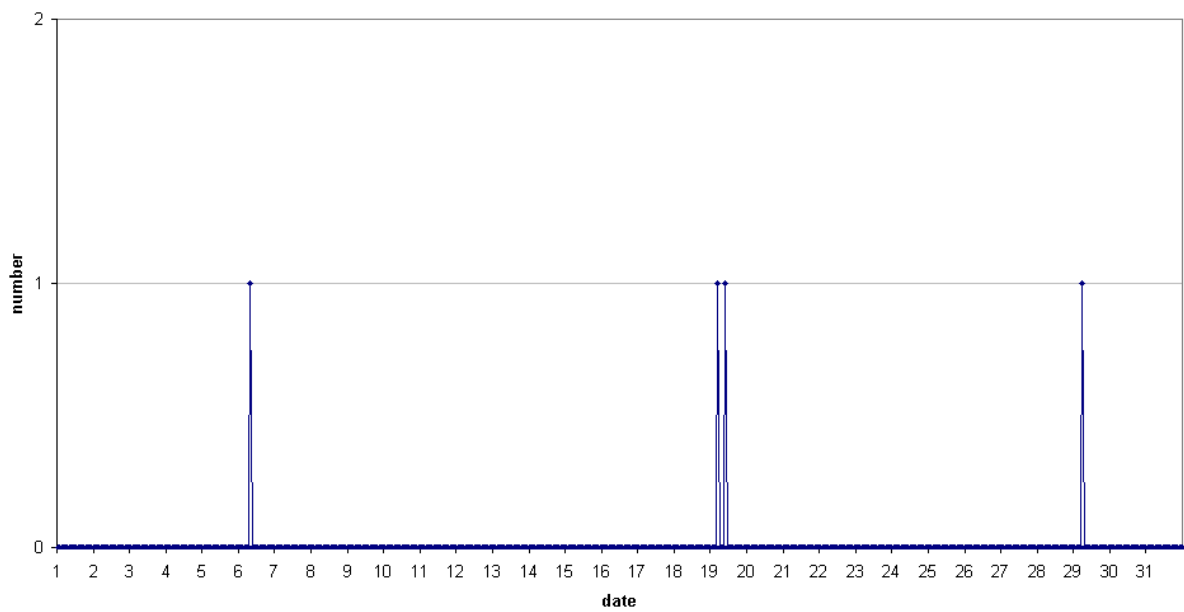*Felix Verbelen (Kampenhout/BE)*

Figure 14 – The hourly numbers of overdense reflections longer than 10 seconds and longer than 1 minute, as observed here at Kampenhout (BE) on the frequency of our VVS-beacon (49.99 MHz) during March 2018.

Radiometeors – April 2018

Felix Verbelen

Vereniging voor Sterrenkunde & Volkssterrenwacht MIRA, Grimbergen, Belgium
`felix.verbelen@skynet.be`

An overview of the radio observations during April 2018 is given.

1   Introduction

The graphs show both the daily totals (*Figure 1 & 2*) and the hourly numbers (*Figure 3 & 4*) of "all" reflections counted automatically, and of manually counted "overdense" reflections, overdense reflections longer than 10 seconds and longer than 1 minute, as observed here at Kampenhout (BE) on the frequency of our VVS-beacon (49.99 MHz) during April 2018.

The hourly numbers, for echoes shorter than 1 minute, are weighted averages derived from:

$$N(h) = \frac{n(h-1)}{4} + \frac{n(h)}{2} + \frac{n(h+1)}{4}$$

As expected the Lyrids shower peaked on 22–23 April.

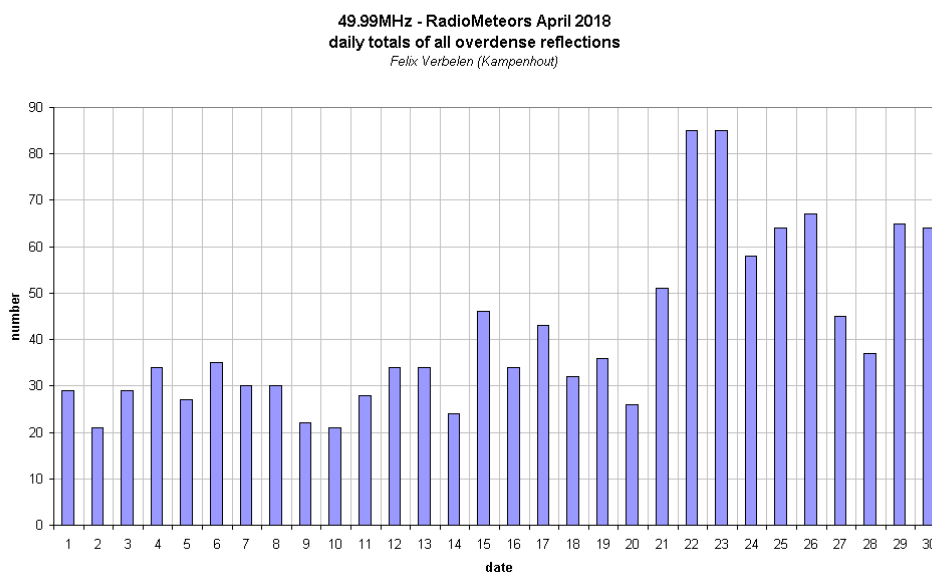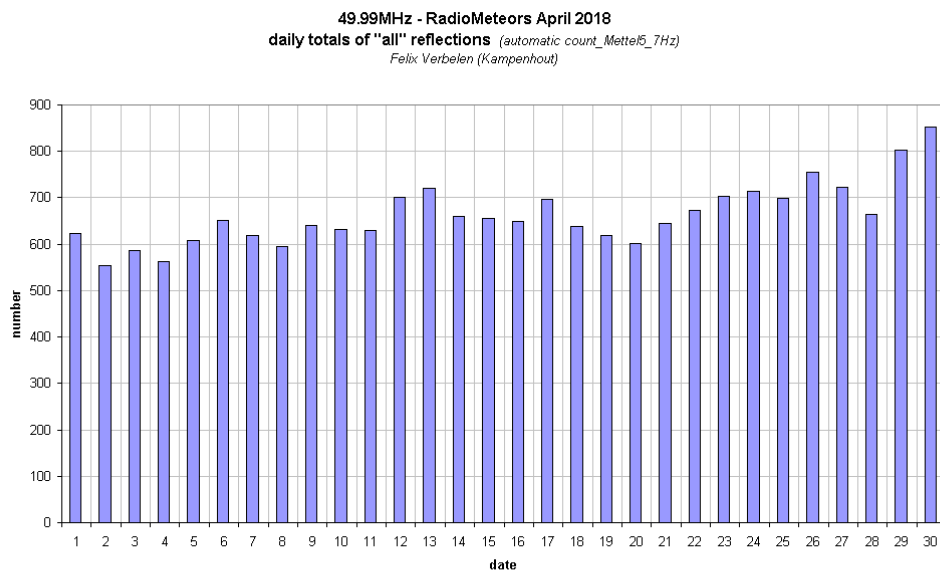If you are interested in the actual figures, please send me an e-mail.

Figure 1 – The daily totals of "all" reflections counted automatically, and of manually counted "overdense" reflections, as observed here at Kampenhout (BE) on the frequency of our VVS-beacon (49.99 MHz) during April 2018.

49.99MHz - RadioMeteors April 2018
daily totals of reflections longer than 10 seconds
Felix Verbelen (Kampenhout)
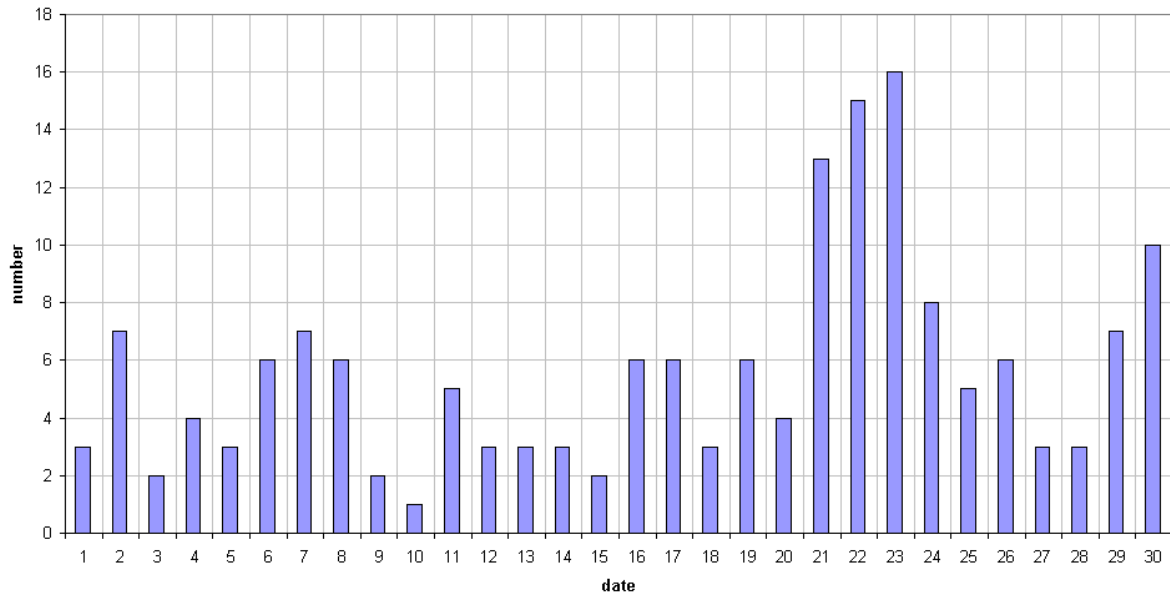
49.99MHz - RadioMeteors April 2018
daily totals of reflections longer than 1 minute
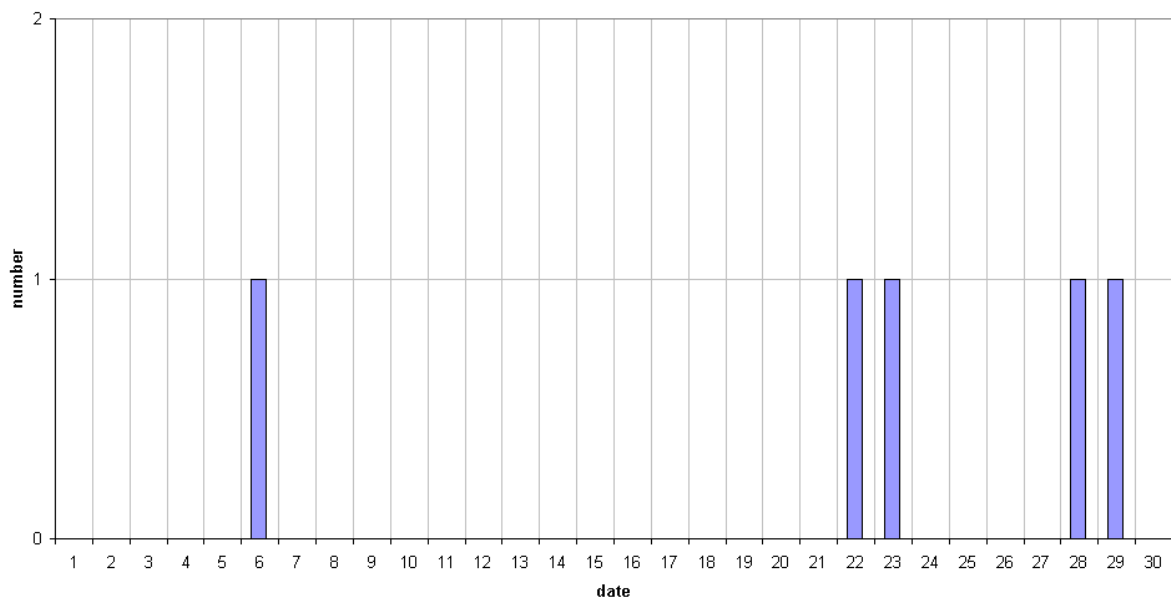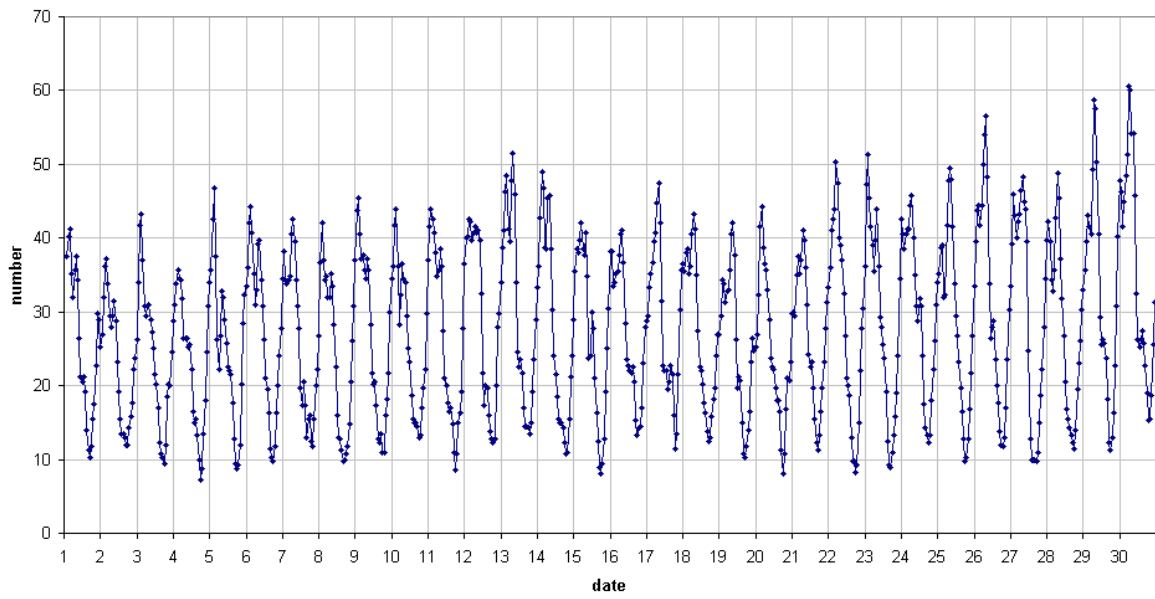*Felix Verbelen (Kampenhout)*

Figure 2 – The daily totals of overdense reflections longer than 10 seconds and longer than 1 minute, as observed here at Kampenhout (BE) on the frequency of our VVS-beacon (49.99 MHz) during April 2018.

49.99 MHz - RadioMeteors April 2018
number of "all" refections per hour (weighted average) *(automatic count_Mettel5_7Hz)*
Felix Verbelen (Kampenhout)

49.99MHz - RadioMeteors April 2018
number of overdense reflections per hour (weighted average)
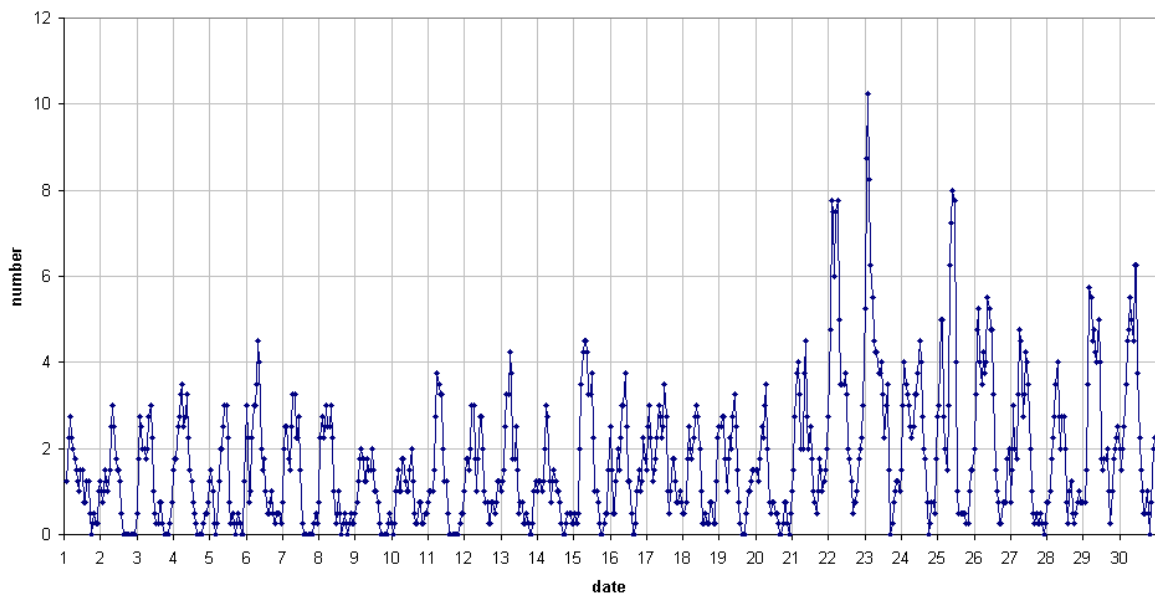*Felix Verbelen (Kampenhout)*

Figure 3 – The hourly numbers of "all" reflections counted automatically, and of manually counted "overdense" reflections, as observed here at Kampenhout (BE) on the frequency of our VVS-beacon (49.99 MHz) during April 2018.

49.99MHz - RadioMeteors April 2018
number of reflections >10 seconds per hour (weighted average)
Felix Verbelen (Kampenhout)

49.99MHz - RadioMeteors April 2018
hourly totals of overdense reflections longer than 1 minute
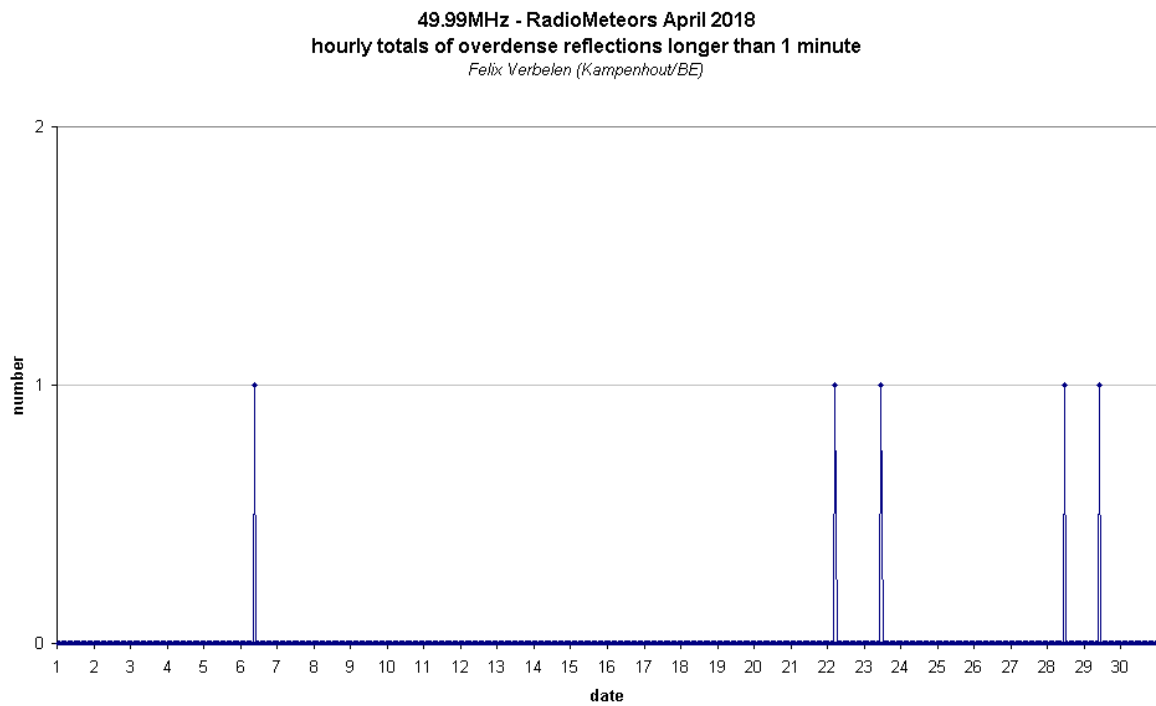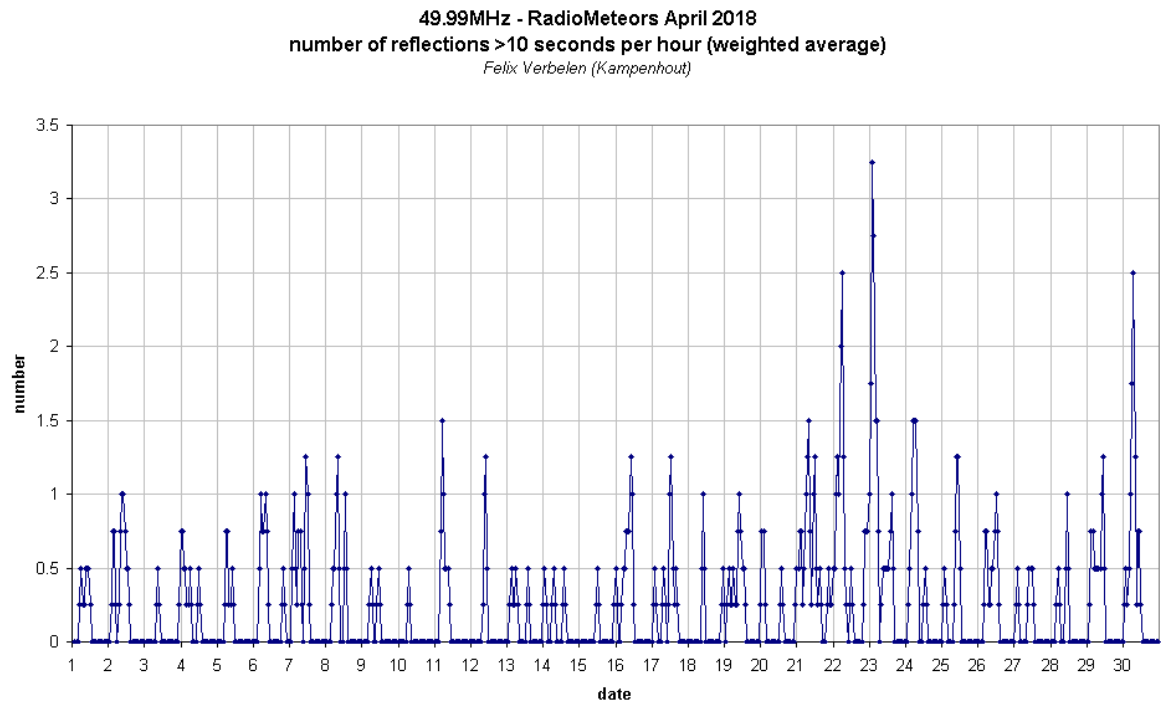*Felix Verbelen (Kampenhout/BE)*

Figure 4 – The hourly numbers of overdense reflections longer than 10 seconds and longer than 1 minute, as observed here at Kampenhout (BE) on the frequency of our VVS-beacon (49.99 MHz) during April 2018.

Fireball events

José María Madiedo

Universidad de Huelva, Facultad de Ciencias Experimentales
jmmadiedo@gmail.com

An overview is presented of exceptional fireball events by the meteor observing stations operated by the SMART Project (University of Huelva) from Sevilla and Huelva during the period April – May 2018.

1 Fireball over Spain on 14 April 2018

This beautiful fireball overflew Spain on 14 April 2018 at 23:41 local time (21:41 universal time)[19]. According to the orbital analysis, it was produced by a fragment from an asteroid that hit the atmosphere at about 100.000 km/h. The event begun at an altitude of about 98 km and ended at a height of around 55 km. It was recorded in the framework of the SMART Project (University of Huelva) from the meteor-observing stations located at the astronomical observatories of Calar Alto (Almería), La Sagra (Granada), La Hita (Toledo) and Sevilla.
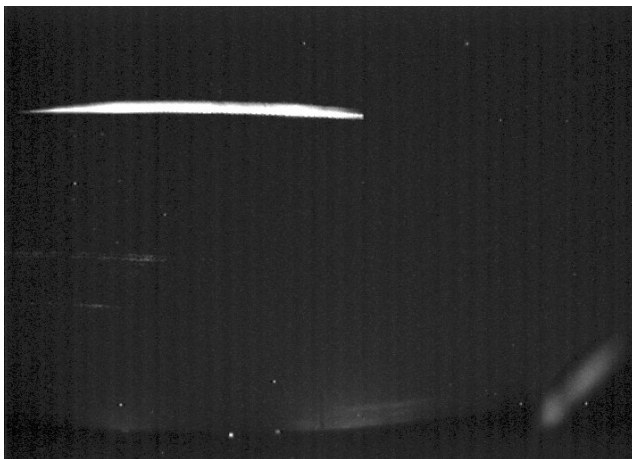

Figure 1 – Fireball 14 April 2018 at 21ʰ41ᵐ UT.

2 Beautiful Virginid fireball behind the clouds on 28 April at 23:50 UT

This Virginid fireball was spotted over Spain on 29 April at 1:50 local time (23:50 universal time on 28 April)[20]. The meteoroid entered the atmosphere at around 65.000 km/s. The event began at an altitude of about 80 km over the province of Almería, and ended at a height of 42 km over the province of Granada. It was recorded in the framework of the SMART Project (University of Huelva) by the meteor-observing stations located at the astronomical observatories of La Sagra (Granada), Sierra Nevada (Granada) and Sevilla.

Figure 2 – Virginid fireball 29 April 2018 at 23ʰ50ᵐ UT.

3 Fireball over the Mediterranean Sea on 15 May 2018

This fireball was recorded over the Mediterranean Sea on 15 May at 3:54 local time (1:54 universal time)[21]. The event was produced by a cometary meteoroid that hit the atmosphere at about 54000 km/h. The luminous phase began at an altitude of around 102 km over the sea, and ended at a height of about 61 km.
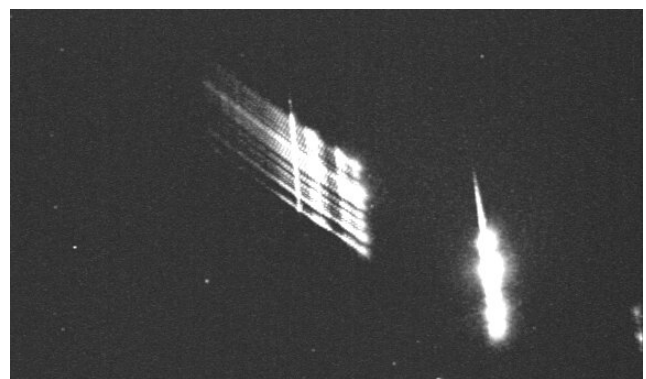

Figure 3 – Fireball 15 May 2018 at 1ʰ54ᵐ UT.

The fireball was recorded by the meteor-observing stations operating in the framework of the SMART Project (University of Huelva) from the astronomical observatories of Calar Alto, La Sagra (Granada), La Hita (Toledo), Sierra Nevada (Granada) and Sevilla.

---

[19] https://youtu.be/87ON51Y7EbY
[20] https://youtu.be/y2nTHnjfkik
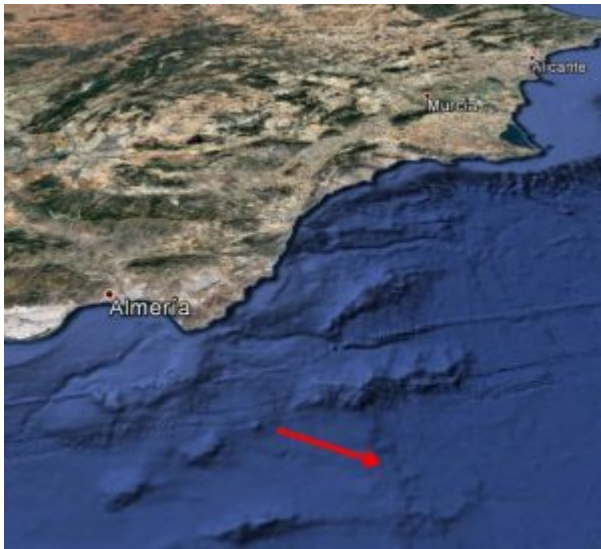[21] https://youtu.be/f72etAgk20c

Figure 4 – Fireball 15 May 2018 at 1h54m UT, trajectory.

4 Meteorite-producing fireball on 22 May 2018

This sporadic fireball was recorded over the Mediterranean Sea on 22 May 2018 at 23:37 UT. The event was produced by a fragment from an asteroid that hit the atmosphere at about 90,000 km/h. Its luminous phase began at an altitude of around 89 km over the sea, and ended at a height of about 19 km. The analysis of its atmospheric path shows that this was a meteorite-producing fireball. The meteorite would have fallen into the sea.

Figure 5 – Fireball 22 May 2018 at 23ʰ37ᵐ UT.

This event was recorded by the meteor-observing stations operating in the framework of the SMART Project (University of Huelva) from several astronomical observatories in Spain: Calar Alto, La Sagra, La Hita and Sevilla.

The following video[22] shows the apparent path of the fireball over the domes of the Calar Alto Astronomical Observatory.

---

[22] https://youtu.be/DVx5XkAJwzA

Eta Aquariids 2018 observed from Florida

Paul Jones

jonesp0854@gmail.com

A summary is given of the visual observations of the 2018 eta Aquariid observations in Florida.

1   Introduction

Even with the moonlight, clouds and some minor harassment by the no-see-um gnats, I was able to do some observing for the 2018 eta Aquariid meteor shower (ETAs) from Matanzas Inlet, Florida. I saw a few real nice eta Aquariid meteors (ETAs) and a couple of equally nice eta Lyrid meteors (ELYs) as well. All told, in three nights, during 4.5 hours of observing, I recorded data on 28 ETAs, 11 ELYs, 4 Anthelions (ANTs) and 33 sporadics (SPOs) for a total of 77 meteors. The moonlight probably hid several fainter ETAs during the watches.

The best and brightest meteors of the three watches were a pair of gorgeous, –2 ETAs, both streaking north out of the radiant in eastern Cygnus. They left glowing smoke trains behind them for a few seconds on the sky. I also noted the super-fast speed of all the ETA meteors I saw. The ETAs of course, are the meteors caused by Halley's Comet and are among the fastest of the meteor showers at upwards to 42 miles per second in speed! That equates to a typical ETA lasting less than 1/10 of a second in duration. One must really concentrate to catch these babies.

In addition to the ETAs, I also noted some nice meteors coming from the ELY radiant this year, just as I have in recent past years. The ELYs are fairly bright meteors and their slower apparent speed is very noticeable when one is seen. I plan to carefully monitor this minor radiant in the years to come. Here is my data:

Observed for radiants:

- ETA: eta Aquariids
- ELY: eta Lyrids
- ANT: Anthelions
- SPO: sporadics

2   May, 8/9, 2018

Observer: Paul Jones, Location: north bank of Matanzas Inlet, Florida, 15 miles south of St. Augustine, Florida, Lat: 29.75 N, Long: 81.24W, LM: variable 5.5 - 6.2, sky conditions: clear, with 30% degradation due to moonlight and twilight interference, Facing: South.

0400 – 0500 EDT (0800 – 0900 UT), T_{eff}: 1 hour, clear, no breaks

- 7 ETA: 0, +1, +2(3), +3(2)
- 3 ELY: +1, +2, +3
- 2 ANT: +1, +3
- 5 SPO: +2, +3(2), +4(2)
- 17 total meteors

4 of the 7 ETAs and 1 of the ELYs left visible trains, blue and yellow tints were noticed in the brighter ETAs.

0500 – 0530 EDT (0900 – 0930 UT), T_{eff}: .5 hour, clear, no breaks

- 4 ETA: –2, 0, +2(2)
- 2 SPO +3(2)
- 6 total meteors

All four of the ETAs left visible trains, the –2 ETA left a train that lasted for about three seconds on the sky.

3   May, 9/10, 2018

Observer: Paul Jones, Location: north bank of Matanzas Inlet, Florida, 15 miles south of St. Augustine, Florida, Lat: 29.75 N, Long: 81.24W, LM: variable 5.5 – 6.2, sky conditions: clear, with 20% degradation due to moonlight and twilight interference, Facing: South.

0330 – 0430 EDT (0730 – 0830 UT), T_{eff}: 1 hour, clear, no breaks

- 5 ETA: –2, +2(2), +3(2)
- 1 ELY: +3
- 8 SPO: 0, +2, +3(3), +4(2), +5
- 14 total meteors

4 of the 5 ETAs left visible trains, the –2 ETA left a train that lasted for about three seconds on the sky. Blue and yellow tints were noticed in the brighter ETAs.

0430 – 0530 EDT (0830 – 0930 UT), T_{eff}: 1 hour, clear, no breaks

- 9 ETA: 0(2), +1, +2(3), +3(3)
- 3 ELY: +2, +3(2)
- 1 ANT: +3
- 9 SPO +2, +3(4), +4(3), +5
- 22 total meteors

Six of the 9 ETAs left visible trains.

4   May, 10/11, 2018

Observer: Paul Jones, Location: north bank of Matanzas Inlet, Florida, 15 miles south of St. Augustine, Florida, Lat: 29.75 N, Long: 81.24W, LM: variable 5.5 – 6.2, sky conditions: clear, with 35% degradation due to cirrus clouds and haze, Facing: South.

0400 – 0500 EDT (0800 – 0900 UT), T_{eff}: 1 hour, cirrus clouds and haze, no breaks

- 3 ETA: +1, +2, +3
- 4 ELY: +1. +2, +3(2)
- 1 ANT: +2
- 9 SPO: +2(2), +3(4), +4(2), +5
- 17 total meteors

2 of the 3 ETAs left visible trains and one ELY left visible trains.

5   Conclusion

Overall, considering the still bright moon, twilight, cloud issues and being past their maximum activity date, the ETAs performed pretty well each morning. The two gorgeous –2 ETAs I saw were quite memorable and the highlight of the watches! I continue to be impressed with the ELYs also both in terms of numbers of meteors seen and their brightness - a very nice little minor meteor shower indeed!

I used an old meteor watchers trick during the watches to mitigate the distraction of the rising moon in the east. I used a book to block out the direct light of the moon from shining in my eyes while observing. That makes a surprising difference in seeing meteors under moonlight conditions.

The mission statement of MeteorNews is: "Minimizing overhead and editorial constraints to assure a swift exchange of information dedicated to all fields of active amateur meteor work." Easy and fast submission of content online, no subscription registration and no membership fees. MeteorNews is free available and dedicated to active amateur meteor observers.

To contribute on a regular bases you are welcome to become Meteor-News-editor, please contact Jakub Koukal (Account administrator) to create your editor account. To contribute on a casual bases, please send your text to one of the editors.

For more info read: https://meteornews.net/writing-content-for-emeteornews/

Contributing to this issue:

- *Jean-Marie Biets*
- *Peter Cambell-Burns*
- *Tioga Gulon*
- *Carl Johannink*
- *Richard Káčerek*
- *Jakub Koukal*
- *José María Madiedo*
- *Koen Miskotte*
- *Paul Roggemans*
- *Enrico Stomeo*
- *Felix Verbelen*